2011

Self Assembled Monolayers on Pd Substrates and Kubas based hydrogen storage materials

Van Hung Mai
University of Windsor

Recommended Citation

Mai, Van Hung, "Self Assembled Monolayers on Pd Substrates and Kubas based hydrogen storage materials" (2011). *Electronic Theses and Dissertations.* Paper 72.

Self Assembled Monolayers on Pd Substrates and Kubas based hydrogen storage materials

by

Van Hung Mai

A Thesis
Submitted to the Faculty of Graduate Studies
through the Department of Chemistry and Biochemistry
in Partial Fulfillment of the Requirements for
the Degree of Master of Science at the
University of Windsor

Windsor, Ontario, Canada

2011

Self Assembled Monolayers on Pd Substrates and Kubas based hydrogen storage materials

by

Van Hung Mai

APPROVED BY:

Dr. Rupp Carriveau, External Reader
Department of Civil and Environmental Engineering

Dr. Stephen J. Loeb, Departmental Reader
Chemistry and Biochemistry Department

Dr. Ricardo Aroca, Departmental Reader
Chemistry and Biochemistry Department

Dr. Tricia Breen Carmichael, , Advisor
Chemistry and Biochemistry Department

Dr. S. Ananvoranich, Chair of Defense
Chemistry and Biochemistry Department

Author's Declaration of Originality

I hereby certify that I am the sole author of this thesis and that no part of this thesis has been published or submitted for publication.

I certify that, to the best of my knowledge, my thesis does not infringe upon anyone?s copyright nor violate any proprietary rights and that any ideas, techniques, quotations, or any other material from the work of other people included in my thesis, published or otherwise, are fully acknowledged in accordance with the standard referencing practices. Furthermore, to the extent that I have included copyrighted material that surpasses the bounds of fair dealing within the meaning of the Canada Copyright Act, I certify that I have obtained a written permission from the copyright owner(s) to include such material(s) in my thesis and have included copies of such copyright clearances to my appendix.

I declare that this is a true copy of my thesis, including any final revisions, as approved by my thesis committee and the Graduate Studies office, and that this thesis has not been submitted for a higher degree to any other University or Institution.

Abstract

The focus of this thesis work is on the formation of new types of SAMs including DTPA and dialkyldiselenide on palladium substrates. With major differences in the headgroups with thiolate SAMs, DTPA and dialkyldiselenide SAMs on palladium will help to reveal the interfacial structures of SAMs and other variations in the macroscopic properties. We also investigated the binding behavior of the new SAMs molecules with palladium through XPS experiments.

To my beloved Dad, Mom and Sister

&

and my beloved girl friend Phuong Tong

Acknowledgements

I am deeply indebted to my thesis advisor.

This work would not have been possible without the support of many people, whether directly or indirectly. First and foremost, I would like to express my sincere gratitude to my supervisor Prof Tricia Breen Carmichael, whose patience and kindness, as well as incredible support and guidance have been invaluable to walk me through this work. Special thanks also to all members of Carmichael group, especially Ronan San Juan, Mike Miller, Heather Filiatrault, Michael Anthony Ferrato, Gyllian Porteous, Stan Amyotte, Steve Carmichael who have been the source of friendship as well as good advice and collaboration during the time I spent here.

I would like to acknowledge Tuan Hoang, Ahmad Hamaed, who worked with me when I was in Antonelli group. We worked together on hydrogen storage project, and I very much appreciated their enthusiasm and willingness to make highly risk and easily explosive organolithium reagent with me. A special thank goes to Dr. David Antonelli for being my supervisor in a short period time.

For this dissertation, I would like to thank my reading committee members, Dr. Ricardo Aroca, Dr. Steven Loeb and Dr Rupp Carriveau. A deepest gratitude is also due to Dr. James Gauld, our graduate coordinator, whose helpful suggestion and advice in proofreading my thesis. Thanks also to Dr. Matthew Revington (our NMR coordinator) and Dr Holger Eichhorn who trained and helped me with NMR and XRD experiments. I would also like to thank specially to Ms. Marlene Bezaire, our graduate secretary, for helping me most with love and care.

I would like to thank my housemates and Vietnamese friends here, Tuan Hoang, Thanh Nguyen, Phan Duy, Thao Tran, Tuan Nguyen, Anh Le, Hoai Vu, Xuan Nguyen and a little niece Emily Le, who lived with me for the past three years. We had a lot of funs together, wonderful moments, and we will never forget nice memories with severe winter as we went to market in a broken car under snowstorm ^^.

And last, but most certainly not least, I would like to thank my family for all their love and encouragement. For my parents, who have raised, nourished and supported me in all my pursuits of science love. For my sister, Ngoc Ha, who always is not only my beloved friend but also my soul guardian to help me through 'bad days' of my life. For my beloved Phuong Tong, I am forever grateful for being with you and wish to continue arguing with you until my very last breath. Thank you.

Van Hung Mai

The University of Windsor
June 2011

Table of Contents

List of Figures

List of Tables

Symbols and Abbreviations

DTPA	:	Dialkyldithiophosphinic acid
BHDS	:	Bis(hexadecyl)-diselenide
EIS	:	Electrochemical Impedance Spectroscopy
XPS	:	X-ray Photoelectron Spectroscopy
AFM	:	Atomic force microscopy
RAIRS	:	Reflection Absorption Infrared Spectroscopy
SAMs	:	Self assembled monolayers
CA	:	Contact Angle
HD	:	Hexadecane
ν_s	:	Symmetric vibrational mode
$\nu_a s$	:	Anti-symmetric vibrational mode

Chapter 1

Intro

PART I Self Assembled Monolayers

1.1 General Introduction

”No problem is too small or too trivial if we can really do something about it from Richard Feynman to Koichi Mano (3 February 1966)”

Nanotechnology research and application have been thriving in last three decades. The idea that we can rule the nature through changing the smallest items leads nanotechnology to become a powerful combination of science and engineering ever seen.

Obviously, the most remarkable impact of nanotechnology is apparent in medical and biological applications; we have seen how dramatical changes are in this field from such the design of minute drug to the establishment of new low-cost, point-of-care clinical diagnostic techniques.Working with this influential technology requires a detailed understanding of the underlying physical, chemical, and biological processes across a range of scientific disciplines and at the nanoscale[1]. Due to the fact that there is no boundary for idea and mind, scientists have played the game of god on creating millions of differently magnificent nano-materials with diverse applications in (bio)sensors [2], medicine [3], electronics [4], energy [5], and optics [6], etc. The early exploration of nanostructures and the later enormous expansion of nano-science ignited around the 1980s, not long after the invention of the scanning tunneling microscope (STM) [7]. Later, the term ”nanotechnology” for this new and specific science research field was firstly framed up by K.E. Drexler [8]. As defined by many scientists, nano-materials are any materials having at least one dimension less than 100nm [9]. Nano-materials can be classified based on types of substances (carbon based nanomaterials [10]), shapes (nanorods [11], nanowires [12]), compositions [13] and etc; however, with regardless to the origin of employed materials, the most common way to distinguish nanomaterials is separating them into four general classifications [14] (Figure 1.1): 0D nanomaterials (all dimensions x, y, z at nanoscales such as nanoparticles [15] like colloids and quantum dots), 1D nanomaterials (two dimensions x, y at nanoscales such as nanowires, nanotubes [16] , 2D nanomaterials (one dimensions x at nanoscales such as layers [17]) and 3D nanomaterials (no bulk dimension at nanoscale such as nanocrystalline, nanocomposite).

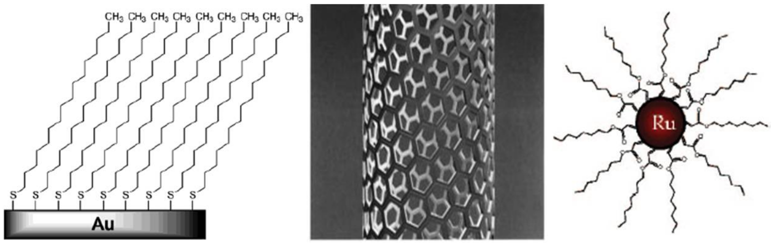

Figure 1.1: Images of 2D, 1D and 0D nanomaterials.

The use of a simple, flexible and convenient system as the basic building blocks of nanoscale structures capitalizes on a wealth of knowledge that can be obtained from the study of self assembled monolayers (SAMs) systems [18]. As one-dimensional nanometer-sized materials, SAMs have attracted considerable interests because of its intrinsic size - dependent properties and enormous number of applications such as corrosion prevention [19], device fabrication [20], membrane mimicry [21] and etc. With the fact that the states of individual molecules, molecules on surface or interfaces has a greater effect on the properties of nanomaterials than the properties of the bulk materials [22], SAMs chemistry provide remarkably the capabilities to manipulate custom-designed surfaces or interfaces for forming and investigating to specific nano-systems. The aim of this chapter is to provide an overview of important milestones, formation, mechanism, structure, and potential application of SAMs, limiting ourselves primarily to a discussion of the thiolate related SAMs structures such as, chelating thiolate SAMs, selenium-based SAMs, and SAMs on palladium surfaces.

1.2 Thiolate SAMs

1.2.1 Thiolate SAMs formation

Based on the strong affinity of sulfur to many transition metal surfaces, thiolate SAMs is considered to be a simplified model system for investigating fundamental properties of SAMs. The most typical investigated thiolate SAMs is the layers of alkyl thiol molecules organized on gold substrates (Figure 1.2), first manipulated by Nuzzo and Allara group [24]. Gold substrates, in both particles [25] and planar surfaces [26] forms, have been extensively exploited as ideal substrate materials for SAMs formation. This is due not only to its malleability to form thin films, but also its availability in high purity, little or no active ability to be oxidized by oxygen at normal conditions, and capability to be cleaned easily [27]. Despite of different available gold substrate forms, the most commonly used crystal lattice configuration of gold thin films is the planar Au (111) (Figure 1.3), deposited on silicon wafers, due to its smooth, order and well defined surfaces and lowest energetic crystalline face [28]. Usually, thin adhesion layers which can be Cr or Ti layers on the silicon wafers is followed by the deposition of gold by thermal evaporation [29] - [30].

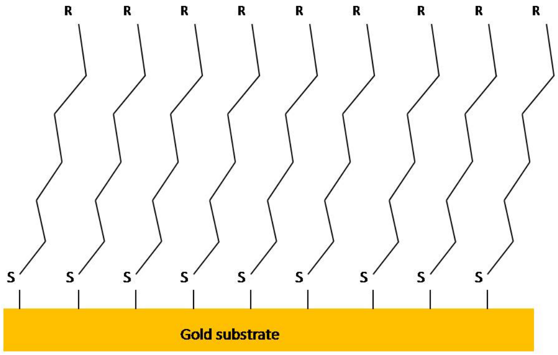

Figure 1.2: Self assembled monolayers of alkyl thiol on gold thin films

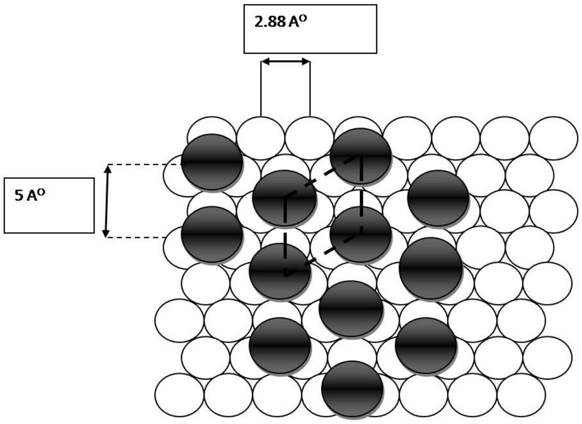

Figure 1.3: Planar Au (111) surface, with black dots are positions of anchored thiolates at the trigonal pocket of gold atoms

The formation of thiol-based SAMs is typically formed by the immersion of gold substrates to a solution containing the thiol [31] or by the exposure of gold substrates under vapor-phase of thiol precursors [32]. However, the solution method generally tends to be preferred due to its cheaper, more convenient, and less hazardous than vapor phase method [32]. As contacted to gold substrate, the thiol molecules spontaneously adsorbed to gold surface due to the ability to reduce surface energy of substrate and to form stable chemical bond between sulfur head group and gold interfacial atoms [33]. The oxidation reaction between thiols and gold atoms is described in the equation below (equation 1.1.1) [32]. X-ray photoelectron spectroscopic (XPS) studies confirmed the formation of gold thiolate Au(I) thiolate $\{(RS^{-}Au^{+} \bullet Au_n)\} : S(2p^{\frac{3}{2}}) \sim 162eV$ as the product of thiol chemisorption on such gold surfaces [34]. In addition, other spectroscopes, such as raman spectroscopy [35] and fourier transform mass spectrometry [36] also supported evidences about the thiolate (RS^{-}) species absorbed on the gold surface.

$$RSH + Au(0)_n \rightarrow RS^{-} \bullet Au(0)_n + \frac{1}{2}H_2 \qquad (1.1)$$

The fact that thiol SAM formation on gold proceeds with two steps adsorption kinetics was well established by many early kinetic studies about thiol adsorption onto Au(111) surfaces [37] - [40]. In the initial step, the thiols absorb onto Au to form disorder regions of molecules with coverage of about 80 - 90% of substrates [37]. This steps is a very fast one, within a few minutes, and mainly depend on the concentration of thiols in the incubate solution due to diffusion-controlled adsorption mechanism. The second step is much slower, over a period of hours, as thiolate self organize into a more ordered layer to form crystalline or semi-crystalline structures on the substrate surface [40]. Therefore, the second step can be described as a two-dimensional (2-D) crystallization process within the layer. The kinetic rate of the second step is strongly based on the interactions (van der waals, dipole-dipole and etc) between alkyl chains (or spacer) and alkyl structures (defects) [41]. The Langmuir adsorption kinetic behavior of thiols SAMs on gold has also been investigated in some detail by a number of kinetic studies using various types of experiments such as near-edge X-ray absorption fine structure (NEXAFS) [42], X-ray photoelectron spectroscopy (XPS) [43] - [44], infrared reflection-absorption spectroscopy IRRAS [45].

Evidences from scanning tunneling microscopy (STM) [46] - [47], IRRAS [48] and low-energy He atom diffraction [49] - [50] demonstrated that the self organizing process of alkyl thiolate molecules on gold substrates has three phases (Figure 1.4). The first stage is the formation of the ”lying down” phase with the random dispersion of absorbate molecules on the surface. The second is the intermediate phase with higher density of absorbate molecules

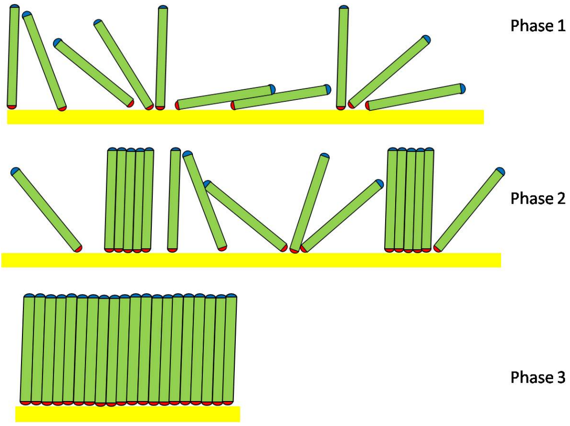

Figure 1.4: Three phase of SAMs formation

and disordered regions. The last one is characterized by the fully coverage of SAMs, close packed structure and the average molecular tilt angle getting the maximum values. The orientation, conformation and 2-D structure of the long chain alkyl ($n \geq 8$) thiolate SAMs at saturation coverage on Au(111) have been well characterized by a number of methods, including NEXAFS [51], IR-RAS [52], Raman spectroscopy [53], and ultraviolet photoemission spectroscopy [54]. It is found that for long chain alkylthiolate SAMs, the conformation of alkyl-chains is nearly all-trans configuration with tilted angle 30^0(from the surface normal) and closely packed to generate a high dense, crystalline two dimentional layer onto substrate surface [55]. The difference of molecular surface density for bulk crystalline n-alkanes ($18.4(A^o)^2$/chain [56]) and Au(111) (21.6 $(A^o)^2$ /molecule [47] - [57]) is accounted for the chain tilting which enables the maximizing the interchain dispersion interations between alkyl-chains of thiolate SAMs.

1.2.2 Chelating thiolate SAMs

Although appearing as one of the initial reports of SAMs on gold [58], surprisingly, chelating thiol-based monolayers have received relatively little attention from surface science researchers. With the primary goal to have a systematic comparison of the SAMs generated from two species: the chelating aromatic dithiols [59] - [60](Figure 1.5) and xanthates [61](Figure 1.6) to those generated from their normal alkanethiol analogues; Randall Lee and co-workers found that a new class of SAMs formed from bis-chelating thiols on gold exhibited stabilities greater than the sum of two sulfur-gold enthalpies and the van der Waals stabilization common to self-assembled organic thin films. Since then, attempts to explore these new chelating thiolate SAMs have been approached mainly by Randall Lee groups involving many aspects such as forming loosely packed SAMs [62] - [64] , investigating desorption and adsorption kinetics [65] - [68], and preparing homogeneously mixed multicomponent SAMs [69].

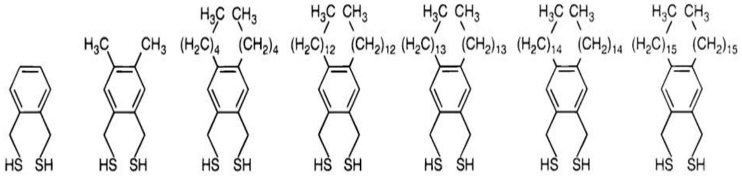

Figure 1.5: Chelating aromatic dithiols molecules

Furthermore, using not only typical chelating aromatic dithiols and xanthates, but also a new type of bis-chelating thiol, 2-Alkyl-2-methylpropane-

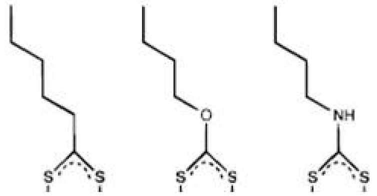

Figure 1.6: Xanthates

1,3-dithiols (Figure 1.7), Park et al [70] was successful to generate a unique homogeneously mixed SAMs which showed some special properties like the less conformationally disordered monolayer film, greater wettabilities and frictional responses when compared to SAMs manipulated from mixtures of normal alkanethiols having analogous chain lengths. Moreover, these new chelating SAMs with, more than one, sulfur binding sites to metal surface showed exceptional thermodynamic stable when compared to analogous n-alkanethiolate SAMs. These unique properties were account by chelating effect of two sulfur bonds which generated a formation of cyclic disulfide with metal on the surface.

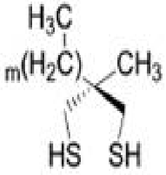

Figure 1.7: 2-Alkyl-2-methylpropane-1,3-dithiols

Employing different type of head groups molecules is also a alternative way to generate chelating thiolate SAMs; Weinstei [71] et al used dialkyldithio molecules (Figure 1.8) which have two sulfur binding sites on the structure to form SAMs; with the specific structure of these molecule, they suggested that their prepared SAMs would exceed traditional thiol counterparts SAMs with different structures, packing densities, electron-transfer properties, and thermal stabilities. With two different alkane chains which can be modified separately, dialkyldithiocarbamates molecules could be potentially employed to design SAMs surface containing variety of structure and packing densities. In addition, the fixed inter-atomic distances between the two sulfur atoms would yield the resonant bidentate structure of the anchored dithiocarbamate on the metal surface. This resonant structure of this specific SAMs is account for many unique electronic characteristic properties which enables to develop many applications for molecular electronics.

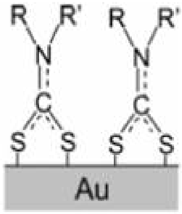

Figure 1.8: Dialkyldithiocarbamate salts into monolayers on gold

1.3 SAMs on Pd substrates

Palladium has generated interest as substrate for self assembled monolayers (SAMs) within metal-insulator-metal junctions because of its potential compatibility with CMOS technology, its resistance to oxidation and its tendency to bind organic thiols strongly [9]. Comparing to other coinage metals, palladium was known as the most practical substitution to gold for being employed as a substrate on thiolate based SAMs [72]. Love [73] et al showed that n-alkanethiolates SAMs formed on thin films of palladium are better etch resistance layer for patterning SAMs based on microcontact printing than thin films on gold and other metals, due to specific properties of n-alkanethiolates/Pd SAMs, such as smaller edge roughness, greater selectivity against wet chemical etchants, and higher compatibility with CMOS devices. Furthermore, on the other thiols/Pd SAMs studies, John et al [74] employed mixtures of long-chain thiols to form SAMs on palladium and showed that these mixed palladium thiolates self assemble into hybrid bilayer mesophase consisting of disordered chain with fair amounts of gauche defects, in contrast with the analogous monothiolates structruces with highly ordered chains in a fully extended all-trans conformation. Palladium substrates were also used to investigate the reductive desorption of n-alkanethiolate (RS^-) self assembled monolayers (SAMs) and to quantify the relative electrochemically accessible surface area of SAMs [75]. In addition to investigate interactions between cells and surfaces and the study of cell biology, OEG-terminated thiolate SAMs on palladium films was employed as inert platform substrates which are useful in studies of certain cellular behaviors-morphogenesis of tissues, oncogenesis, and the effects of toxins on cells - that require long-term observation [76].

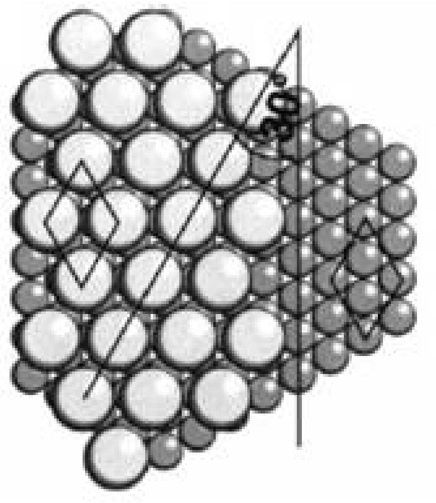

Figure 1.9: $\sqrt{3} \times \sqrt{3}R30^o$-S structure

Despite of the fact that the formation of thiolate SAM on palladium has been demonstrated by several investigations mentioned above, the structure of thiol/Pd(111) interface in the thiolate SAMs is, however, still not clear due to the complex structure of sulfur on palladium. Via the adsorption of H_2S gas on the Pd(111) sample under UHV conditions, several model of S-Pd interface structure have been proposed by applying many types of surface analysis such as, normal incidence X-ray standing wave (NIXSW) absorption [77], surface extended X-ray absorption fine structure (SEXAFS) [78], scanning tunneling microscopy (STM) [79], Auger electron spectroscopy (AES) [80] and Low-energy electron diffraction (LEED) [81] - [82]. In general, these structural models, based on a simple S overlayer on Pd(111) surface, results in the formation of $\sqrt{3} \times \sqrt{3}R30^o$ phase (Figure 1.9) at room temperature, and with increasing coverage and elevated temperature, the more complex $\sqrt{7} \times \sqrt{7}R19.1^o$ phase (Figure 1.10) is formed. However, due to the $\sqrt{3} \times \sqrt{3}R30^o$ structure of the

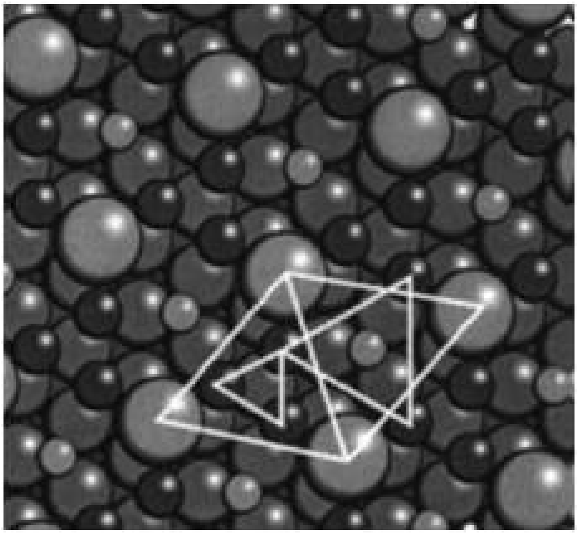

Figure 1.10: Complex $\sqrt{7} \times \sqrt{7}R19.1^o$ phase

elemental sulfur phase is a simple adlayer, the compound palladium-sulfide interphase structure is still not revealed.

Recently, by applying XPS to investigate thiolate SAMs structures on palladium surface, Love et al [73] revealed that the adsorption of n-alkanethiols on palladium formed monolayers on the top of a complex surface phase - palladium sulfide interphase. They also proposed that the ratio of sulfur species on Pd (111) surface could be nearly 2 sulfide species for every one bonded as a thiolate, and showed that the formation of thiolate SAMs on the surface of Pd might generate a metastable palladium sulfide interphase which is similar to that found on thiolate/silver SAMs [83]. Moreover, their XPS results about additional sulfur on Pd surface didn't account with the surface structures of sulfur/Pd suggested by some previous LEED studies. Recently, by means of

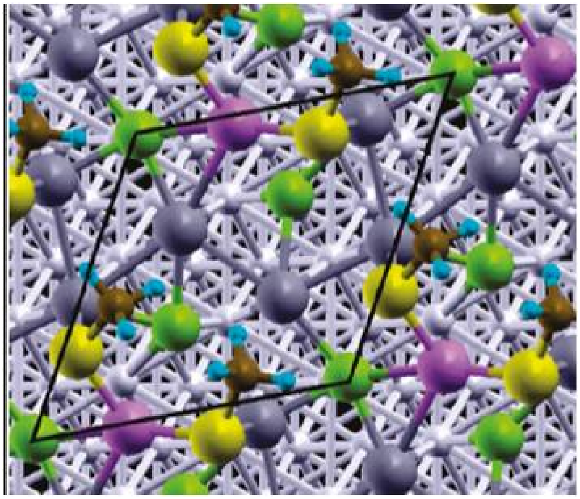

Figure 1.11: S-Pd surface structure model proposed by means of DFT calculations of Carro et al

DFT calculations and experimental XPS studies, Carro et al [84] proposed a new model of S-Pd surface structure (Figure 1.11) which suggested the coverages of $\theta_{sulfide}$ and $\theta_{thiolate}$ are about 0.4 and 0.3 respectively, and mixed S-Pd structure (S_3Pd_5) with a packed arrangement of Pd pentagons with one S atom inside and two triangles with two S atoms. These computational results provide useful information to understanding S-Pd surface structure, however, further evidences from experimental surface analysis techniques are essential for reveal the nature of the interface between the palladium and sulfur containing species.

1.4 Selenium based SAMs.

With substantial advances made in methods suitable for characterizing SAMs, using scanning tunneling microscopy, atomic force microscopy, optical ellipsometry, X-ray photoelectron spectrometry, reflection absorption infrared spectroscopy, and near-edge X-ray absorption fine structure spectroscopy [85] - [92], the nature of thiol/gold interface has been understood at the qualitative lever with the organization of the thiolates structure and interactions of sulfur-gold bonds. However, in general, the structure of head-groups/metals interface in SAMs systems are still ambiguous [9], especially when replacing gold by other coinage metals, such as silver [83], copper [92], palladium [72] - [74], and platinum [93]. To investigate the origin of headgroups /metals interface, using alternatives to thiol-based monolayers and alternatives metals substrates to gold would be of fundamental interest.

The most promising alternative to thiol based monolayers is organoselenium monolayers. Due to stronger metallic properties and other unique properties, like photovoltaic and photoconductivity of selenium, the substitution of sulfur with selenium can be significant to form a new SAMs based on the different anchor head. Despite their promising utility for a variety of applications [94] - [95], such as in photoresists, photocatalysts, preparation of semiconductor quantum dots, photoinduced electron-transfer systems, and so on, selenol/diselenide monolayers still have not received enough attention. There has been relatively little work studied on selenium based monolayers to build similarly ordered organic monolayers on metals as substitution for sulfur anchor group.

In one of the first organo-selenolate monolayers studies; in 1992, Samant et al [96] provided evidences of a compact selenium based SAMs by using docosaneselenol on gold (111) surfaces; and by employing X-ray scattering experiments, they suggested an incommensurate structure of SAMs with the tilt angle of 15^o and an distortion structure about 3% from ideal hexagonal closely packed layer comparing to the typical $(\sqrt{3} \times \sqrt{3})R30^o$ structure of thiolate based SAMs. Despite of the fact that there are no obvious experimental evidences for comparing Au-Se and Au-S bond strength, they proposed a hypothesis that the thiolate chemisorbs more strongly than the selenolate. This hypothesis may have discouraged other research groups from using organoselenolates to form SAMs. It was not until another organoselenium monolayers studies was carried out by Dishner et al in 1997 that the hypothesis proposed by Samant was challenged by new experimental evidences. By employing STM, Dishner et al [97] revealed that images of well-ordered benzenesenolate SAMs could be obtained while these images of benzenethiolate SAMs cannot. This STM evidence suggested that Au-Se interaction is stronger than Au-S interaction. Furthermore, in order to determine whether selenolates form more robust monolayers than thiolates, Huang et al [98] investigated the adsorptivities and the oxidative stabilities of diphenyl disulfide (DPDS) and diphenyl diselenide (DPDSe) mixed monolayers formed by displacement and competitive adsorption under long term exposure to air and UV radiation. Their results demonstrated a stronger adsorbate-surface interactions and lower surface coverage were observed with selenolates SAMs. They also revealed similar degradation mechanisms of selenolates and thiolates under photo-oxidize upon UV radiation, and suggested that the Se-Se bond is cleaved to form benzeneselenolate upon adsorption, analogous to formation of benzenethiolate monolayers from DPDS.

However, the surface coverage of selenium based monolayers is totally different as shown in the studies of Bandyopadhyay et al [99] employing electrochemical characterization techniques; their results of cyclic voltametric and impedance measurements demonstrated that small aromatic diselenides, such as diphenyl diselenide, can form a self-assembled monolayer with 99% surface coverage on polycrystalline gold similar to disulfides. Furthermore, in the case of using dialkyl diselenide and dialkyl selenide molecules to form SAMs, Shaporenko et al [100] found that didodecyl diselelenide forms densely packed and well-ordered SAMs, while the adsorption of didodecyl selelenide results in the formation of a SAMs with a low packing density and a conformational disorder. Thus, there has been an enormous effort to understand factors for determining surface structure of selenium based monolayers due to many controversial statements about this type of SAMs such as, Se-Se bond cleavage or preserve, multilayers or monolayer formation, stronger or weaker strength bond of Au-Se comparing to Au-S bond.

Recently, a number of complementary experimental and theoretical

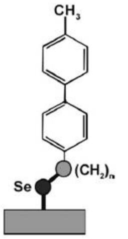

Figure 1.12: Hybrid 4,4-biphenyl-substituted alkaneselenolates

studies has been investigated extensively to clarify controversies related to selenium based SAMs formed on Au(111). Using bis(biphenyl-4-yl) diselenide (BBPDSe) to form biphenyl selenolate (BPSe) SAMs on Au surface, Shaporenko et al [101] showed evidences that the arrangement of the BPSe molecules within every domain deviates from the commensurate $(2\sqrt{3}\times\sqrt{3})R30^o$ structure with an average tilt angle of about 20^o, suggesting the restructuring of the adsorbate-mediated substrate. Moreover, Shaporenko et also investigated related selenolates SAMs systems, hybrid 4,4ω-biphenyl-substituted alkaneselenolates, $CH_3(C_6H_4)_2(CH_2)_nSe-$ (BPnSe, n = 2-6) on Au (Figure 1.12) substrates, and found that the bonding configuration of the selenium head-group is the deciding factor in the balance of structure-building interactions and molecular packing of the alkaneselenolate SAMs. Later, to further gain insight into the odd-even effect in molecular packing of hybrid ω -(4'-methylbiphenyl-4-yl) alkaneselenolates $CH_3(C_6H_4)_2(CH_2)_nSe$ (BPnSe, n = 2-6) SAMs on Au, Cyganik et al [102] (from the same research group with Shaporenko) showed that, for n= even, lower packing density structure with an area per molecule of about 0.260-0.275 nm^2 than that for n = odd which is about $0.216nm^2$, and also demonstrated that their BPnSe SAMs has larger crystalline domains which are typically ca. 30-80nm, about 5 times larger than their thiol analogues. By combining STM experimental data and results of slab-type band-structure calculations, Track et al [103]showed that π - conjugated selenolates SAMs (Figure 1.13) structures exhibit a particular long range and high degree of order, with $(\sqrt{3} \times 4)$ surface unit cell.

In addition to investigations on structure of selenium based SAMs, many research groups also study others properties of this class of SAMs such as electronic properties [104] - [105], behaviors upon exposure to irradiation, and thermal desorption [106] - [107]. However, interestingly, despite the large number of present studies, there was still insufficient evidence to clarify the structure of selenium based SAMs. Therefore, further studies, from both experimental and theoretical surface science, would be required to give a better picture of selenium based SAMs.

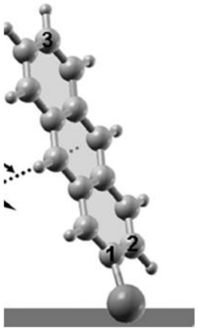

Figure 1.13: π-conjugated selenolates SAMs

References

[1] Horton, M.A.; Khan, A. *Nanomedicine: Nanotechnology, Biology, and Medicine,* **2006**, 2, 42.

[2] Lee, S. J.; Anandan, V.; Zhang, G. *Biosensors Bioelectronics*, **2008**, 23, 1117.

[3] Bourgeois, O.; Skipetrov, S.E.; Ong, F. and Chaussy, J. *Phys. Rev. Lett.* **2005**, 94, 057007.

[4] Feng, X. D.; Sayle, D. C.; Wang, Z. L.; Paras, M. S.; Santora, B.; Sutorik, A. C. *Science* **2006**, 312, 1504.

[5] Sargent, E. H. *Adv. Mater.* **2005**, 17, 515.

[6] Yu, P. K. L.; Wu, M. C. in: 2nd German-American Frontiers of Engineering, **1999**, 8, 10. Irvine, CA, USA.

[7] Binnig, G.; Rohrer, H.; Gerber, C.; Weibel, E. *Phys. Rev. Lett.* **1982**, 49, 57.

[8] Drexler, K. E. Engines of creation: The coming era of nanotechnology, **1986**, Oxford University Press, Oxford.

[9] Love, J. C.; Estroff, L. A.; Kriebel, J. K; Nuzzo, R. G.; Whitesides, G. M. *Chem. Rev.* **2005**, 105, 1103.

[10] Gu, Z.; Fang, J.; Deng, B. *Environ. Sci. Technol.* **2005**, 39, 3833.

[11] Seo, J. W.; Jun, Y. W.; Park, S. W.; Nah, H.; Moon, T.; Park, B. *Angew Chem Int. Ed.* **2007**, 46, 8828; Zijlstra, P.; Chon, J. W. M.; Gu, M.; *Nature* **2009**, 459, 410.

[12] Yoo, P. J.; Nam, K. T.; Qi, J.;Lee , S. K.; Park , J.; Belcher , A. M.; Hammond P. T. *Nature Materials* **2006**, 5, 234; Huang, J. X.; Fan, R.; Connor, S.; Yang, P. *Angew. Chem. Int. Ed.* **2007**, 46, 2414.

[13] Murray, C. B.; Sun, S.; Gaschler, W.; Doyle, H.; Betley, T. A.; Kagan, C. R. *IBM J. Res. Dev.* **2001**, 45, 47.

[14] Ashby, M. F.; Schodek, D. L. *Nanomaterials, Nanotechnologies and Designs*, **2009**, Elsevier Ltd.

[15] Guldi, D. M.; Zilbermann, I.; Anderson, G. A.; Kotov, N. A.; Tagmatarchis, N.; Prato, M. *J. Am. Chem. Soc.*, **2004**, 126, 14340.

[16] Gindulyte, A.; Lipscomb, W. N.; Massa, L. *Inorg. Chem.* **1998**, 37, 6544.

[17] Ulman, A. An introduction to Ultra-thin Film from Langmuir Blodgett to Self-Assembly **1991**, Academic Press, Inc.: New York.

[18] Ulman, A. *Acc. Chem. Res.*, **2001**, 34, 855; Ajayan, P. M.; Ebbesen, T. W. *Rep. Prog. Phys.* **1997**, 60, 1025; Chen, W.; Chen, S.; Ding, F.; Wang, H.: Brown, L. E.; Konopelski, J. P. *J. Am. Chem. Soc.* **2008**, 130, 12156.

[19] Ulman. A. Self-Assembled Monolayers of Thiols. Thin Films **1998**, Vol. 24. San Diego, CA, Academic.

[20] Laibinis, P. E.; Whitesides. G. M. *J. Am. Chem Soc.* **1992**, 114, 9022.

[21] Xia, Y. N.; Whitesides, G. M. *Annu. Rev. Mater Sci.*, **1998**, 28, 153-184; Xia, Y. N.; Rogers, J. A.; Paul, K. E.; Whitesides, G. M. *Chem. Rev.* **1999**, 99, 1823.

[22] Plant, A. L. *Langmuir*, **1999**, 15, 5128.

[23] Adamson, A. W.; Gast, A. P. *Physical Chemistry of Surfaces*, 6th ed.; **1997**, Wiley-Interscience: New York.

[24] Nuzzo, R. G.; Allara, D. L. *J. Am. Chem. Soc.* **1983**, 105, 4481.

[25] Fenter, P.; Eberhardt, A.; Eisenberger, P. *Science* **1994**, 266, 1214.

[26] Allara, D. L.; Nuzzo, R. G. German Patent 1983-3322009, 1983; *Chem. Abstr.* **1984**, 100, 107883.

[27] George, M. A.; Glaunsinger, W. S.; Thundat, T.; Lindsay, S. M. *Thin Solid Films* **1990**, 189, 59.

[28] Hasan, M.; Bethell, D.; Brust, M. *J. Am. Chem. Soc.* **2002**, 124, 1132.

[29] Hou, Z.; Dante, S.; Abbott, N. L.; Stroeve, P. *Langmuir* **1999**, 15, 3011.

[30] Bain, C. D.; Whitesides, G. M. *Adv. Mater.* **1989**, 28, 506.

[31] Widrig, C.; Chung, C.; Porter, M. *J. Electroanal. Chem.* **1991**, 310, 335.

[32] Ulman, A. *Chem. Rev.* **1996**, 96, 1533.

[33] Bain, C. D.; Beibuyck, H. A.; Whitesides, G. M. *Langmuir* **1989**, 5, 723.

[34] Widrig, C. A.; Chung, C.; Porter, M. D., *J. Electroanal. Chem.* **1991**, 310, 335.

[35] Nuzzo, R. G.; Dubois, L. H.; Allara, D. L. *J. Am. Chem. Soc.* **1990**, 112, 558.

[36] Li, Y.; Huang, J.; McIver, R. T., Jr.; Hemminger, J. C. *J. Am. Chem. Soc.* **1992**, 114, 2428.

[37] Bain, C. D.; Troughton, E. B.; Tao, Y-T.; Evall, J.; Whitesides, G. M.; Nuzzo, R. G. *J. Am. Chem. Soc.* **1989**, 111, 321.

[38] Thomas, R. C.; Sun, L.; Crooks, R. M.; Ricco, A. J. *Langmuir* **1991**, 7, 620.

[39] DeBono, R. F.; Loucks, G. D.; Manna, D. D.; Krull, Can. U. J. *J. Chem.* **1996**, 74, 677.

[40] Karpovich, D. S.; Blanchard, G. J. *Langmuir* **1994**, 10, 3315.

[41] Buck, M.; Eisert, F.; Fischer, J.; Grunze, M.; Trager, F. *Appl Phys A* **1991**, 53, 552.

[42] Hahner, G.; Wll, C.; Buck, M.; Grunze, M. *Langmuir* **1993**, 9, 1955.

[43] Berkovic G.; Shvartsberg, E. *Appl. Phys. B* **1991**, 53, 333.

[44] Buck, M.; Eisert, F.; Fischer, J.; Grunze, M.; Trager, F. J. Vac. *Sci. Technol. A* **1992**, 10, 926.

[45] Truong, K. D.; Rowntree, P. A. *J. Phys. Chem.* **1996**, 100, 19917.

[46] Yamada, R.; Uosaki, K. *Langmuir* **1998**, 14, 855.

[47] Poirier, G. E. *Langmuir* **1999**, 15, 1167

[48] Dubois, L. H.; Nuzzo, R. G. *Annu. Rev. Phys. Chem.* **1992**, 43, 437.

[49] Camillone III, N.; Leung, T. Y. B.; Schwartz, P.; Eisenberger, P.; Scoles, G. *Langmuir* **1996**, 12, 2737.

[50] Schwartz, P.; Schreiber, F.; Eisenberger P.; Scoles, G. *Surf. Sci.* **1999**, 423, 208.

[51] Hiner, G.; Kinzler, M.; Thiimmler, C. Ch.; Grunze, M. *J. Vacuum Sci. Technol. A* **1992,** 10, 2758.

[52] Laibinis, P. E.; Whitesides, G. M.; Allara, D. L.; Tao, Y. T.; Parikh, A. N.; Nuzzo, R. G. *J. Am. Chem. Soc* **1991**, 113, 7152.

[53] Bryant, M. A.; Pemberton, J. E. *J. Am. Chem. Soc.* **1991**, 113, 3629.

[54] Duwez, A. S. ; Di Paolo, S.; Ghijsens, J.; Riga, J.; Deleuze M., Delhalle, J. *J. Phys. Chem. B* **1997**,101, 884.

[55] Ulman, A.; Eilers, J. E.; Tillman, N. *Langmuir* **1989**, 5, 1147.

[56] Abrahamsson, S.; Dahldn, B.; Lofgren, H.; Pascher, I. *Prog. Chem. Fats Other Lipids* **1978**, 16, 125.

[57] Poirier, G. E. *Chem. Rev.* **1997**, 97, 1117.

[58] Nuzzo, R. G.; Allara, D. L. *J. Am. Chem. Soc.* **1983**, 105, 4481.

[59] Garg, N., and Lee, T. R. *Langmuir.***1998**, 14, 3815.

[60] Garg, N.; Carrasquillo-Molina, E.; Lee, T. R. Langmuir 2002, 18,. 2717-2726

[61] Colorado, R., Jr.; Villazana, R. J.; Lee, T. R. *Langmuir* **1998**, 14, 6337.

[62] Shon, Y. S.; Colorado Jr., R.; Williams, C. T.; Bain, C. D.; Lee, T. R. *Langmuir* **2000**, 16,. 541-548

[63] Shon, Y.S.; Lee, S.; Colorado, R.; Perry, S. S.; Lee, T. R. *J. Am. Chem. Soc.* **2000**, 122, 7556-7563.

[64] Wang, W., Zhang,S., Chinwangso,P., Advincula,R.C. and Lee, T. R. *J. Phys. Chem. C* **2009**, 113, 3717.

[65] Shon, Y. S.; Lee, T. R. *J. Phys. Chem. B* **2000**, 104, 8192-8200.

[66] Shon, Y. S.; Lee, T. R. *J. Phys. Chem. B* **2000**, 104, 8182-8191

[67] Lee, T. C.; Hounihan,D. J.; Colorado, R.; Park, J. S.; Lee, T. R. *J. Phys. Chem. B* 108 **2004** 2648-2653.

[68] Garg, N.; Friedman, J. M.; Lee, T. R. *Langmuir* **2000**,16, 4266-4271.

[69] Park, J. S.; Vo, A. N.; Barriet, D.; Shon, Y. S.; Lee, T. R. *Langmuir* **2005**,. 21, 2902-2911

[70] Park, J. S.; Smith, A. C.; Lee, T. R. *Langmuir* **2004**, 20, 5829.

[71] Weinstein, R. D.; Richards, J. *Langmuir* **2007**, 23, 2887.

[72] Love, J. C.; Wolfe, D. B.; Chabinyc, M. L.; Paul, K. E.; Whitesides; G. M. *J. Am. Chem. Soc.* **2002**, 124, 1576.

[73] Love, J. C.; Urbach, A. R.; Prentiss, M. G.; Whitesides, G. M. *J. Am. Chem. Soc.* **2003**, 125, 2597.

[74] John, N. S., Thomas, P. J., and Kulkarni, G. U *J. Phys. Chem. B* **2003**, 107, 11376.

[75] James A. W. and Christopher B. G., *J. Phys. Chem. C*, **2007**, 111, 12804-12810.

[76] Jiang, X., Bruzewicz, D. A., Thant, M. M. and Whitesides, G. M., *Anal. Chem.*, **2004**, 76, 6116-6121.

[77] Dhanak, V.R. ; Shard A.G.; Cowie, B.C.C.; Santoni, A., *Surface Science* **1998** 410, 321.

[78] Bmermann,J.;Huck, M.; Rauch, T.; Speller, S.; Heiland, W. **Surf., Sci. 1996** S.849-854, 357.

[79] Maca,F.; Scheffler, M.; Berndt, W. *Surf. Sci.* **1985** 160 467.

[80] Laibinis P. E. , Whitesides G. M.,Allara D. L.,Tao Y. T.,Parikh A. N.,Nuzzo R. G., *J. Am. Chem. Soc,* **1991**, 113, 7152.

[81] Hans A. B.,Whitesides G. M., *Langmuir,* **1993**, 9 (7),1766.

[82] Hahner, G.; W611, Ch.; Buck, M.; Grunze, M *Langmuir*, **1993**, 9, 1955.

[83] Laibinis, P. E.; Whitesides, G. M.; Allara, D. L.; Tao, Y. T.; Parikh, A. N.; Nuzzo, R. G. *J. Am. Chem. Soc.* **1991**, 113, 7152.

[84] Carro,P.; Corthey, G.; Rubert, A. A.; Benitez, G. A.; Fonticelli, M. H.; Salvarezza, M. H. *Langmuir* **2010**, 26, 14655.

[85] Castner, D. G.; Hinds, K.; Grainger, D. W, *Langmuir*, **1996**, 12 (21), 5083.

[86] Noh, J.; Kato, H. S.; Kawai, M. and Hara, M. *J. Phys. Chem. B*, **2002**, 106 (51), 13268.

[87] Yamada, R. and Uosaki, K. , *Langmuir*, **1998**, 14, 855.

[88] Hiner,G.; Kinzler, M.; Thiimmler, C.; W611, Ch. and Grunze, M. *J. Vacuum Sci. Technol. A*, **1992**, 10, 2758.

[89] Prato, M.;Moroni, R.; Bisio, F.; Rolandi, R.; Mattera,L.; Cavalleri, O. and Canepa, M. *J. Phys. Chem. C*, 2008, 112 (10), 3899.

[90] Jennings, G. K. , Tseh-Hwan Y,, Jeffrey C. M,, and Laibinis P. E. , *J. Am. Chem. Soc.*, **2003**, 125 (10), 2950.

[91] Li, Z.; Chang, S. C.; Williams, S. R. *Langmuir*, **2003**, 19 (17), 6744.

[92] Waitkins, G. R., Bearse, A. E., Shutt, R., *Ind. Eng. Chem.*, **1942**, 34 (8), 899.

[93] Ellis, A. B.; Kaiser, S. W.; Wrighton, M. S. *J. Am. Chem. Soc.*, 1976, 98 (22), 6855.

[94] Reinerth, W. A.; Burgin, T. P.; Dunbar, T. D.; Bumm, L. A.; Arnold, J. J.; Jackiw, J. J.; Zhou, C.; Deshpande, M. R.; Allara, D. L.; Weiss, P. S.; Reed, M. A.; Tour, J. M. *Polym. Mater. Sci. Eng.* **1998**, 78, 178.

[95] Pandey, G.; Poleshwar Rao, K. S. S. *Angew. Chem., Int. Ed. Engl.* **1995**, 34, 2669.

[96] Samant, M. G.; Brown, C. A.; Gordon, J. G., II. *Langmuir* **1992**, 8, 1615.

[97] Dishner, M. H.; Hemminger, J. C.; Feher, F. J. *Langmuir* **1997**, 13, 4788-4790.

[98] Huang, F. K.; Horton, R. C., Jr.; Myles, D. C.; Garrell, R. L. *Langmuir* **1998**, 14, 4802.

[99] Krisanu Bandyopadhyay and K. Vijayamohanan, *Langmuir* **1998**, 14, 625.

[100] Shaporenko, A.; Ulman, A.; Terfort, A.; Zharnikov, M., *J. Phys. Chem. B* **2005**, 109, 3898.

[101] Shaporenko, A.; Cyganik, P.; Buck, M.; Terfort, A.; Zharnikov, M *J. Phys. Chem. B* **2005**, 109, 13630-13638

[102] Cyganik, P.; Szelagowska-Kunstman, K.; Terfort, A.; Zharnikov,. M. *J. Phys. Chem. C* **2008**, 112, 15466

[103] Track, A. M.; Rissner, F.; Heimel, G.; Romaner, L.; Kafer, D.; Bashir, A.; Rangger,G. M.; Hofmann, O. T.; Bucko, T.; Witte, G.; and Zojer, E. *J. Phys. Chem. C* **2010**, 114, 2677

[104] Monnell, J. D.; Stapleton, J. J.; Dirk, S. M.; Reinerth, W. A.; Tour, J. M.; Allara, D. L.;. Weiss, P. S., *J. Phys. Chem. B*, **2005**, 109, 20343.

[105] Llave, E.; Scherlis D. A. *Langmuir* **2010**, 26, 173

[106] K fer, D., Bashir, A. and Witte, G. *J. Phys. Chem. C* **2007**, 111, 10546

[107] Weidner, T.; Shaporenko, A.; Ballav, N.;Ulman, A.; and Zharnikov, M. *J. Phys. Chem. C* **2008**, 112, 1191.

Part II Hydrogen Storage Materials

1.5 Hydrogen storage introduction

Petroleum dependence, especially in the transportation field, over the world leads human to many undesirable issues such as, the rapid depletion of hydrocarbon fuel resources, the environmental pollution impact of fuels consumption, the serious geopolitical tension among countries for the demand of fossil resources [1] - [3]. For long term, alternative energy sources to substitute the fossil fuels need to be developed. With its much higher energy density (143MJ/kg, or 40kWh/kg) comparison to gasoline fuels (46.4MJ/Kg), hydrogen becomes one of the most promising alternatives to replace petroleum [4]. Hydrogen exists as a ubiquitous, clean, and reproducible energy carrier which can be produce directly from water or other organic compounds by systems analogous to photovoltaics; and as employed in combustion engine, its emitted gas is only water which offers no pollutants, other toxics gas and carbon dioxide. Moreover, hydrogen can be used to combine with oxygen in the fuel cell to generate electricity [3] - [6].

To efficiently employ hydrogen as energy carrier, however, many challenges related to storage and transport hydrogen need to be addressed [5]. There are many great efforts from both engineering and science fields to solve this obstacle, including using physical compressed tanks [7], designing new hydrogen storage materials [8](like MOF, metal hydride) and etc. In the narrow scope of this chapter, we only review several popular trends for storage hydrogen goal.

1.5.1 High pressure and cryogenic vessels for hydrogen storage

The major used methods for hydrogen storage are limited to compressed gas and liquefaction; which are now still being applied to many transportation vehicles [5]. Compressed hydrogen gas technique has unavoidable drawbacks; for example even at the highest practical pressure ∼80 MPa, the volumetric density of compress gas is still very low ($\sim 40kgH_2/m^3$) [9]. As compared to gasoline (31.6 MJ/L) which is also compressed at the same pressure ∼70 MPa, the energy density of compressed hydrogen gas is much lower (4.4MJ/L). Moreover the safety concerns with using high pressure compressed hydrogen gas cannot be neglected. Although advances in the material science are employed to fabricate new material with high physical strength like carbon fiber-reinforced composite which allow forming higher pressure tanks; other challenges such as the cost of vessels and pressurization process, limit of high pressure, refueling time and etc, are also need to be considered [10].

Using cryogenic hydrogen tanks is also another approach for hydrogen storage; in principle, liquid hydrogen tanks can store almost twice as high storage capacity by volume as pressurized hydrogen tanks [5]. Even with its double volumetric capacity (0.070 kg/L) comparing to compressed hydrogen techniques (0.039 kg/L at 700bar); the cryogenic hydrogen storage technique is still lower than the requirement of DOE technical target (Table 1.1) [10] for on board hydrogen storage systems. Moreover, the key challenges with liquid hydrogen storage are a big cost of liquefaction, the handling of cryogenic liquids, thermal insulation, boil-off loss and similar problems with compressed hydrogen gas such as safety concerns, refilling time and etc.

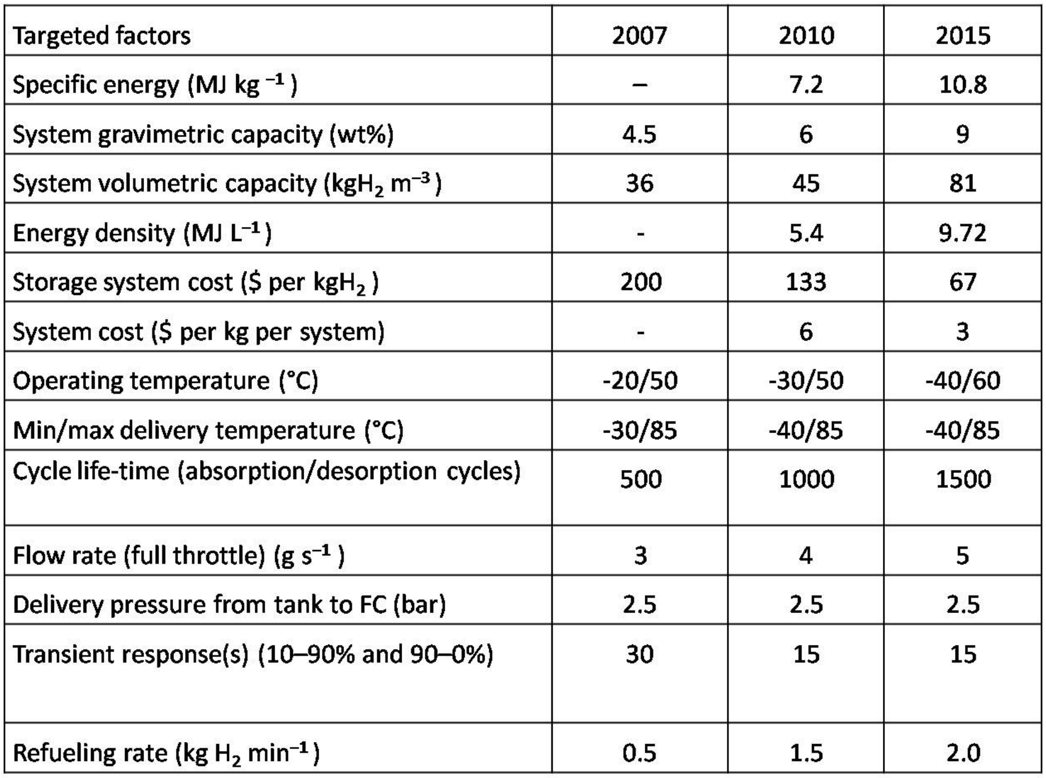

Targeted factors	2007	2010	2015
Specific energy (MJ kg $^{-1}$)	–	7.2	10.8
System gravimetric capacity (wt%)	4.5	6	9
System volumetric capacity (kgH$_2$ m^{-3})	36	45	81
Energy density (MJ L^{-1})	-	5.4	9.72
Storage system cost ($ per kgH$_2$)	200	133	67
System cost ($ per kg per system)	-	6	3
Operating temperature (°C)	-20/50	-30/50	-40/60
Min/max delivery temperature (°C)	-30/85	-40/85	-40/85
Cycle life-time (absorption/desorption cycles)	500	1000	1500
Flow rate (full throttle) (g s^{-1})	3	4	5
Delivery pressure from tank to FC (bar)	2.5	2.5	2.5
Transient response(s) (10–90% and 90–0%)	30	15	15
Refueling rate (kg H$_2$ min^{-1})	0.5	1.5	2.0

Table 1.1: DOE technical hydrogen storage targets for automotive

1.5.2 Hydrogen storage materials

Carbon based materials

Even the fact that the interactions between hydrogen molecules are relatively weak, and only become importance at the critical temperature of hydrogen (33.25K); the weak Van der Waals interactions of hydrogen and absorbent molecules, however, take the major role to keep hydrogen physisorped within porous materials at low temperatures which are usually near cryogenic temperature 77K [11]. Depended on the types of absorbent was used, the heat of adsorption can vary from 4-10kj/molH_2 [11] - [13]. These binding energies of hydrogen and surface atoms of absorbents based on Van der Waals forces are relatively lower than the 10-50 kJ/mol range [14] - [16], which is proposed by many calculations as the ideal enthapy for reversible hydrogen storage at room temperature operation.

Narrow single wall nanotubes [17] was proclaimed as the ideal candidate for hydrogen storage due to its high hydrogen adsorption capacities up to 10 wt% (even at ambient temperature), based on the condensation of hydrogen inside pores of these materials. Many experiments were performed to re-measure gravimetric and volumetric capacity of these materials, but no studies could reproduce these spectacular high uptake capacities. Lee et al [18] investigations on single wall nanotubes for hydrogen storage showed that the hydrogen uptake capacity only less than 1% at 80bar at room temperature; this number was extremely lower than the proposed capacity mentioned above. Miyamato et al [19] also employed single wall nanotubes for cryogenic hydrogen physisorption, but the result did not show any better on the hydrogen capacity, 0.54wt% at 77K, 0.05MPa, (even an optimistic linear extrapolation for 80bar will have 4%wt) compared to the DOE targets.

With great advances in computational studies, many theoretical calculations have predicted even higher hydrogen uptakes for metal-doped carbon-based materials. By using DFT calculations, Froudakis et al [20] suggested the formation of Ti- and Sc-coated CNTs and fullerenes which was also predicted to exhibit high hydrogen storage capacities up to 8 wt% with a binding energy of about 0.5 eV/H_2 molecule. In a hypothetical molecule (Figure 1.14) designed by Zhao et al [21] computational studies, organoscandium bulkyballs $C_{60}[ScH_2]_{12}$ was proposed to have the uptake of 7.0 wt%, hydrogen with the suitable binding energy of hydrogen molecules range within 0.3-0.4 eV for ambient temperature applications.

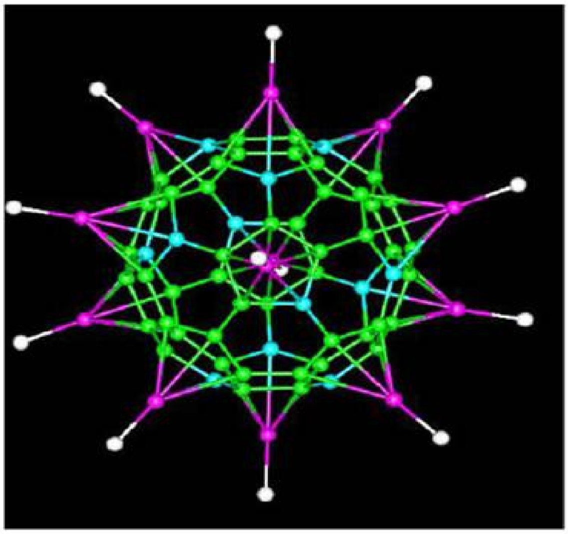

Figure 1.14: Organoscandium bulkyballs $C_{60}[ScH_2]_{12}$ designed by Zhao calculations.

However, now it is not easy to fabricate metals into carbon based materials due to the fact that the vapor deposition technique only yield metal doped on the outside surface of materials, not in the pores which attribute to the large portion of surface area of substrate materials [22]. The formation of metal clusters on the modified materials also effect on the number of expectedly active metal sites for hydrogen binding. The ideal scenery for these metal doped materials to be capable for hydrogen storage are metal centers existing on the nanotube surface in the atomic form and not as clusters in order to maximize the available binding sites for hydrogen adsorption.

Metal-organic frameworks

With especially high surface areas and large micropore volumes, MOFs have been considered as very promising hydrogen storage materials, particularly for physisorption processes. Not long after the first report about gas adsorption behavior of MOFs by Kitagawa et al [23] in 1997; Yaghi et al [24] employed MOF-5, which had extraordinarily high surface area of 2,500-4,000 m^2/g, as H_2 storage materials. And hydrogen absorption measurements of MOF-5 showed very interesting results, with up to 4.5wt% at 78K, 0.8 bar and 1wt% at 298K, 20bar. Another strikingly result with a storage hydrogen capacity of 7.5 wt% at 7 MPa and 77 K from O. M. Yaghi et al groups for MOF-177 [25] - [26], having an estimated Langmuir surface area of 4500 m^2/g, really have ignited return of interest in hydrogen storage based on physisorption.

However, the potential for hydrogen storage at room temperature of most MOF materials may be not as great as they show in the cryogenic temperature. The adsorption capacities of these materials are relatively low at room temperature, with only 0-1.0 wt% [27] - [28].

Metal hydrides

Until now, no hydrogen physisorption based materials can compete with chemical and metal hydrides for gravimetric storage density on a materials basis. For example, borohydrides [29] have significant storage capacities, up to 19% of the mass of the molecule for $LiBH_4$; and ammonia (NH_3) is also high-capacity storage medium with 17 wt% hydrogen. However, the challenges for practical hydrogen storage are their high decomposition temperatures and large activation barriers to rehydrogenation [30] - [32].

One of promising systems, which still has been employed for hydrogen storage, is sodium alanate (NaAlH4) [33], with its theorical reversible hydrogen content 5.5 wt%, although in practice only about 5 wt% capacity has been reported so far. This material releases hydrogen through two decomposition steps (Equation 1.2.1) [34]. The decomposition temperatures for the first and second steps at 0.1MPa are 30^oC and 100^oC, respectively. Obviously, the temperature range required for desorption of this material is not far away from the $60-80^oC$ range targeted by the US DOE (Table 1.1), comparing to other conventional metal hydrides. Even with its acceptable gravimetric storage capacity and favourable thermodynamics, however, sodium alanate has a very severe obstacle with re-hydrogenationon processes, which require temperatures of $200-400^oC$ and pressures of 10-40 MPa [35].

$$3NaAlH_4 \rightarrow Na_3AlH_6 + 2Al + 3H_2 \tag{1.2}$$

$$Na_3AlH_6 \rightarrow 3NaH + Al + 1.5H_2 \tag{1.3}$$

Furthermore there are many other reasons prevent metal hydrides from being applied for on board applications, for example infrastructure implications, the storage of the waste material on-board, recycling and energy issues, operation conditions; it is quite possible that more research could improve hydride based materials properties even further [36] - [40].

1.6 Kubas hydrogen storage materials

In 2010, Yakobson, a Rice University theoretical physicist, suggested that a new class of hydrogen storage materials, known as metallacarborane, could store amount of hydrogen equal or greater than the 2015 target of DOE; this great new brought back inspirations to many hydrogen storage researchers for developing metallacarborane (Figure 1.15) which is mainly composed by boron, carbon and metal atoms in a cage like structure Yakobson [41] claimed that the adsorption of hydrogen to metal center of metallacarborane is based on the Kubas interactions. Despite the fact that when Yakobson et al calculations proposed a new class of hydrogen storage based on Kubas type materials, it attracted considerable attentions of hydrogen storage scientists, but actually before Yakobson; there were several computational and experiment studies investigating Kubas type materials by employing other different structures, such as, computational studies of Zhao et al with organoscandium bulkyball using Sc(0) [21], of Kim et al with B and Be doped small carbon nanostructures [42], and experimental studies of Hoang et al with V and Cr doped mesoporous silica [43] and of Hu et al with microporous titanium oxides [44].

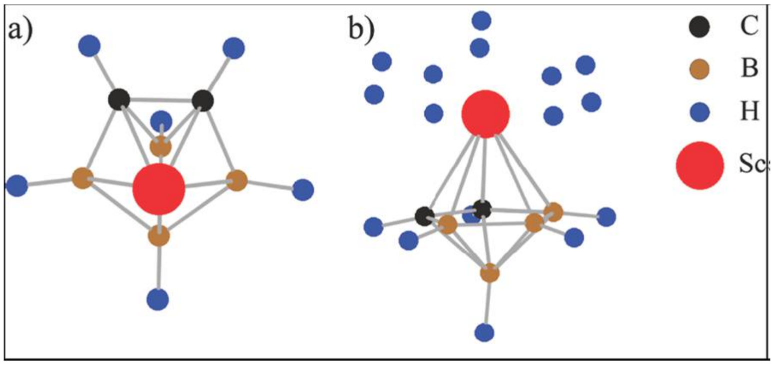

Figure 1.15: Proposed structures of Yakobson about metallacarborane materials (a) $C_2B_4H_6Sc$ and (b) fully hydrogen saturated $C_2B_4H_6Sc - 5H_2$

As mentioned in Yakobson calculations, Kubas interactions allows for reversible storage of hydrogen in ambient conditions that would make Kubas type materials highly attractive for hydrogen storage applications. Although hydrogen storage applications of kubas type materials have only began recently; Kubas interactions were discovered through the isolation of the first dihydrogen complex (Figure 1.16) by Kubas et al in 1984 [45]. The bonding of hydrogen in Kubas complexes has been described totally different from classical dihydrogen complexes (Figure 1.17) [46]. Kubas bonding model for dihydrogen complexes was presented in Figure 1.18. In Kubas interaction, the H-H σ orbital binds to an empty d orbital of metal center via electron density donations [47]; and this interaction is also augmented by the back donation from filled d orbitals of metal center and form a stable dihydrogen complex. The binding strength of Kubas interactions, which is in the middle of strong

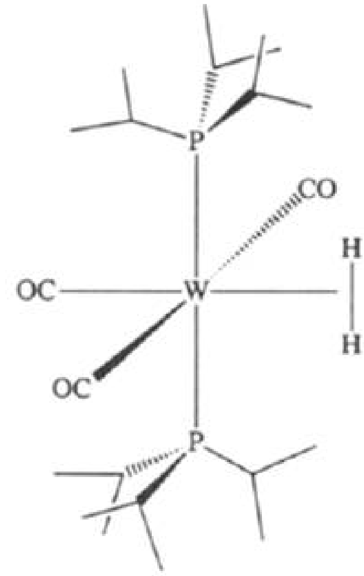

Figure 1.16: Structure of $[W(\eta^2 - H_2)(CO)_3(P - i - \mathrm{Pr}_3)_2]$ the first dihydrogen complex

hydrides chemisorption and weak van der Waals physisorption, would be ideal kind of binding for reversible hydrogen storage systems operating at ambient conditions.

Figure 1.17: Dihydrogen and classical dihidrides complex

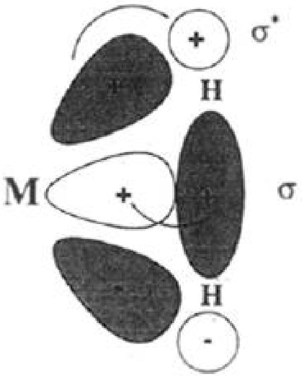

Figure 1.18: Bonding model in transition metal dihydrogen complex

References

[1] Winter, C. J. & Nitsch, *J. Hydrogen as an Energy Carrier*: Technologies, Systems, Economy (Springer, **1988**).

[2] Fichtner, M. *Adv. Eng. Mater.* 2005, 7, 443.

[3] Berry, G. D.; Aceves, S. M. *Energy & Fuels.* **1998**, 12, 49.

[4] Bain, A. and Van Vorst, W. D. Int. *J. Hydrogen Energy* **1999**, 24, 399.

[5] Schlapbach, L.; Zuttel, A. *Nature* **2001**, 414, 353-358.

[6] Yildiz, B.; Kazimi, M. S. *Int. J. Hydrogen Ener.* **2006**, 31, 77.

[7] Bockris, J. O. M. *Int. J. Hydrogen Ener.* **2007**, 32 153.

[8] Turner,J. A.; Williams, M. C.; Rajeshwar, K. *The Electrochem. Soc. Interface 13* **2004**, 3, 24.

[9] Sandi, G. *The Electrochem. Soc. Interface 13* **2004**, 3, 40.

[10] DOE Office of Energy Efficiency and Renewable Energy Hydrogen, Fuel Cells & Infrastructure Technologies Program Multi-Year Research, Development and Demonstration

Plan(http://www.eere.energy.gov/hydrogenandfuelcells/mypp), Millennium Cell Project Report, FY2005 Annual Progress Report for the DOE Hydrogen Program, November **2005**, available at: http://www.hydrogen.energy.gov/annual−progress05−storage.html.

[11] Heine, T.; Zhechkov, L.; Seifert, G. *Phys. Chem. Chem. Phys.* , **2004**, 6, 980.

[12] Nijkamp, M. G.; Raaymakers, J. E. M. J.; Van Dillen, A. J.; De Jong, K. P. *Appl. Phys. A* , **2001**, 72, 619.

[13] Strobel, R.; Garche, J.; Moseley, P. T.; Jorissen, L., Wolf, G. *J. Power Sources* , **2006**, 159, 781 − 801

[14] Dinca, M.; Long, J. R. *Angew. Chem. Int. Ed.* **2008**, 47, 6766.

[15] Yildirim, T.; Ciraci, S. *Phys. Rev. Lett.* **2005**, 94, 175501.

[16] Bhatia, S. K.; Myers, A. L. *Langmuir*, **2006**, 22, 1688.

[17] Becher, M.; Haluska, M.; Hirscher, M.; Quintel, A.; Skakalova, V.; Detlaff−Weglikowska, U.; Chen, X., Hulman, M.; Choi, Y.; Roth, S.; Meregalli, V.*Physique* , **2003**, 4, 1055.

[18] Lee, S. M.; An, K. H.; Lee Y. H.; Seifert, G.; Frauenheim, T. *J. Am. Chem. Soc.* , 2001, 123, 5059.

[19] Miyamato, J.; Hattori, Y.; Noguchi, D.; Tanaka, H.; Ohba, T.; Utsumi, S.; Kanoh, H.; Kim, Y. A.; Muramatsu, H.; Hayashi, T.; Endo, M.; Kaneko, K. *J. Am. Chem. Soc.* , **2006**, 128, 12636.

[20] Froudakis, G. E. *Nano Lett.* 2001, 1, 531.

[21] Zhao, Y.; Kim, Y.; Dillon, A. C.; Heben, M. J.; Zhang S. B. *Phys. Rev. Lett.* **2005**, 94, 155504.

[22] Homma, Y.; Kobayashi, Y.; Ogino, T.; Takagi, D.; Ito,. R.; Jung. Y. J.; Ajayan, P. M. J. *J. Phys. Chem. B*, **2003**, 107 (44), 12161.

[23] Kondo, M.; Yoshitomi, T.; Seki, K.; Matsuzaka, H.; Kitagawa, S. *Angew. Chem. Int. Ed.* **1997**, 36, 1725.

[24] Rosi, N. L.; Eckert, J.; Eddaoudi, M.; Vodak, D. T.; Kim, J.; OKeeffe, M.; Yaghi, O. M. *Science* **2003**, 300, 1127.

[25] Wong Foy, A. G.; Matzger, A. J. and Yaghi, O. M. *J. Am. Chem. Soc.*, **2006**, 128, 3494.

[26] Chae, H. K.; Siberio Perez, D. Y.; Kim, J.; Go, Y. B.; Eddaoudi, M.; Matzger, A. J.; OKeeffe, M. and Yaghi, O. M. *Nature*, **2004**, 427, 523

[27] Hirscher, M.; Panella, B. *Scripta Mater.* **2007**, 56, 809.

[28] Poirier, E.; Chahine, R.; Benard, P.; Dorval - Douville, G.; Lafi, L.; Chandonia, P. A.; *Langmuir* **2006**, 22, 8784.

[29] Vajo, J. J.; Skeith, S. L. and Mertens, F. *J. Phys. Chem. B*, **2005**, 109, 3719.

[30] Von Helmolt, R. and Eberle, U. *J. Power Sources*, **2007**, 165, 833.

[31] Mamatha, M.; Bogdanovic,B.; Felderhoff, M.; Pommerin, A.; Schmidt, W.; Schu th, F. and Weidenthaler, C. *J. Alloys Compd.*, **2006**, 407, 78.

[32] Bogdanovic, B.; and Schwickardi, M. *J. Alloys Compd.*, **1997**, 253, 1.

[33] Kay, B. D.; Schmid, B.; Shaw, W.; Gutowski, M.; Autrey, T. *Angew. Chem. Int. Ed.* **2005**, 44, 3578.

[34] Ramachandran, P. R. and Gagare P. D.*Inorg. Chem.* **2007**, 46, 7810-7817

[35] Bogdanovic, B. and Schwickardi, M. *J. Alloys Comp.*, **1997**, 253, 1.

[36] Claudy, P.; Bonnetot, B.; Letoffe, J. M. *J. Therm. Anal.*, 1979, 15, 119.

[37] Kim, Y.; Lee, E. K.; Shim, J.H.; Cho, Y. W.; Yoon, K. B. *J. Alloys Compd.*, **2006**, 422, 283.

[38] Bogdanovic, B.; Felderhoff, M.; Pommerin, A.; Schth, F.; Spielkamp, N. *Adv. Mater*, **2006**, 18, 1198.

[39] Matus, M. H.; Anderson, K. D.; Camaioni, D. M.; Autrey, S. T.; Dixon, D. A. *J. Phys. Chem.* **2007**, 111, 4411.

[40] Yoon, C. W.; Sneddon, L. G. *J. Am. Chem. Soc.* **2006**, 128, 13992.

[41] Singh, A. K.; Sadrzadeh, A.; Yakobson, B. I. *J. Am. Chem. Soc.*, **2010**, 132, 14126.

[42] Kim, J. Y.; Frisbie, C. D. *J. Phys. Chem. C,* **2008**, 112, 3515.

[43] Hoang, T. K. A.; Hamaed, A.; Trudeau, M.; Antonelli, D. M. *J. Phys. Chem. C*, **2009**, 113 17240.

[44] Hu, X.; Trudeau, M.; Antonelli, D. M *Chem. Mater.*, **2007**, 19, 1388.

[45] Kubas, G. J.; Ryan, R. R.; Swanson, B. I.; Vergamini, P. J.; Wasserman, H. J. *J. Am. Chem. Soc.*, **1984**, 106, 451.

[46] Kubas, G. J. *Comments Inorg. Chem.* **1988**, 7,. 17

[47] Kubas, G. J. *Acc. Chem. Res.* **1988**, 128, 21120

[48] Yildirim, T.; Ciraci, S., *Phys. Rev. Lett.* **2005**, 94, 175501.

[49] Zhou, W.; Yildirim, T.; Durgun, E.; Ciraci, S. *Phys. Rev. B* **2007**, 76, 085434.

[50] Durgun, E.; Ciraci, S.; Zhou, W.; Yildirim, T. *Phys. Rev. Lett.* **2006**, 97, 226102.

1.7 Scope of the Thesis

1.7.1 Chapter 02 Bidentate and monodentate chelating mixture SAMs on Pd substrates generated from Dialkyldithiophosphinic acids (DTPAs) molecules

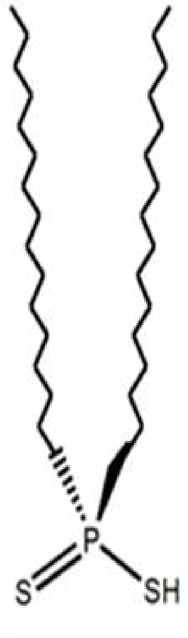

Figure 1.19: Image of DTPA molecules

In chapter 2, we will use a new molecule Dialkyldithiophosphinic (DTPA) to form SAMs on Pd. This molecule (Figure 1.10) has two sulfur available binding sites to interact with the Pd surface through dative bonds. By using this new molecule, we wish to further investigate the binding interface between sulfur head groups and palladium substrates. In this study, we also investigate the formation of DTPA on two different types of Pd surface: "template stripping" Pd films and "as deposited" Pd films. Moreover, we want to provide evidence about using different morphology surfaces to form SAMs also causes effect on charge transfer though alkyl chain through EIS investigation. XPS is also employed to study binding mode of sulfur-palladium bond.

1.7.2 Chapter 03 A new selenide based Self−Assembled Monolayers (SAMs) on Pd film with the homogeneous binding nature at headgroups-metal interface

In chapter 3, we will describe the preparation and characterization of self-assembled monolayers (SAMs) formed by the chemisorption of bis(hexadecyl)-diselenide (BHDS) on surfaces of palladium. We also wish to study the self-assembled monolayers of dialkyl diselenide on palladium subtrates to determine the nature of the interface formed by palladium film and selenium-based SAMs, the optimum conditions to form bis(hexadecyl)diselenide SAMs, and the structural organization of alkane chains in these new monolayers. The focus of this thesis work is on the formation of new types of SAMs including DTPA and dialkyldiselenide on palladium substrates. With major differences in the headgroups with thiolate SAMs, DTPA and dialkyldiselenide SAMs on palladium will probably reveal the interfacial structures of SAMs and other variations in the macroscopic properties. We also investigated the binding behavior of the new SAMs molecules with palladium through XPS experiments.

1.7.3 Chapter 04 Cyclopentadienyl Chromium Hydrazide Materials for hydrogen storage

Intriguing by the Kubas interations between transition metal with hydrogen and by prediction of Yildirim calculations[48] - [50] about an increase in binding enthalpy with increasing hydrogen ligation in Kubas compounds, in chapter 4, we designed new transition metal-based materials with hydrazine used as linker. Cyclopentadienyl Cr hydrazide gels (Figure 1.20) were synthesized from the protonolysis reaction between bis(cyclopentadienyl) Cr and hydrazine. The material is amorphous, contains low valence chromium species and used as substrates for Kubas-type hydrogen storage. These materials have ΔH values that rise from 10-45 kJ/mol and retain 49 % of the adsorption capacity at 298 K relative to 77 K, over three times higher than the best MOFs and amorphous carbons (10-15%).

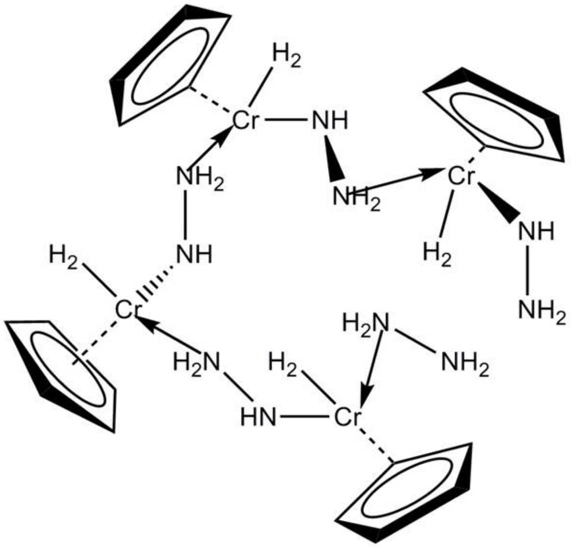

Figure 1.20: Cyclopentadienyl Cr hydrazide gels

Chapter 2

Bidentate and monodentate chelating mixture SAMs on Pd substrates generated from Dialkyldithiophosphinic acids (DTPAs) molecules

2.1 Introduction

Besides the exploitation of adsorbates conformations to generate controlled interfacial properties of SAMs, the morphology of substrates on which a SAM forms also contributes to manipulate the interfacial/surface properties of these materials [1] - [4]. By changing the experimental methods, compositions and conditions to form metal thin films, various types of substrate's surface can be composed with different roughness, grain sizes and defects [5] - [6]. For example, as deposited (As-dep) normally by e-beam deposition, the grains size of thin palladium films formed on silicon wafer are 15-30 nm in diameter; while employing "template stripping (TS) methods [7] (Figure 2.1)" after e-beam deposition can create much smaller grains size <1 nm on palladium surface. The smaller grains size of metal thin film is, the more suitable it is to use as substrate for microcontact printing and etching [8] - [9].

As outline in the previous chapter, chelating thiolate SAMs works from Randall groups and SAMs on palladium surfaces have intrigued us to investigate the structure and properties of new chelating molecules (DTPA) on different types of Pd substrates. In this study, we will describe the SAMs prepared from DTPA molecules (Figure 2.2) through characterization of crystallinity and composition by reflection absorption infra red spectroscopy (RAIRS), wettability by contact angles measurement (CA), thickness and barrier properties by electrochemical impedance spectroscopy (EIS), the morphology of grains on the substrate surface by atomic force microscopy (AFM) and additional

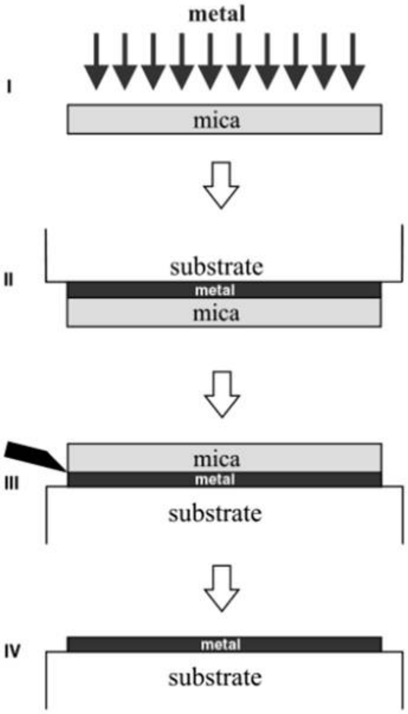

Figure 2.1: Principle of the template-stripping method. (I)The metal is e-beam deposited onto silicon wafer surface in an ultrahigh vacuum. (II) The metal side of the metal-coated silicon is glued to a glass slide or a silicon wafer substrate with epoxy glue. (III) The glass slide is stripped off to leave, ideally, a clean, flat, metal surface (shown in IV)

analysis of the SAMs by X-ray photoelectron spectroscopy (XPS) which is permitted a direct calculation of the packing densities and binding mode of the DTPA SAMs on palladium. We also compare properties of DTPA SAMs with two different Pd substrates (TS and As-dep) and with thiols/Pd SAMs. Our works demonstrate DTPA can forms a relatively stable SAMs on Pd substrates compare to thiol SAMs on Pd and the minor difference in the roughness of two kinds of palladium films doesn't affect much on the macroscopic properties of two DTPA/Pd SAMs.

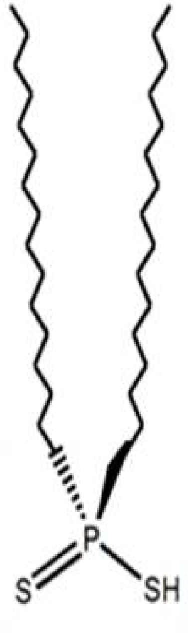

Figure 2.2: Image of DTPA molecules.

2.2 Experimental Section

2.2.1 Materials

All anhydrous solvents were directly obtained from an Innovative Technologies solvent purification system. All commercially available chemicals, unless otherwise stated, were purchased and used as received from Sigma-Aldrich and Alfa-Aesar. All chemicals were stored under appropriate conditions.

2.2.2 Preparation of Pd films

The palladium surfaces were prepared by vapour deposition of 20 ÅCr or Ti (adhesive layer) on silicon wafers, followed by 1000 ÅPd. The deposition of Pd was held with the typical deposition rate 1Å/s. The evaporator pressure was reduced to 5×10^{-6} mbar before the crucible was subjected to e-beam with 10mA of emission current. The thickness of Pd surfaces was monitored during the deposition process using SQC-310 Deposition Controller. The freshly made substrates should be used within 1h after they were taken out of the evaporation chamber to avoid any possible oxidation of Pd films.

2.2.3 Formation of Self-Assembled Monolayers of Dialkyldithiophosphinic acids (DTPAs)

The freshly evaporated Pd substrates were immersed into 2m M solutions of DTPAs in degassed anhydrous ethanol, at room temperature for at least 24 hours to ensure monolayer coverage. During the formation of DTPA SAMs, solutions were stored under nitrogen in sealed scintillation vials (20mL). The treated substrates were rinsed thoroughly with pure ethanol and toluene to remove excess molecules beyond the first layer, and then dried in a stream of nitrogen gas.

2.2.4 Atomic force microscopy (AFM)

AFM measurements of Pd surfaces were determined by contact-mode of a Digital Instruments Multimode atomic force microscope. The typical scan size was $1\mu m \times 1\mu m$

2.2.5 X-ray Photoelectron Spectroscopy (XPS)

The samples were analyzed by XPS using a Kratos Axis Ultra X-ray photoelectron spectrometer using a 60 degree sample tilt (30 degree electron take-off angle). XPS can detect all elements except hydrogen and helium, probes the surface of the sample to a depth of 7-10 nanometres, and has detection limits ranging from 0.1 to 0.5 atomic percent depending on the element. Survey scan (15 sweeps, 120s sweep time) analyses were carried out with an analysis area of 300 x 700 microns and a pass energy of 160 eV. High resolution analyses were carried out with an analysis area of 300 x 700 microns and a pass energy of 20 eV (long runs of $\sim$ 200 scans for S and P).

2.2.6 Reflection Absorption Infrared Spectroscopy (RAIRS)

RAIRs spectra of the monolayers of DTPAs were obtained using a Bruker IFS 66v/S spectrometer equipped with a narrow band liquid nitrogen cooled MCT detector in single reflection mode with an Autoseagull accessory. The incident reflection angle was set at 85^o. Spectra of SAMs were measured on silicon substrates bearing 1000 Åfilms of palladium. The background spectra were collected from a palladium reference taken from the same set of substrates as the samples. Spectra were obtained using 1024 scans at 2 cm^{-1} resolution after evacuating for 2h for each sample. The samples were rinsed in ethanol and dried with a stream of nitrogen gas before the measurements were taken.

The baselines of the spectra were corrected using 75 iterations for each.

2.2.7 Contact Angle Goniometry

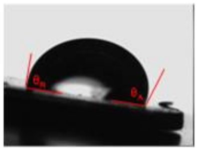

Figure 2.3: Advancing and receding contact angles measurements

Contact angles were measured with a Ram-Hart contact angle goniometer equipped with a microlitre syringe. ACS reagent-grade water was purchased from Sigma-Aldrich. The static water contact angles were measured on both sides of 5 μL drops placed on at least three different areas of the sample. The dynamic hexadecane and water contact angles were measured by placing a 5 μL drop on the surface, to which the contact angle is measured as the instrument is tilted for every 5^o tilting increment until a maximum advancing contact angle is measured (just before the drop moves). The side of the drop on the lower portion will give the advancing contact angle and the side of the drop on the higher portion will give the receding contact angle (Figure 2.3).

2.2.8 Electrochemical Impedance Spectroscopy (EIS)

EIS was performed using a BAS-Zahner IM6 ex impedance unit. The saturated calomel electrode was used as reference electrode, and courter electrode was a 1.0mm-diameter Pt wire (purchased from Sigma-Aldrich). Solutions of

1mM $K_4Fe(CN)_6$, 1mM $K_3Fe(CN)_6 \cdot 3H_2O$ and 100 mM Na_2SO_4 in distilled water was used as electrolyte solution. The working electrode in contact with the aqueous solution was a confined circle with an area of 1 cm^2. The measurements were made at an open circuit potential set at ~450 mV with a 10 mV ac perturbation that was controlled from 5×10^{-2} to 1.6×10^4.

Simple SAMs systems which are usually under charge transfer on the homogeneous surfaces can be described by the simple equivalent circuit[10] in Figure 2.4. C_{SAM} and R_{SAM} are the capacitance and the resistance of the SAMs; and R_{SAM} is inversely proportional to the current density which is applied between SAM-containing electrode and platinum wire counter electrode. All other resistances in this simple system, such as the electrolyte resistance, cable resistances, etc. are combined in $R_{Solution}$, the solution resistance term. Obviously, this simple equivalent circuit allows the establishment of the correlations between electrochemical system parameters and characteristic impedance elements.

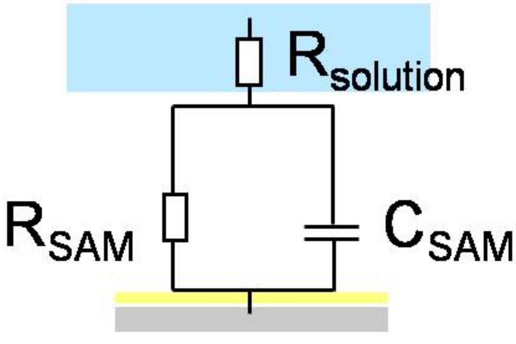

Figure 2.4: Simple equivalent circuits

The impedance modulus Z ($j\omega$) for the simple equivalent circuit in Figure 2.4 can be expressed as a function of frequency f in Equation 2.1.

$$Z\left(j\omega\right) = R_{solution} + R_{SAM}/(1 + j\omega C_{SAM}R_{SAM}) \tag{2.1}$$

A number of different methods are proposed by Mansfeld[11]-[12] et al for displaying the experimentally determined complex impedance $Z\left(j\omega\right) = Z^{'} + jZ^{''}$. The capacitance of the interface can be obtained from the frequency f_{max} of the maximum of the imaginary impedance $Z^{''}$ and R_{SAM} as following equation:

$$C_{SAM} = 1/2\pi f_{max}R_{SAM} \tag{2.2}$$

The values of $R_{Solution}$ and R_{SAM} can be determined from the high and low frequency limits of the measured impedance spectra, respectively:

$$R_{solution} = \lim_{f\to\infty}\left|Z\right| \tag{2.3}$$

$$R_{solution} + R_{SAM} = \lim_{f\to 0}\left|Z\right| \tag{2.4}$$

2.3 Results and discussion

2.3.1 AFM results

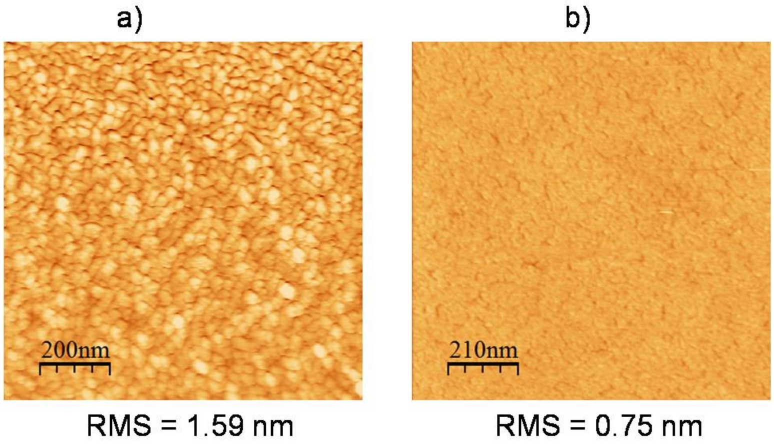

Figure 2.5: AFM images of (a) As-deposited Pd film and (b) Template stripped Pd film. These images of palladium films (100 nm thick) have range of z-scale 10 nm for as-deposited films and z-scale 5 nm for template stripped films.

Upon investigation of the template-stripped and as-deposited palladium film samples by means of AFM, it was found that the surface of the template-stripped samples was rather less step edge defects and smaller roughness (RMS = 0.75nm) compare to the surface of as-deposited samples (RMS = 1.59nm).As our AFM data about grain size of as-deposited (15 - 30 nm) and template stripped (100-150 nm), the surface of template-stripped Pd films was atomically flat over large areas with minor amount of holes comparing to that of as-deposited palladium films which had clearly visible great number of peak and valley regions. With the morphology difference between these two prepared surfaces of Pd substrates, we expect to govern the interactions between head groups of DTPA and Pd surfaces. XPS experiments were applied to investigate the binding mode and composition of interface between Pd substrates and monolayer formed by DTPA molecules.

2.3.2 XPS results

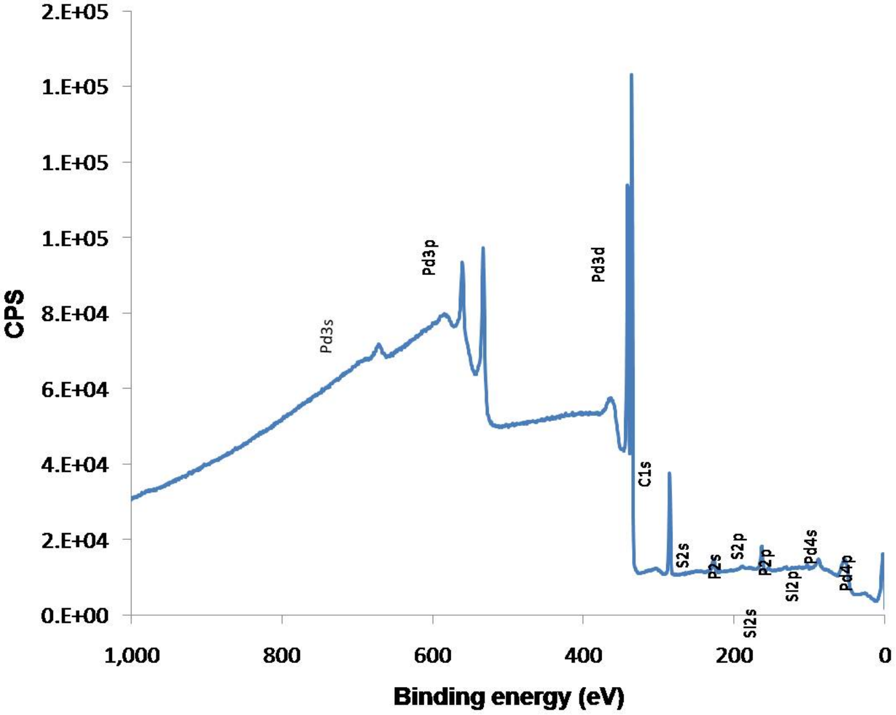

Figure 2.6: XPS survey scan of $(C_{16})_2DTPA$ SAMs on as-deposited Pd film.

XPS survey scan of $(C_{16})_2DTPA$ SAMs on the surface of as-deposited Pd substrate (Figure 2.6) show all component elements of this SAMs including Pd, P, S and C. As mentioned detail in chapter 3, although in this spectrum the binding energy of the O(1s) cannot observe clearly due to the overlap with binding energy region of the $Pd(3p^{3/2})$ peak, the missing of oxygen peak at O(2s) binding energy region (21-29eV) in this survey scan suggest that there is no oxygen present in this SAMs surface. The XPS survey scan data showed that this SAM is not oxidized under the formed DTPA SAMs conditions. It is an important issue to minimize the effects of oxidation and contamination, since the appearance of PdO_x on the interface of Pd films can effect significantly on the macroscopic properties of SAMs surface like wettability, barrier properties and etc.

XPS survey scan of $(C_{16})_2DTPA$ SAMs on template-stripped Pd film (in Figure 2.7) showed similar features with that of $(C_{16})_2DTPA$ SAMs on as-deposited Pd film. It also confirmed the presence of expected elements in $(C_{16})_2DTPA$ SAMs by the occurrence of palladium, carbon, phosphorus, and sulfur peaks. The most significant feature in this sample is that there are no signs of content of residual oxygen in the interface of DTPA SAMs on template-stripped Pd film as inferred from the absence of O(2s) peak from the survey scan. It means that surface of both DTPA SAMs samples on different Pd substrates are not contaminated by oxygen oxidation.

The high-resolution S (2p) XPS spectra of $(C_{16})_2DTPA$ SAMs on two different Pd substrates was exploited for determining the nature of the chemical bonds between the DTPA head-groups and Pd surface. The interpre-

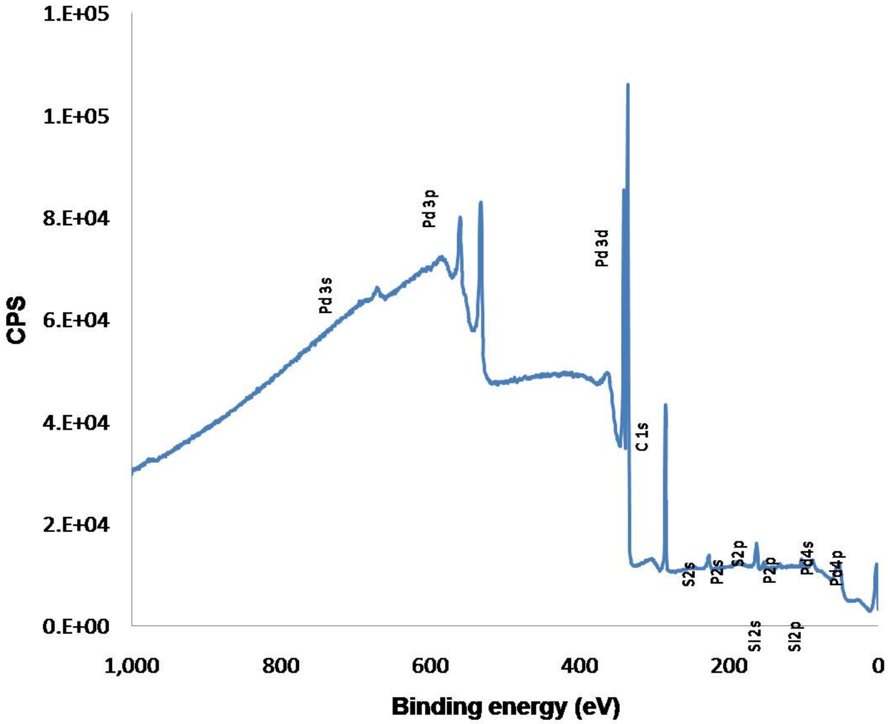

Figure 2.7: XPS survey scan of $(C_{16})_2DTPA$ SAMs on template-stripped Pd film

tation of the high resolution XPS spectra for sulfur region of $(C_{16})_2DTPA$ SAMs on As-dep Pd sample was showed in the Figure 2.8 and Table 2.1. The XPS results of our $(C_{16})_2DTPA$ SAMs suggest that the bonding nature of palladium and sulfur head-groups from DTPA molecules is totally different with that of palladium and alkyl-thiol, due to the fact that XPS results of thiol/Pd SAMs[8] showed at least three sulfur peaks which are assigned to Pd-S (162.3eV), $CH_3(CH_2)_nS^-$ (163.2eV) and $-S-S-$ (164.9eV); however, there are only two types of sulfur species were found from the simulation data of our DTPA samples. Moreover, as exposed to atmospheric oxygen, thiol/Pd SAMs

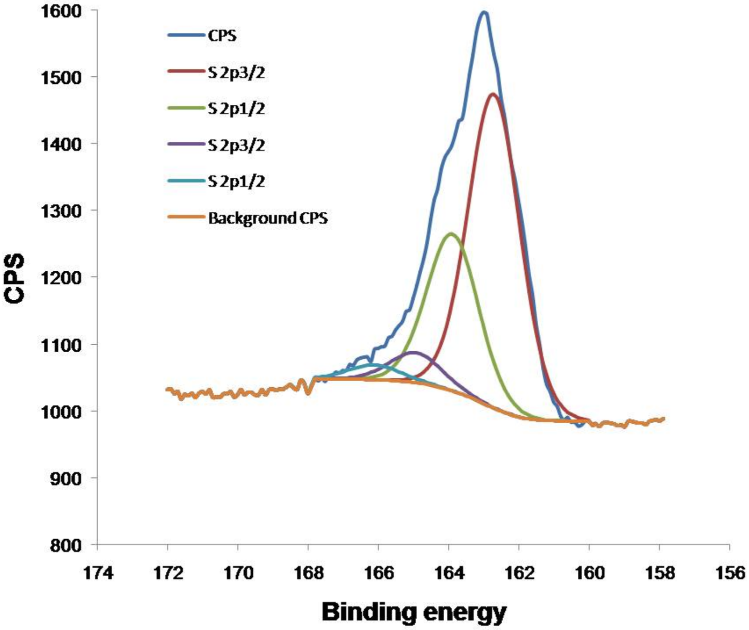

Figure 2.8: High-resolution XPS data for the S(2p) core levels of $(C_{16})_2DTPA$ SAMs formed on As-deposited Pd films.

are oxidized[8]. And, the formation of two new oxidized sulfur-containing species are observed at binding energies of 166.3 and 168.6 eV. Since there is no detectable oxidized sulfur species (no peaks at 166- 169 eV binding energy region), we can conclude that our DTPA/Pd SAMs didn't oxidise by air oxygen. Based on the XPS studies of our group about the formation of DTPA on as-deposited and template stripped gold surfaces [13], we suggest the similar assignment for the sulfur species appeared at our XPS simulation data: the one at 162.70 eV was for sulfur species which are bound to Pd surface and another at 164.93 eV assigned for unbound species. The ratio between bound and unbound sulfur species is 8.7 : 91.3 based on the percentage of peak areas.

	Binding energy (eV)	% Area	Type
S $2p_{3/2}$	164.93	8.7	unbound
S $2p_{3/2}$	162.70	91.3	bound

Table 2.1: XPS Binding energy and assigned peaks of S (2p) core lever of $(C_{16})_2DTPA$ SAMs formed on As-deposited Pd films

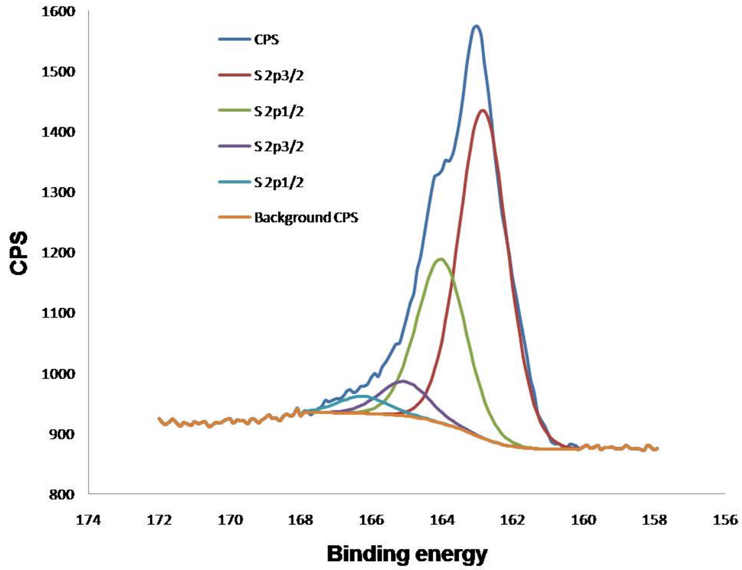

Figure 2.9: High-resolution XPS data for the S(2p) core levels of $(C_{16})_2DTPA$ SAMs formed on template - stripped Pd films

The interpretation of the high resolution XPS spectra for sulfur region of $(C_{16})_2DTPA$ SAMs on template-stripped Pd sample was showed in the Figure 2.9 and Table 2.2. As comparing to $(C_{16})_2DTPA$ SAMs on as-deposited Pd sample, a similar binding behavior between the palladium and sulfur species of this SAMs sample was observed with minor difference in binding energies and the relative concentrations of bound and unbound sulfur species (Table 2.2). We believe that the changing roughness between two Pd substrates contribute

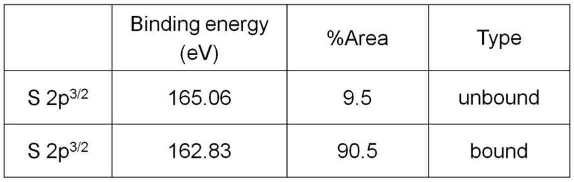

	Binding energy (eV)	%Area	Type
S $2p^{3/2}$	165.06	9.5	unbound
S $2p^{3/2}$	162.83	90.5	bound

Table 2.2: XPS Binding energy and assigned peaks of S (2p) core lever of $(C_{16})_2DTPA$ SAMs formed on Template-stripped Pd films

to these differences. However, due to the ratio between bound (~ 90 %) and unbound (~ 10 %) sulfur species (Table 2.1 and 2.2) which is almost the same for two kinds of Pd substrates, we proposed the ratio of bidentate and monodentate chelating DTPA molecules (4:1 ratio) anchored on palladium surface (Figure 2.10).

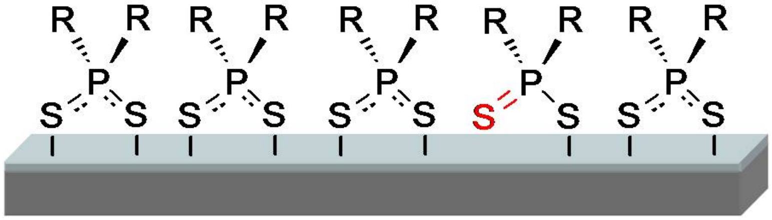

Figure 2.10: Proposed ratio of bidentate and monodentate chelating DTPA molecules on Pd surfaces

2.3.3 Reflection Absorption Infrared Spectroscopy (RAIRS)

Figure 2.11 shows RAIRS spectra for SAMs prepared from DTPA $(C_{16})_2DTPA$ SAMs and $C_{16}SH$ SAMs with different palladium substrates. The C-H stretching region in the infrared spectra of hydrocarbon SAMs is strongly influenced by the conformation of the alkyl chains and the chain environment[14][15].

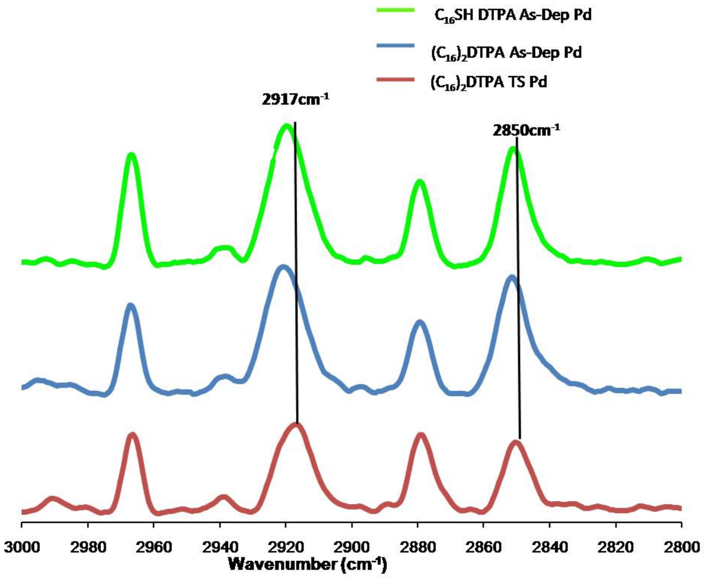

Figure 2.11: RAIRS spectra of $(C_{16})_2DTPA$ SAMs and $C_{16}SH$ SAMs on Pd substrates

Interpretation of this region follows by assigning the C-H stretching bands (Table 2.3). The IR spectra for SAMs prepared from $(C_{16})_2DTPA$ on both As-Dep Pd and TS Pd show sharp methylene stretching $\nu_{as}(CH_2)$ peak at 2919-1917cm^{-1} and $\nu_s(CH_2)$ at 2851-2849 cm^{-1} respectively. The $CH_2(s)$ and $CH_2(as)$ stretches of these two $(C_{16})_2DTPA$ SAMs on As-Dep Pd and TS Pd are consistent with a largely all-trans organization of the alkyl chains, similar to $C_{16}SH$ SAMs on Pd with $\nu_{as}(CH_2)$ peak at 2918cm^{-1} and $\nu_s(CH_2))$ at 2850cm^{-1}. The shift of wavenumbers of (C16)2DTPA SAMs on As-Dep Pd compare to that of $(C_{16})_2DTPA$ SAMs on TS Pd indicate that $(C_{16})_2DTPA$ SAMs on As-Dep Pd are less crystalline than $(C_{16})_2DTPA$ SAMs on TS Pd and $C_{16}SH$ SAMs on As-Dep Pd, implying that the packing of alkyl chains is less dense.

Modes	Wavenumbers (cm^{-1})		
	$(C_{16})_2$DTPA As-Dep Pd	$(C_{16})_2$DTPA TS Pd	C_{16}SH As-Dep Pd
$\nu_{as}(CH_2)$	2919	2917	2918
$\nu_s(CH_2)$	2851	2849	2850

Table 2.3: Wavenumbers values of antisymmetric and symmetric CH_2 vibrations

2.3.4 Contact Angle Goniometry

Substrates	H_2O		Hexadecane	
	Adv (θ_a)	Rec (θ_r)	Adv (θ_a)	Rec (θ_r)
C_{16}SH As-Dep Pd	116 ± 3	103 ± 2	40 ± 1	36 ± 1
$(C_{16})_2$DTPA As-Dep Pd	110 ± 2	94 ± 2	39 ± 2	34 ± 1
$(C_{16})_2$DTPA TS-Pd	113 ± 1	96 ± 1	43 ± 2	38 ± 1

Table 2.4: Advancing and receding water contact angles (θ_a and θ_r) of $(C_{16})_2DTPA$ SAMs and $C_{16}SH$ SAMs on Pd substrates

Wettability is a highly sensitive tool for probing the structure and composition of surfaces[16]-[17]. The values for the advancing and receding water and hexadecane contact angles, (θ_a and θ_r), of all investigated $(C_{16})_2DTPA$ SAMs and $C_{16}SH$ SAMs are summarized in Tables 2.4. For the two symmetrically long chains $(C_{16})_2DTPA$ SAM on Pd substrates, we observe contact angles that essentially match the expected values for methyl-terminated monolayers (110^o-113^o respectively). It suggests that $(C_{16})_2DTPA$ SAMs was formed stably and typical of well-ordered monolayers. The difference between the advancing and receding contact angles, $\Delta\theta = \theta_a - \theta_r$, is hysteresis which characterize for surface heterogeneity, roughness and mobility of surface[18]. The water contact angle hysteresis observed for $C_{16}SH$ SAMs is lower than the hysteresis for other two DTPA SAMs; it implies that the SAMs surface formed by $C_{16}SH$ somewhat more homogenous and ordered than the surface formed by DTPA. Due to its sensitivity to the hydrophobic surface, hexadecane contact angles measurements also was used to investigate the macroscopic properties of SAMs. It is know that the advancing angles will be sensitive to the hydrophobic domains. Hexadecane contact angle values confirms the fact that denser packed monolayers were formed with $(C_{16})_2DTPA$ SAMs on TS Pd and $C_{16}SH$ SAMs on As-Dep Pd comparing to monolayers of $(C_{16})_2DTPA$ SAMs on As-Dep Pd. The hysteresis of HD contact angle observed in this study hardly to interpret due to the overlap of mean values as including deviations.

2.3.5 Barrier Properties

As shown in Figure 2.12 and equations (Equation 2.1 and 2.3) mentioned in experimental section related to EIS measurement, $R_{Solution}$ can be determined as the experimental impedance modulus at high frequencies extrapolated to infinite limit of frequency. It means that at highest frequencies, the impedance

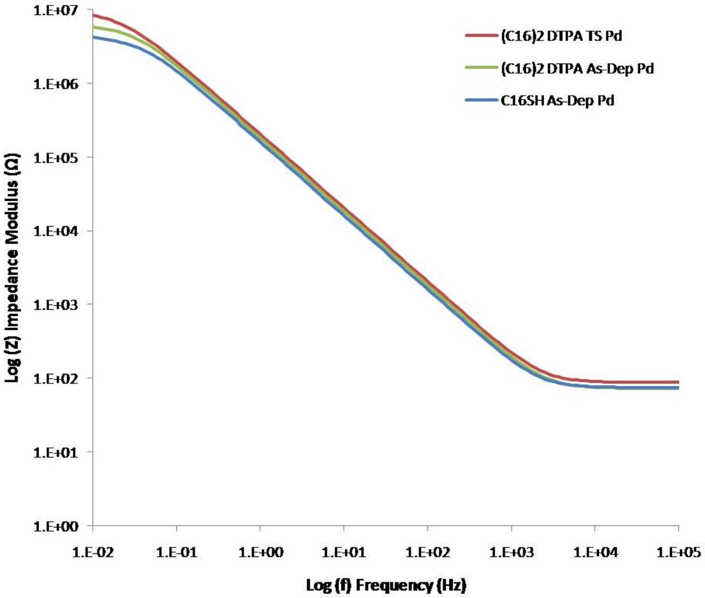

Figure 2.12: Electrochemical impedance spectra of $(C_{16})_2DTPA$ SAMs and $C_{16}SH$ SAMs on Pd substrates

modulus of the whole systems is caused mainly by the resistance of solution. However, according to equation 2.1 and equation 2.4, the total impedance of $R_{Solution} + R_{SAM}$ can be extrapolated from the impedance modulus of systems at lowest frequencies which is inferred close to the zero limit of frequency. As observing from Figure 2.12, much higher values of total impedance of $R_{Solution}$ + R_{SAM} comparing to that of $R_{Solution}$ suggests that the SAMs provides effective resistance against electron transfer from electrolyte solution to Pd substrates. At moderate frequencies, the linear correlation (with a slope of -1) between the log of impedance modulus and log of frequency indicates that the overall impedance modulus is dominated by the capacitances of the SAMs, and the SAM structure functions as a physical dielectric, separating the conductive Pd substrate from the ion-containing electrolytes solution.

The simulated impedance and capacitance values of SAMs by applying the simple model (Figure 2.4) was shown in Table 2.5; and from capacitance values we also can calculate thickness of SAMs by using equation 2.5

$$d = \frac{\varepsilon\varepsilon_o}{C} \tag{2.5}$$

Where:

C is the capacitance per area (in Fm^{-2})

ε is the dielectric constant of polyethylene (2.3)

ε_o is the permittivity of free space (8.54×10^{-12}Fm^{-1}).

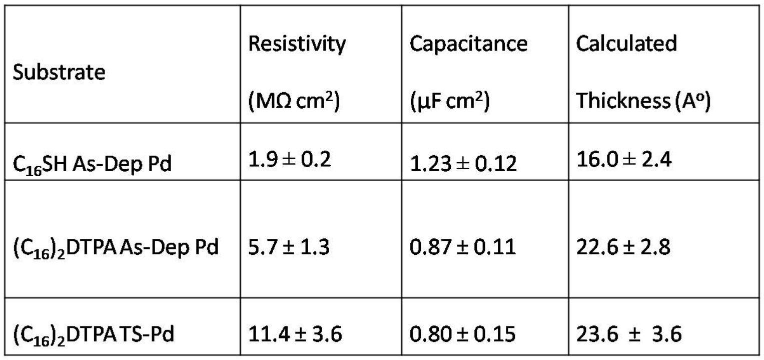

Substrate	**Resistivity (MΩ cm^2)**	**Capacitance (μF cm^2)**	**Calculated Thickness (A^o)**
C_{16}SH As-Dep Pd	**1.9 ± 0.2**	**1.23 ± 0.12**	**16.0 ± 2.4**
(C_{16})$_2$DTPA As-Dep Pd	**5.7 ± 1.3**	**0.87 ± 0.11**	**22.6 ± 2.8**
(C_{16})$_2$DTPA TS-Pd	**11.4 ± 3.6**	**0.80 ± 0.15**	**23.6 ± 3.6**

Table 2.5: Resistance and capacitance values of $(C_{16})_2DTPA$ SAMs and $C_{16}SH$ SAMs on Pd substrates

The capacitance values of $(C_{16})_2DTPA$ SAMs from Table 2.5 indicate that there are similar thicknesses of $(C_{16})_2DTPA$ SAMs on both As-Dep and TS Pd. Moreover, the higher thicknesses of DTPA SAMs comparing to $C_{16}SH$

SAMs suggest that monolayers formed by DTPA may be less tilted than monolayers formed by $C_{16}SH$. DTPA SAMs on Pd substrates show better electrical resistivity under electrolyte solutions than the $C_{16}SH$ SAMs. The occurrence of unbound thiol species on DTPA SAMs maybe account for the difference in electrical resistivity. However, the lower resistivity of the $(C_{16})_2DTPA$ SAM on As-Dep Pd suggests either lower coverage or packing density of this SAM compare to $(C_{16})_2DTPA$ SAM on TSPd. This result is expectable due to the obviously higher number of step edge defects, peaks and valleys of As-deposited Pd films than template-stripped ones.

2.4 Conclusion

In summary, we showed that $(C_{16})_2DTPA$ molecules can form stable SAMs on both kinds of Pd substrates by RAIRs and contact angle evidence. Furthermore, we have revealed the binding nature of sulfur head-groups of DTPA molecule with Pd substrates and suggested a chelating model for the anchor of DTPAs molecules on the surface of Pd films. Despite the changing the surface roughness and morphology of the Pd substrate, it has no effect on the binding of the DTPA headgroup. Even similar DTPA headgroup binding on As-Dep and TS Pd, there are subtle differences in the crystallinity and packing density of the alkyl chains in SAMs formed on the two substrates. We attribute these differences to the presence of fewer defects (such as step edges) in the TS Pd substrate. It is also interesting to know that DTPA SAMs having such a better resistance comparing to $C_{16}SH$ SAMs; and it suggests another approach for using DTPA SAMs where higher resistance applications are demanded.

References

[1] Bain, C. D., Joe E., Whitesides, G. M., *J. Am. Chem. Soc.*, 1989, 111 (18), 7155.

[2] Tamada, K.; Hara, M.; Sasabe, H.; Knoll, W. *Langmuir* **1997**, 13, 1558−1566

[3] Joon-Seo, P.; Aaron, C. S.; and Lee, T. R. *Langmuir*, **2004**, 20 (14), 5829.

[4] Shon, Y.-S.; Lee, S.; Colorado, R., Jr.; Perry, S. S.; Lee, T. R. *J. Am. Chem. Soc.* **2000**, 122, 7556

[5] Skaife, J. J.; Brake, J. M.; Abbott, N. L. *Langmuir* **2001**, 17, 5448.

[6] Semaltianos, N. G.; Wilson, E. G. *Thin Solid Films* **2000**, 366, 111

[7] Hegner, M.; Wagner, P.; Semenza, G. *Surf. Sci.* **1993**, 291, 39; Fernanda F. Rossetti, Ilya Reviakine, and Marcus Textor, *Langmuir* **2003**, 19, 10116.

[8] Love, J. C.; Wolfe, D. B.; Chabinyc, M. L.; Paul, K. E.; Whitesides; G. M. *J. Am. Chem. Soc.* **2003**, 125, 2597.

[9] Love, J. C.; Estroff, L. A., Kriebel, J. K. , Nuzzo, R. G., and Whitesides, G. M., *Chem. Rev.* **2005**, 105, 1103.

[10] Mansfeld, F., Kendig, M. W., and Lorenz, W. J., *J. Electrochem. Soc.* **1985**, 132, 290.

[11] Mansfeld,F. , *Corrosion*, **1981**, 37, 301.

[12] Mansfeld, F., and Kendig, M. W. W., *Korros.* **1983**, 34, 397.

[13] Miller, M. S.; San Juan, R. R.; Ferrato, M. A.; Carmichael, T. B. *Langmuir* **2011**, 27, 10019.

[14] Snyder, R. G.; Strauss, H. L.; Elliger, C. A. *J. Phys. Chem.* **1982**, 86, 5145.

[15] MacPhail, R. A.; Strauss, H. L.; Snyder, R. G.; Elliger, C. A. *J. Phys. Chem.* **1984**, 88, 334.

[16] Whitesides, G. M.; Laibinis, P. E. *Langmuir* **1990**, 6, 87.

[17] Ulman, A. An Introduction to Ultrathin Organic Films; Academic: Boston, **1991**

[18] Bain, C. D.; Troughton, B.; Tao, Y.-T.; Evall, J.; Whitesides, G. M.; Nuzzo, R. G. *J. Am. Chem. Soc.* **1989**, 111, 321

Chapter 3

A new selenide based Self–Assembled Monolayers (SAMs) on Pd film with the homogeneous binding nature at headgroups-metal interface

3.1 Introduction

In this chapter, we will report a new selenium based SAMs from Bis(hexadecyl)diselenide developed on surfaces of palladiums. Although there are several studies related to SAMs on Pd surfaces[1]-[5], to the best of our knowledge, this is the first study employing palladium as substrate for selenium based SAMs. Not only trying to form new selenium based SAMs on Pd, we also aimed to optimize formation conditions of this SAMs by using RAIRS, and compare characterization results of this SAMs film to those of SAMs formed by adsorption of thiols on Pd. AFM and XPS evidences also revealed the rough topography of SAMs and the nature of Pd/Se interface. Electrochemical Impedance Spectroscopy (EIS) was applied to examine the metallic effect of selenium head group to electron-transfer ability of SAMs. The data were collected from contact angles measurement to confirm the relative higher roughness of SAMs and hydrophobic property of Se-based SAMs compare to these of thiol based SAMs on Pd.

3.2 Experimental Section

3.2.1 Synthesis of Bis(hexadecyl)diselenide

All reactions were carried out under nitrogen in absolute solvents. The synthesis of Bis(hexadecyl)diselenide has already been described. Synthesis procedure was reproduced according to literature[6].

3.2.2 Pd films preparation

Palladium substrates were prepared by evaporation of approximately 2 nm of Ti followed by 100nm of Pd onto on silicon wafers with the typical deposition rate 1 Å/s, in a vacuum of 5×10^{-6} mbar in an e-beam evaporation machine. The thickness of Pd surfaces was monitored during the deposition process using SQC-310 Deposition Controller. After taking out of the evaporation chamber, the freshly prepare substrate should be used within 1h to prevent any possible oxidation of Pd films.

3.2.3 Preparation of monolayers

Self assembled monolayers of Dihexadecyldiselenide were formed by immersing the freshly made Pd films into a dilute solution (1mM) of corresponding compound in degassed anhydrous toluene, at room temperature, and the monolayer formation time was 6h, 12h, 18h, 24h, 48h and 96h).

After incubation for in sealed scintillation vials (20mL), the substrates were removed from solution, rinsed carefully five times with the pure solvent and absolute ethanol, and then dried in a stream of N_2. Measurements were performed immediately after the monolayer preparation.

Denotation: Self assembled monolayer of $(C_{16}H_{33}Se)_2$ formed with 6h immersion was denoted as 6h-$(C_{16}Se)_2$ and respectively with other different immersion time samples.

3.2.4 Atomic force microscopy (AFM)

AFM measurements of Pd surfaces were determined by contact-mode of a Digital Instruments Multimode atomic force microscope. The typical scan size was $1\mu m \times 1\mu m$ with a scan rate of 0.5 Hz and a scanning resolution of 512 samples/line.

3.2.5 Reflection Absorption Infra Red Spectroscopy (RAIRS)

The RAIR data were obtained using a Bruker IFS 66v/S spectrometer equipped with liquid nitrogen cooled MCT detector in single reflection mode with an Autoseagull accessory. For minimizing the absorption of CO_2 and sometimes water, the background and SAMs treated samples were rinsed carefully with pure ethanol and evacuated under the chamber for 2h before measuring. Spectra were obtained using 1024 scans at 1 cm^{-1} resolution. Finally they were baseline corrected with 75 iterations.

3.2.6 Wettability Measurements.

Water and hexane (ACS reagent-grade) contact angles were measured by a Ram-Hart contact angle goniometer equipped with a microlitre syringe. A drop of 5 μL was placed on the monolayer. Readings of the static angles were taken at least three times on both sides of the drop at three different locations of the sample. These values were then averaged over at least three different monolayers. The contact angles were typically reproducible to within 2^o.

3.2.7 Electrochemical Impedance Spectroscopy (EIS)

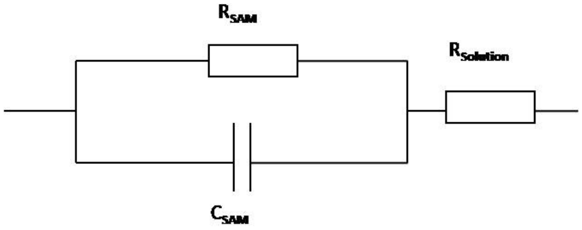

Figure 3.1: Simple equivalent circuits

EIS was performed using a BAS-Zahner IM6 ex impedance unit. The saturated calomel electrode was used as reference electrode, and courter electrode was a 1.0mm-diameter Pt wire (purchased from Sigma-Aldrich). Solutions of 1mM $K_4Fe(CN)_6$, 1mM $K_3Fe(CN)_6 \cdot 3H_2O$ and 100 mM Na_2SO_4in distilled water was used as electrolyte solution. The measurements were made at an open circuit potential set at ~450 mV with a 10 mV ac perturbation that was controlled from 3.0×10^{-2}to1.0×10^5Hz. Film resistances and capacitance values were determined by fitting the EIS data with a simple equivalent circuit model (Figure 3.1) (mentioned in chapter 2) equivalent circuit using software provided by BAS-Zahner Company.

3.2.8 X-ray Photoelectron Spectroscopy

X-ray photoelectron spectroscopy (XPS) surface analysis was performed on a Kratos Axis Ultra X-ray photoelectron spectrometer. The X-ray source was a monochromatized Al Kσ source with a 35^o takeoff angle; operating pressure was $< 10^{-9}$ Torr. Survey scan (15 sweeps, 120s sweep time) analyses were carried out with an analysis area of 300 x 700 microns and a pass energy of 160 eV. High resolution analyses were carried out with an analysis area of 300 x 700 microns and a pass energy of 20 eV (long runs of ~200 scans for Se and Pd).

3.3 Results and discussion

3.3.1 AFM results

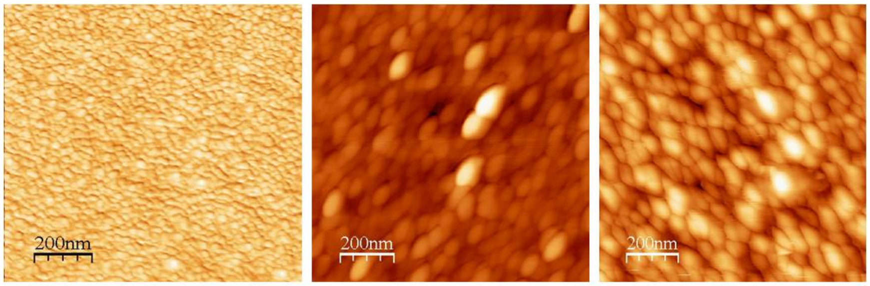

Blank Pd **24h-$(C_{16}Se)_2$ SAM** **48h-$(C_{16}Se)_2$ SAM**

Figure 3.2: AFM images of $(C_{16}Se)_2$ SAMs after 24 and 48h immersed in solution with $1\mu m \times 1\mu m$ size and scaning resolution of 512 samples/line

AFM	$(C_{16}Se)_2$ SAMs					
Samples	Blank	6h	12h	24h	48h	96h
RMS(nm)	2.51	2.82	3.08	3.26	3.56	3.72

Table 3.1: RMS roughness values of Pd films at different immersion times

At first, we only tried to form bis(hexadecyl)-diselenide SAMs/Pd from immersing a 100-nm-thick substrate of freshly evaporated polycrystalline Pd into a 1 mM solution of Bis(hexadecyl)diselenide in toluene at 12h and 24h; with AFM experiments, we observed the changing in the roughness of these two samples (Table 3.1) . We suspected that oxygen contaminated in our solvents or atmospheric oxygen may oxidize our samples and make their surface become rougher.

To verify that there is no effect of solvent on structure film and morphology of Pd substrate and to eliminate the possibility of air oxygen which may be oxidized Pd substrates, we also form bis(hexadecyl)-diselenide SAMs/Pd on two different anhydrous solvents, toluene and ethanol, under oxygen-degassed conditions with incubation time (24h). Wetting behaviors of the two samples are similar. We also use AFM to clarify whether there is any encountered changing in morphology of bis(hexadecyl)-diselenide SAMs films of between these two samples. Our AFM result doesn't show any difference between them. We can conclude that solvents doesn't affect on the morphology changing of Pd substrates.

As we tried to form $(C_{16}Se)_2$/Pd SAMs with other different immersion times; the roughness of these $(C_{16}Se)_2$/Pd SAMs still showed a increasing trends along with immersion times. The surface roughness of (bishexadecyl)-diselenide SAMs/Pd films were characterized by atomic force microscopy (AFM). We included blank Pd films in AFMs results as a direct reference for roughness changing observed. Figure 3.2a presents AFM image ($1\mu m \times 1\mu m$) of freshly made Pd (blank substrate) surface after cleaned by anhydrous ethanol and dried under nitrogen gas. Figure 3.2b and c presents AFM images Pd surfaces covered with $(C_{16}Se)_2$ SAMs after 24h and 48h immersion in bis(hexadecyl)-diselenide solution.

The data of Table 3.1 shows RMS roughness values of bishexadecyl)-diselenide SAMs/Pd films at different immersion times. We have show that there is a critical increase in roughness of bishexadecyl)-diselenide SAMs/Pd films during times even after eliminating any possible factors (mentioned above such as oxygen free solution, freshly made substrates and etc) which can cause oxidized surface.

3.3.2 Contact Angle Goniometry

We also employed CA measurements to observe wetting behaviors of bis(hexadecyl)diselenide/Pd SAMs with different immersion times. Obviously, a significant issue, which exists for organized films, is the detailed relationships between molecular features at surfaces, such as orientation and corrugation, and wetting. Wetting is influenced by a number of factors, among them mainly molecular-scale and macroscopic roughness[7]. And the observed increasing trend in surface roughness of bis(hexadecyl)diselenide/Pd SAMs must have a considerable influence on contact angle measurements. We can describe the effect of surface roughness by the so-called Wenzel equation[8] (Equation 3.1). The equation predicts that if a molecularly hydrophobic surface is rough, the appearance is that of an even more hydrophobic surface.

$$cos\theta^* = rcos\theta \tag{3.1}$$

Where:

θ^* is the apparent contact angle.

r is roughness ratio is defined as the ratio of true area of the solid surface to the apparent area.

θ is the Young contact angle[9] as defined for an ideal surface.

CA	$(C_{16}H_{33}Se)_2$ SAMs					$C_{16}H_{33}SH$ SAMs
Immersion time	6h	12h	24h	48h	96h	24h
θ_{H2O}	80 ± 1	103 ± 2	126 ± 2	134 ± 2	133 ± 2	113 ± 2
θ_{HD}	16 ± 2	23 ± 1	18 ± 2	<10	<10	22 ± 1

Table 3.2: Static water and hexane contact angle of $(C_{16}Se)_2$ SAMs at different immersion times.

Static contact angles of water and hexadecane (HD) (Table 3.2) were measured on monolayers prepared by the immersion of Pd substrates in solutions of Bis(hexadecyl)-diselenide at various immersion times, similar to samples used for AFM experiments. The observed static water contact angle is smallest (80 ± 2^o) for 6h-$(C_{16}Se)_2$SAMs. Although we expected higher values of water contact angle for 6h-$(C_{16}Se)_2$SAMs samples due to the effect of roughness mentioned in Wenzel equation. Low contact angle values of 6h-$(C_{16}Se)_2$SAMs samples (comparing to static water contact angle of well ordered thiol/Au SAMs with 113 ± 2^o)

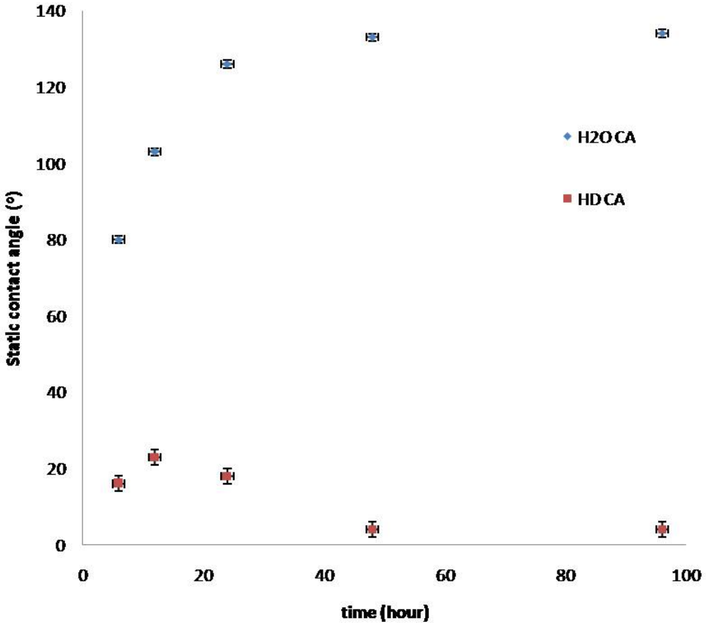

Figure 3.3: Static water and HD contact angles vs immersion times of $(C_{16}Se)_2$ SAMs

support to the evidence from RAIRS (mentioned later) that 6h is not a sufficient time for forming fully covered $(C_{16}Se)_2$SAMs; and because of this reason, there might be some conformational disorder regions on 6h-$(C_{16}Se)_2$SAMs which cause lower static contact angle. At this time the monolayer itself is far from being well ordered yet. With water CA measurement of 12h-$(C_{16}Se)_2$SAMs samples, we have a CA value (103 ± 2^o) comparable to that of our prepared 12h-$C_{16}H_{33}SH$/Pd samples (108 ± 2^o); however, both of these 12h samples also didn't yield highly dense, crystalline monolayers. This is in accordance with investigations using RAIRS of 12h-$(C_{16}Se)_2$SAMs.

However, as immersed longer in $(C_{16}Se)_2$ solution, the collected 24h and 48h samples have higher water contact angles $(126 - 134^o)$ (Table 3.2). These contact angle values of 24h and 48h-$(C_{16}Se)_2$SAMs are much higher than that of 24h-$C_{16}H_{33}SH$/Pd SAMs (113^o) which is considered as a well defined SAMs structures. For the first time we observed such a high degree of hydrophobic behavior of SAMs on Pd substrates, comparing to thiol/Pd systems. Apparently, such high water contact angle is typical of a rough substrate. These larger and larger RMS roughness values explain why the water contact angle of 24h and 48h-$(C_{16}Se)_2$ SAMs also increase with immersion time. The increasing trend of water contact angle values with $(C_{16}Se)_2$ SAMs agree with the increasing of RMS roughness due to the fact that water drop cannot enter inside of the roughness surface[10], a water drop sits on a patchwork of bis(hexadecyl)-diselenide SAMs surface and air which leads the increasing water contact angle to 134^o. Hydrophobicity of our bis(hexadecyl)-diselenide/pd SAMs are definitely reinforced by roughness, in qualitative agreement shown in Figure 3.2, Table 3.1 and 3.2. But this agreement is only qualitative; we do not observe a simple linear relation in contact angle (Figure 3.2) and roughness (Table 3.1), and do not understand the discontinuity in contact angle value found in 96h-$(C_{16}Se)_2$ SAMs sample. This discrepancy is also observed in the studies of other surface scientist about the effect of roughness on wetting behavior of a surface [11] - [12]. They suggested that water CA get the critical values (in our SAMs 134^o); it may be due to surface energy of water drop get minimal values at equilibrium[13].

Due to its greater sensitive to the hydrophobic property of surfaces, HD contact angle is also performed in this study; the HD contact angles for SAMs of bis(hexadecyl)-diselenide that were assembled for different times are shown in Table 3.2. Interestingly, unlike the case of long-chain thiols or disulfides/Pd systems[1] here the HD contact angle data shows much lower values. We suspect that the possible desorption process of (hexadecyl)-diselenide/Pd SAMs may cause rougher surface; this maybe explain why the increasing trend of water contact angle. Moreover, the spread out of HD drops on the SAMs surface ($\theta_{HD} \leq 10^o$) might be caused by the high sensitivity of HD molecules to alkyl chains of bis(hexadecyl)-diselenide molecules which now scattered disorderedly on Pd surfaces. However, further desorption studies of (hexadecyl)-diselenide/Pd SAMs may solve this unknown behaviour of this type of SAMs.

3.3.3 Reflection Absorption Infrared Spectroscopy (RAIRS)

RAIRS Spectroscopy of SAMs formed at different immersion times (up to 96h) in Figure 3.2 reveals the anti-symmetric (ν_{as} at 2920 cm^{-1} region) and symmetry (ν_s at 2850cm^{-1} region) C-H stretching vibrations of CH_2

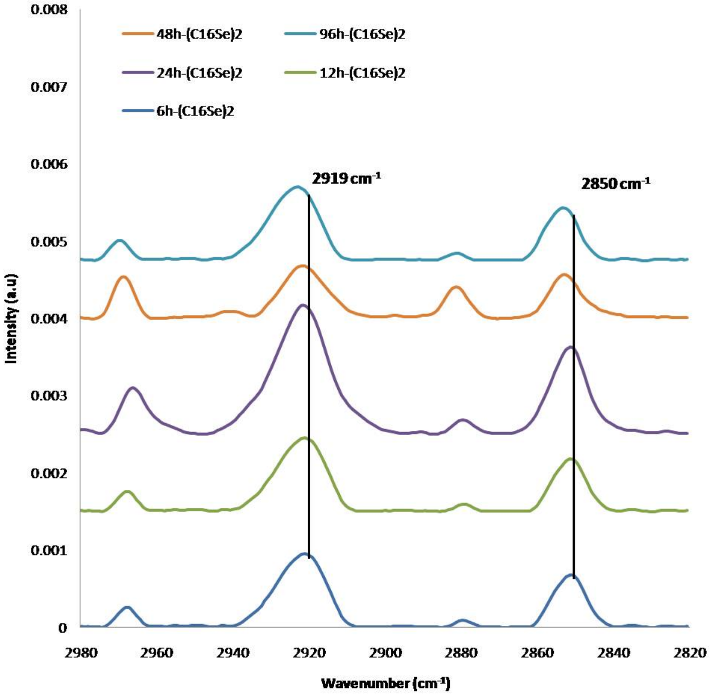

Figure 3.4: RAIRS spectroscopy of $(C_{16}H_{33}Se)_2$ SAMs at different immersion times.

groups. As also shown in the Figure 3.4, the peaks at 2966 cm^{-1} region are assigned to the d-CH_3 stretching mode, ν_{as} (CH3,ip), and the peaks at 2880 cm^{-1} are assigned to the s-CH_3, symmetric stretching mode, $\nu_s(CH_3)$. As absorption is seen for the anti-symmetric (at 2922 cm^{-1}) and symmetric (at 2851 cm^{-1}) C-H stretches in 6h-$(C_{16}Se)_2$SAMs, the environment of the alkyl chains in this SAMs resembles that of a liquid like monolayer[14].

In contrast, for increased immersion time of SAMs formation as in monolayers 12h-$(C_{16}Se)_2$, the peak positions of the absorption and the increase of the intensity for the anti-symmetric (at 2921 cm^{-1}) and symmetric CH_2

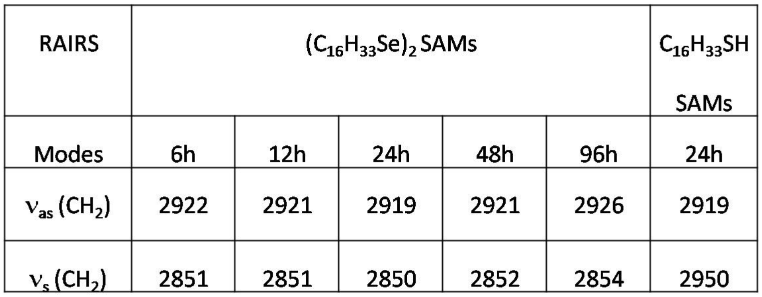

RAIRS	$(C_{16}H_{33}Se)_2$ SAMs					$C_{16}H_{33}SH$ SAMs
Modes	6h	12h	24h	48h	96h	24h
ν_{as} (CH_2)	2922	2921	2919	2921	2926	2919
ν_s (CH_2)	2851	2851	2850	2852	2854	2950

Table 3.3: Wavenumbers values of anti-symmetric and symmetric CH_2 and CH_3 vibrations

groups indicate less liquid-like environment than 6h-$(C_{16}Se)_2$SAMs sample. The influence of immersion time to the arrangement of alkyl chain is obvious in these series of samples, due to the shorter immersion time is, the lesser amount of bis(hexadecyl)diselenide molecules is adsorbed on Pd substrates. Following the trend of increasing immersion time, the coverage of bis(hexadecyl)diselenide molecules on the film may be reach the optimum values with 24h-$(C_{16}Se)_2$ sample; we can see the intensities of two peaks of the anti-symmetric and symmetric modes of CH_2 vibrations of this sample are the highest comparing to these of all other samples; and the peaks frequencies for ν_{as} (at 2919 cm^{-1}) and ν_s (2850 cm^{-1}) of CH_2 vibrations also show shifts to the crystalline phase of alkyl chain. Moreover, the intensities of ν_{as} (CH_3,ip) and $\nu_s(CH_3)$ modes of 6, 12, and 24h samples, which also increases with the increasing of immersion time, suggest that bis(hexadecyl)diselenide molecules may also self align to form a more dense packed region with higher number of CH_3 groups exposed to the surface.

We also extent immersion time to 48h-$(C_{16}Se)_2$ and 96h-$(C_{16}Se)_2$ samples; and surprisingly, as increasing immersion time to over 24h, the alkyl chain of $(C_{16}Se)_2$ on Pd of these samples is even more liquid-like than that of 6h-$(C_{16}Se)_2$ SAMs; and especially, for 96h-$(C_{16}Se)_2$ sample, the molecular environment of the alkyl chains relaxes from this state to one involving more disorder than all other samples, and even can be compared to the liquid-like disorder of the shorter alkyl chain of thiol on Pd[1].

The data also shows the highest values of the intensities of CH_3 vibrations modes of 48h sample and the lower values of these intensities of 96h samples; the probably possible scenery for CH_3 intensity trend is that the occurrence of the increasing roughness trends apparently makes more and more structural defects, such as dense arrangements of intergrain boundaries and other gross structural irregularities[15] - [16], and affect the order of 48h and 96h-$(C_{16}Se)_2$ SAMs. And those defects create some regional disordered areas close to well-ordered ones, and that corresponds with the liquid-like of alkyl chain phase, the decreasing of the CH_3 groups vibrations intensities, and the increasing of the CH_2 groups vibrations intensities comparing to 24h sample.

We also compare the RAIRs spectra of bis(hexadecyl)diselenide/Pd SAMs with those of hexadecanethiol /Pd SAMs. Figure 3.5 shows that the positions of peak frequencies of ν_{as} (CH_2) (at 2922 cm^{-1}) and ν_s (at 2851 cm^{-1}) of both 24h-$(C_{16}Se)_2$ and 24h- $C_{16}H_{33}SH$ spectra suggest the "crystallinelike" nature of both monolayers. The higher intensities

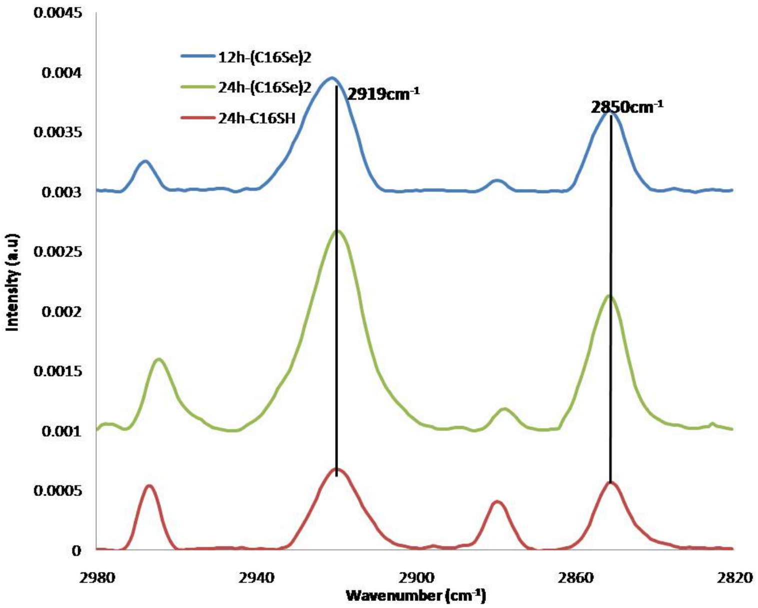

Figure 3.5: RAIRS spectra of $(C_{16}Se)_2$ and $C_{16}H_{33}SH$ SAMs

of $\nu(s)(CH_2)$ modes and lower intensities of $\nu(s)(CH_3)$ modes can be attributed to the lesser dense packed structure and larger tilt angle of bis(hexadecyl)diselenide/Pd SAMs comparing to hexadecanethiol/Pd SAMs. 12h-$(C_{16}Se)_2$ RAIRs spectrum is also added in Figure 3.5 as the benchmark for the comparison between 24h-$(C_{16}Se)_2$/Pd and 24h-$C_{16}H_{33}SH$/Pd SAMs. Further, since we anticipated the differences between bis(hexadecyl)diselenide and hexadecanethiol SAMs might be not only related to the structures of them, but also to electronic properties; we conducted a series of EIS experiments to investigate those properties.

3.3.4 Barrier Properties

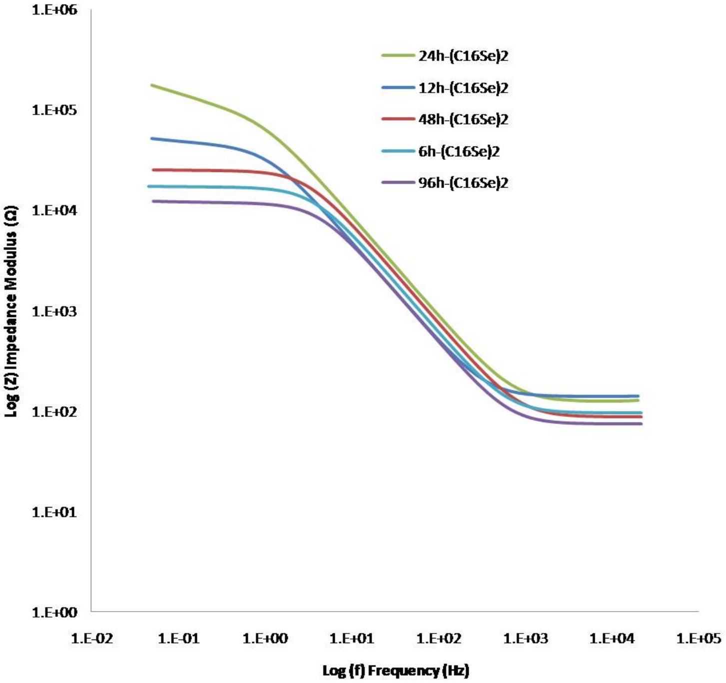

Figure 3.6: Electrochemical impedance spectra in the form of a Bode magnitude plot for $(C_{16}H_{33}Se)_2$ SAMs prepared by exposures to 1 mM $(C_{16}H_{33}Se)_2$ at different immersion time on Pd in an aqueous solution of 1mM $K_4Fe(CN)_6$, 1mM $K_3Fe(CN)_6 \cdot 3H_2O$ and 100 mM Na_2SO_4 with a Ag/AgCl/saturated KCl reference electrode

It is well-known that a self-assembled monolayer can form a lipophilic barrier for electron transfer between the electrode surface and hydrophilic electro-active probes in solution. We further have characterized the barrier properties of our SAMs in the presence of aqueous solutions 1mM $K_4Fe(CN)_6$, 1mM $K_3Fe(CN)_6 \cdot 3H_2O$ and 100 mM Na_2SO_4. Figure 3.6 shows impedance spectra in the form of Bode plots for SAMs formed at different immersion time. Impedance measurements were performed using a three-electrode cell comprising a SAMs as the working electrode, a platinum wire counter electrode, and a saturated calomel reference electrode (SCE). The simulated impedance and capacitance values of SAMs by applying the simple equivalent circuit model was shown in the Table 3.4; and from capacitance values we also can calculate thickness of SAMs by using equation 3.2.

$$d = \frac{\varepsilon\varepsilon_o}{C} \tag{3.2}$$

Where:

C is the capacitance per area (in Fm^{-2})

ε is the dielectric constant of polyethylene (2.3).

ε_o is the permittivity of free space ($8.54 \times 10^{-12}\mathrm{Fm}^{-1}$).

The results of simulated impedance (Table 3.4) of bis(hexadecyl)-diselenide SAMs show the increasing trend of impedance from 6h-24h with the highest resistance value for 24h-sample; while the decrease of impedance is observed with over 24h immersion time samples. The calculated thickness generated from simulated capacitance of these bis(hexadecyl)-diselenide SAMs samples also reveal the same trend with impedance. The information above suggest that 24h is the best immersion time for forming (bishexadecyl)-diselenide SAMs on Pd surfaces with the optimum resistance and thickness comparing to other immersion times. These results may imply that the coverage of SAMs surface decrease with extended immersion time over 24h. The proposed scenery (as mentioned in RAIRs and CA results about the effect of increasing roughness trends on a series of bishexadecyl-diselenide SAMs after immersing Pd substrates over 24h) is also agree with the data of resistance and thickness of these SAMs. The increasing of roughness may be attributed to a higher density of inhole defect sites and an increasing number of conformational defects of $(C_{16}Se)_2$ SAMs as extending immersion time of $(C_{16}Se)_2$ SAMs. These defects on the SAMs interface strongly effect on the dielectric properties of SAMs which plays an important role in controlling charge transfer processes.

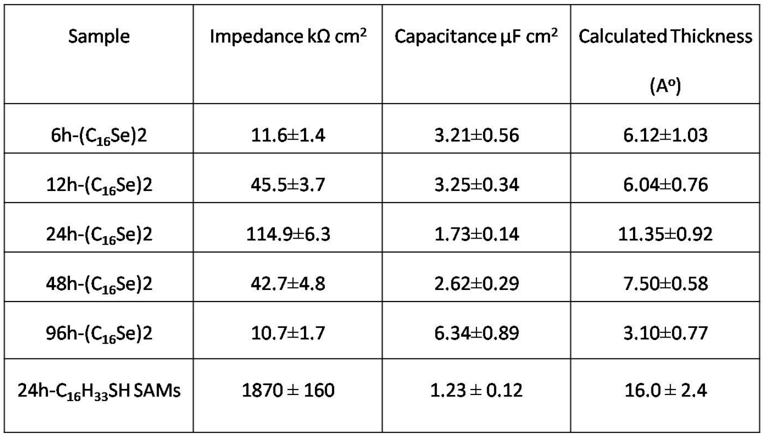

Sample	Impedance kΩ cm^2	Capacitance µF cm^2	Calculated Thickness (A°)
6h-(C_{16}Se)2	11.6±1.4	3.21±0.56	6.12±1.03
12h-(C_{16}Se)2	45.5±3.7	3.25±0.34	6.04±0.76
24h-(C_{16}Se)2	114.9±6.3	1.73±0.14	11.35±0.92
48h-(C_{16}Se)2	42.7±4.8	2.62±0.29	7.50±0.58
96h-(C_{16}Se)2	10.7±1.7	6.34±0.89	3.10±0.77
24h-$C_{16}H_{33}$SH SAMs	1870 ± 160	1.23 ± 0.12	16.0 ± 2.4

Table 3.4: Impedance, capacitance and calculated thickness values of $(C_{16}Se)_2$ SAM at different immersion time and 24h-$C_{16}H_{33}SH$ SAMs

We also include the impedance, capacitance and thickness data of

24h-$C_{16}H_{33}SH$ SAMs on Pd surfaces prepared by our groups in the Table 3.4. As comparing to the impedance value of 24h-$C_{16}H_{33}SH$ SAMs samples, those values of all other $(C_{16}Se)_2$ SAMs are much lower; it is totally along with theoretical calculations from Ratner and co-workers [17]. Based on calculation of the differences between the valence and conduction energies, they claimed that diselenol molecules assembled on Au should conduct 25 times better than the equivalent dithiols. Another reason for such lower resistance of our $(C_{16}Se)_2$ SAMs comparing to $C_{16}H_{33}SH$ SAMs is that the roughness of our $(C_{16}Se)_2$ SAMs definitely create more defects (mentioned above), and make our SAMs have lower order and coverage structure than $C_{16}H_{33}SH$/Pd SAMs. Moreover, studies of thiol/Pd SAMs of Love et al[1] also suggested the hypothesis that a thin interphase of PdS formed between the oriented monolayer of alkanethiolates and the bulk palladium film could account for higher resistance of $C_{16}H_{33}SH$ SAMs. And, the difference between thickness of 24h-$(C_{16}Se)_2$ SAMs and that of 24h-$C_{16}H_{33}SH$ SAMs was about $4A^o$; it indicates that the tilt of alkyl chain of $(C_{16}Se)_2$ SAMs is higher than that of $C_{16}H_{33}SH$ SAMs. This is along with the data collected from RAIRS and CA experiments. Further, to investigate the binding structure of our $(C_{16}Se)_2$ SAMs, we also employed XPS experiments.

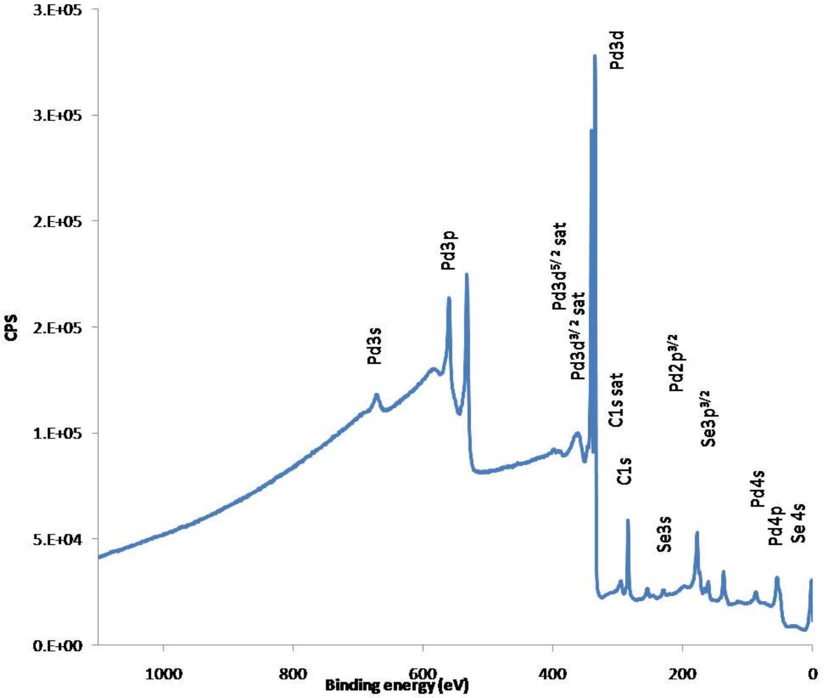

Figure 3.7: Survey scan XPS spectrum of $(C_{16}Se)_2$ SAMs

3.3.5 XPS results

The survey scan spectrum of bis(hexadecyl)-diselenide SAMs formed on Pd films is showed in Figure 3.7 together with high-resolution spectra for the core regions of palladium (Figure 3.8a) carbon (Figure 3.8b) and selenium (Figure 3.9a and 3.9b) atoms. From the XPS survey scan spectrum of the $(C_{16}Se)_2$ SAMs, we found that the evidence of oxygen containing species on bis(hexadecyl)-diselenide SAMs/Pd films is obscure by the fact that the O(1s) binding energy region (from 530eV to 535eV)[18] is merged with the Pd($3p^{3/2}$) core level binding energy region (532-534eV)[19]. We also observe an low intensity and broad peak of oxygen at O(2s) core level (21-29eV)[20]. It suggest a possible presence of oxygen containing species on structure of bis(hexadecyl)-diselenide/Pd SAMs. The selenium species also is present on the surfaces of bis(hexadecyl)-diselenide/Pd SAMs with specific broad peaks at 54.0-59.1 eV assigned to Se(3d)[21], at 229-230eV for Se(3s)[22], and at 159-161eV for Se(3p)[23] core level region. Examination of the SAMs by high resolution XPS spectra of Pd, Se and C may reveal the bonding nature among these elements.

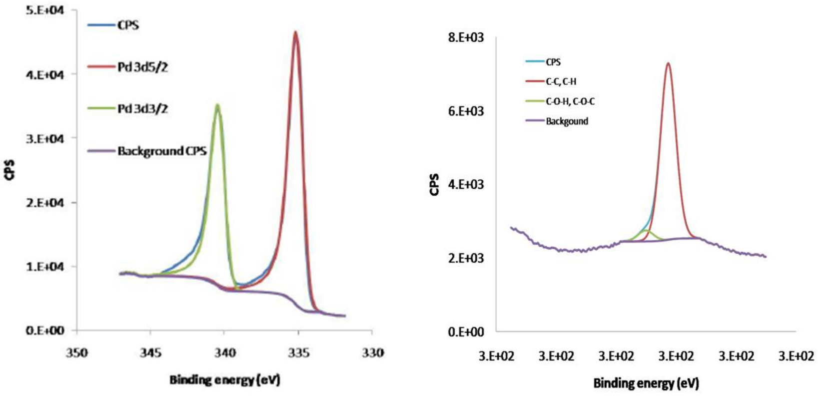

a

b

Figure 3.8: High-resolution XPS data for the Pd(3d)(a) and C (1s)(b) core levels of $(C_{16}Se)_2$ SAMs

The line shape of the high-resolution Pd(3d) core level spectra show two components: one with binding energy at 340.5 eV ($3d^{3/2}$) and another at 335.3eV ($3d^{5/2}$). The high resolution XPS spectrum for Pd(3d) clearly showed photoemission peaks that are attributed to one type of Pd containing species on the interface of bis(hexadecyl)-diselenide SAMs/Pd monolayers. Since there is one type of Pd containing species and the binding energies of Pd($3d^{3/2}$) at 340.5 eV and Pd($3d^{5/2}$) at 335.3eV core level of our sample are lower than those of Pd($3d^{3/2}$) at 342.2eV and Pd($3d^{5/2}$) at 337.1 eV fof PdO and PdOx [24]-[26]; we can confirm that there is no oxidation of Pd substrates by oxygen. Moreover, the high resolution of XPS spectrum at C(1s) core level shows two photoemission peaks of C present on the surface of our prepared sample; one with sharp shape and higher intensity at 285eV can be assigned to C from the aliphatic chain of bis(hexadecyl)-diselenide, other with broad shape and smaller intensity at 286.5eV can be attributed to the existence of C-O, C=O substituted species which was suggested by previous study of decaneselenol/gold SAM[27]. The existence of C-O, C=O substituted species also explains for the present of low intensity and broad peak of oxygen at O(2s) core level observed in survey scan of our sample.

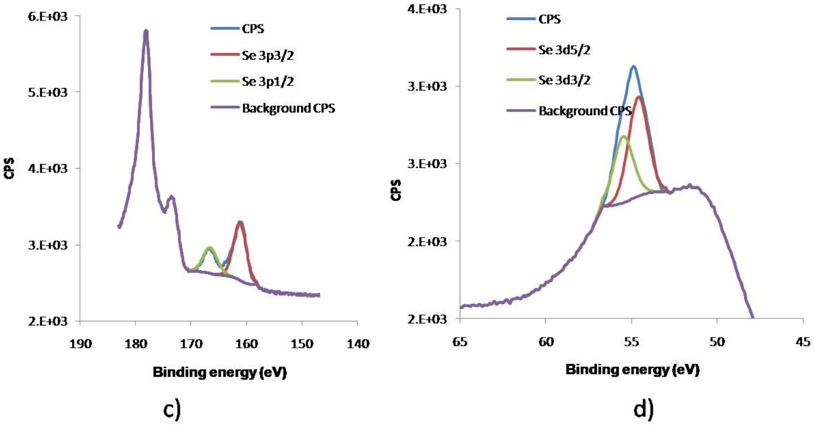

c) d)

Figure 3.9: High-resolution XPS data for the Se(3p) and Se(3d) core levels of $(C_{16}Se)_2$ SAMs

High resolution XPS also is applied to selenium element in order to investigate the Pd-Se bonds and binding energy shift in the core and valence levers of Se. Figure 3.9a shows the fitting data of selenium two spectra lines, Se ($3p^{1/2}$) with only one single peak at 166.2eV and Se ($3p^{3/2}$) also with one peak at 160.9eV. The high-resolution XPS data for the Se (3d) core levels (Figure 3.9b) also shows 2 peaks, at 55.3 and 54.5eV and they can be assigned to Se ($3d^{3/2}$) and Se ($3d^{5/2}$) peaks, respectively. Both high resolution XPS spectra of bis(hexadecyl)-diselenide SAMs at Se(3p) and Se(3d) core levels confirm that there is only one type of selenium containing specie. Since the selenium specie revealed in these XPS data is not likely one that can be related to SeO_2 which shows photoemission peak of Se (3d) at higher binding energy region (59.8 eV)[28], we can assign the selenium specie which present in the surface of our SAMs to the selenium in Pd-Se-C bond. With the fact that XPS spectra of our bis(hexadecyl)-diselenide SAMs on Pd have shown only one type of selenium, we may conclude that the bonding at the surface of bis(hexadecyl)-diselenide SAMs can be heterogeneous binding structure. we successfully make a bis(hexadecyl)-diselenide SAMs on Pd substrates. This results is remarkable as comparing to many failure in preparing high-quality C16Se SAMs on Au and Ag by other groups [29]. It may suggest that selenium based SAMs on the Pd substrate can product well defined monolayer than on other coinage metals.

3.3.6 Conclusion

The data presented in this chapter indicate that a new selenium based SAMs on palladium is formed during the immersion of Pd substrates into $(C_{16}Se)_2$ solution. 24h is also considered as the optimum immersion time to form this SAMs. Electrical and macroscopic properties of the structure $(C_{16}H_{33}Se)_2$/Pd SAMs surface was reveals with different characteristic as comparing to that $C_{16}H_{33}SH$/Pd SAMs due to the stronger metal properties of selenium head-groups and rougher surface of $(C_{16}H_{33}Se)_2$/Pd SAMs. A homogenous bonding environment between Pd and Se atoms was observed through investigations with XPS experiments. This implies that this new SAMs can be applied as alternative to alkylthiol/Pd SAMs when the stronger and homogenous bonding interactions between substrate-headgroups are required. However, this new SAMs with lower resistance may be less useful as an etch resistance materials. Moreover, further studies is necessary for better understanding the roughness changing trends which mainly affect our SAMs properties.

References

[1] Love, J. C.; Wolfe, D. B.; Chabinyc, M. L.; Paul, K. E.; Whitesides; G. M. *J. Am. Chem. Soc.* **2002**, 124, 1576.

[2] Alain, C.; Matthias, G.; Heinz, S.; Bruno, M.; and Emmanuel, D. *Langmuir*, **2002**, 18, 2406.

[3] James, A. W. and Christopher, B. G. *J. Phys. Chem. C* **2007**, 111, 12804.

[4] Pilar, C.; Gaston, C.; Aldo, A. R.; Guillermo, A. B.; Mariano, H. F. and Roberto, C. S. *Langmuir*, **2010**, 26(18), 14655.

[5] Love, J. C.; Urbach, A. R.; Prentiss, M. G.; Whitesides, G. M. *J. Am. Chem. Soc.* **2003**, 125, 12696.

[6] Jan, M.; Andreas, T. Inorganica Chimica Acta **2006**, 359 4821.

[7] Chaudhury, M. K.; Whitesides, G. M. *Science*, **1992**, 256, 1539.

[8] Wenzel, R.N., *Ind. Eng. Chem.* **1936**, 28, 988.

[9] Young, P. T. *Trans. R. Soc. London* **1805**, 95, 65.

[10] Cassie, A. B. D.; Baxter, S. *Trans. Faraday Soc.* **1944**, 40, 546)

[11] Bico, J.; Marzolin, C.; Quere, D. *Europhys. Lett.* **1999**, 47, 220.

[12] Quere, D. *Physica A* **2002**, 313, 32.

[13] Johnson,R.E. , Dettre, R.H. *Adv. Chem. Ser.* **1964**, 43 112.

[14] Ulman, *A. An introduction to Ultra-thin Film from Langmuir Blodgett to Self-Assembly*; **1991**, Academic Press, Inc.: New York.

[15] Poirier, G. E. *Langmuir* **1997**, 13, 2019.

[16] Sun, L.; Crooks, R. M. *Langmuir* **1993**, 9, 1951.

[17] Yaliraki, S. N.; Kemp, M.; Ratner, M. A. *J. Am. Chem. Soc.* **1999**, 121, 3428.

[18] Kim, K.S.; Gossmann, A.F.; Winograd, N. *Anal. Chem.* **1974**, 46, 197.

[19] Hillebrecht, F.U.; Fuggle, J.C.; Bennett, P.A.; Zolnierek, Z. *Phys. Rev. B* **1982**, 27, 2179.

[20] Legare, P.; Fritsch, A. *Surf. Interface Anal.* **1990**, 15, 698.

[21] Agostinelli, E.; Battistoni, C.; Fiorani, D.; Mattogno, G.; Nogues, M. *J. Phys. Chem. Solids* **1989**, 50, 269.

[22] Shalvoy, R.B.; Fisher, G.B.; Stiles, P.*J. Phys. Rev. B* **1977**, 15, 1680.

[23] Thomas, J.M.; Adams, I.; Williams, R.H.; Barber, M. *J. Chem. Soc. Faraday Trans. II* **1972**, 68, 755.

[24] Fleisch, T.H.; Zaiac, G.W.; Schreiner, J.O.; Mains, G.J. *Appl. Surf. Sci.* **1986**, 26, 488.

[25] Moddeman, W.E.; Bowling, W.C.; Carter, D.C.; Grove, D.R. *Surf. Interface Anal.* **1988**, 11, 317.

[26] Noack, K.; Zbinden, H.; Schlogl; R. *Catal. Lett.* **1990**, 4, 145

[27] Ishida, T.; Tsuneda, S.; Nishida, M.; Hara, M.; Sasabe, H.; Knoll, W. *Langmuir* **1997**, 13, 4638.

[28] Malmsten, G.; Thoren, I.; Hogberg, S.; Bergmark, J.E.; Karlsson, S.E. *Phys. Scripta,* **1971**, 3, 96.

[29] Shaporenko, A.; Ulman, A.; Terfort, A.; andZharnikov, M.; *J. Phys. Chem. B* **2005**, 109, 3898.

Chapter 4

Cyclopentadienyl Chromium Hydrazide Materials for hydrogen storage

4.1 Introduction

Because of the environmental and economic problems associated with the overuse of fossil fuels[1], researchers continue to develop a variety of alternative energy sources. Hydrogen is the ideal fuel because it is lightweight, abundant, and water is its only combustion product. However, hydrogen storage still remains a great hurdle[2]. The 2010 target set by the U. S. Department of Energy (DOE) is 4.5 wt% and 1.3 $kWhL^{-1}$ (0.028 kg hydrogen L^{-1}) for a fully reversible system operating near room temperature[3]. Some of the more promising technologies involve the use of chemical carriers such as alloys[4] and metal hydrides[5], or adsorbents such as amorphous carbons[6], zeolites[7], and metal-organic frameworks[8]. While metal hydrides are thwarted by heat management issues and slow kinetics, physisorption materials typically lose 80 - 90 wt% of their performance at room temperature due to low heats of adsorption (typically 5 - 13 kJ mol^{-1})[9]. To achieve the DOE target under ambient conditions, the ideal H_2 binding energy is predicted to be in the range of 20 - 30 kJ.mol^{-1} H_2[10]. Many current experimental[11] and theorical[12] investigations focus on the engineering of adsorption sites on porous solids for improving binding enthalpies. Recent advances in our group indicate that coordinatively unsaturated low-valence transition metal centers supported on mesoporous silica can function as ideal $\sigma - \pi H_2$(Kubas-type)[13] binding sites with enthalpies as high as 23 kJ.mol^{-1}[14]. These composites demonstrate up to 40% relative retention of storage capacity per metal site at room temperature; however the low concentration of active metal sites and the high degree of unused void space prevent the overall capacities from reaching practical values.

4.2 Experimental Section

4.2.1 Synthesis of Cyclopentadienyl Chromium Hydrazide Materials

Bis(cyclopentadienyl) chromium was purchased from Aldrich. Anhydrous hydrazine was prepared by aezotropic distillation using toluene as entrainer fluid[24]. The reaction between bis(cyclopentadienyl) chromium and hydrazine were carried out in dry toluene solvent. After that, the reaction mixture was filtered and the obtained solid which was then heated in vacuum at 60 ^oC, 100 ^oC, and 150 ^oC. *All reactions were conducted in an argon glove box using rigorously moisture and air-free conditions.

1) CrN21 materials. Bis (cyclopentadienyl) chromium (4g, 22mmol), purchased from Strem Chemicals, was mixed with 100ml toluene and stirred at 50^oC for 60 minutes under argon until a homogeneous solution was obtained. Anhydrous hydrazine (0.37ml, 11mmol), dried and distilled

using a toluene azeotrope, was added dropwise to the solution. The reaction vessel was sealed and the stirred at 50C for 4hours, 75^oC for 4 hours, and 100^oC for 24 hours. The precipitate was collected by filtration and dried under vacuum at room temperature for 6 hours, and the collected black solid was then heated in vacuo at 0.02mmHg and $60^oC$for 48 hours to yield CrN2160, 100^oC for 48 hours to yield CrN21100, and 150^oC for 48 hours to yield CrN21150.

2) CrN11 materials. The materials CrN1160, CrN11100, and CrN11150 were made by the same procedure described above for the CrN21 materials, however a molar ratio of $1:1$ between bis (cyclopentadienyl) chromium and hydrazine was used.

3) CrN12 materials. The materials CrN1160, CrN11100, and CrN11150 were made by the same procedure described above for the CrN21 materials, however a molar ratio of $1:2$ between bis (cyclopentadienyl) chromium and hydrazine was used.

*All cyclopentadienyl chromium hydrazide materials samples was named in Table 4.1.

4.2.2 Hydrogen adsorption measurements

The hydrogen adsorption/desorption isotherms were measured by a computer controlled commercial Sieverts apparatus manufactured by Advanced Materials Corporation, Pittsburgh, PA. Highly purified

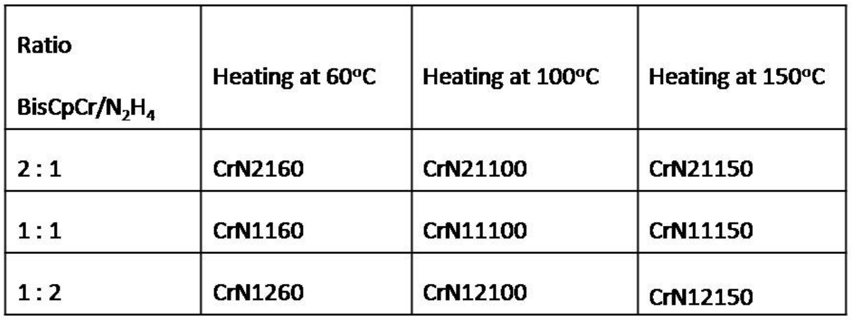

Ratio BisCpCr/N_2H_4	Heating at 60°C	Heating at 100°C	Heating at 150°C
2 : 1	CrN2160	CrN21100	CrN21150
1 : 1	CrN1160	CrN11100	CrN11150
1 : 2	CrN1260	CrN12100	CrN12150

Table 4.1: Sample names for cyclopentadienyl chromium Hydrazide Gels

hydrogen (99.9995% purity) was used as the adsorbent. Typically the mass used for the hydrogen sorption measurement was 500-1000mg. The size of the sample chamber is 2.5 cm^3. Lightly packed powder materials were used for all measurements. Before all measurements the materials were degassed at 200^oC under high vacuum for at least one day in order to remove any volatile impurities. A simplified sketch of this apparatus is shown in Figure 4.1. The temperature of the gas reservoir was measured by two AD590 IC thermometers that are calibrated against a standard mercury thermometer within 0.1^oC at room temperature. The sample temperature was measured with type K thermocouple by converting a voltage reading to temperature according to ITS-90 (The International Temperature Scale of 1990). The limits of error are 2^oC or 0.75 % above 0^oC and 2^oC or 2 % below 0^oC. The pressure of both the gas reservoir and sample chamber was measured by Heise model HP0 pressure transducer, which has a range of 1500 psi (about 100 bar). The accuracy of this transducer was rated to be 0.05 % of the full scale including non-linearity, drift, and hysteresis. The GRC operates by admitting an appropriate amount of gas to the reservoir and determines its molar amount from its pressure and temperature. The system then manipulates the valves between the reservoir and the reaction chamber and transfers a desired amount of the gas from the reservoir to the gas reaction chamber. After equilibrium is attained, the system re-calculates the number of hydrogen molecules. The number missing from the gas phase corresponds to the number of molecules absorbed by the sample. The system employs a modified Benedict-Webb-Rubin equation of state in calculating the amount of absorbed hydrogen from the pressure, temperature, and volume. The apparatus gradually increases the hydrogen pressure to the maximum specified value, while summing the sorbed hydrogen. The amount of hydrogen released from the sample is then determined by pumping out the gas reservoir and gradually bleeding hydrogen from the sample chamber into the gas reservoir. During the test process the sample chamber was immersed in water for room temperature measurements and liquid nitrogen or liquid argon for cryogenic measurements, and the liquid level was maintained unchanged.

$$\ln\left(\frac{P_1}{P_2}\right) = \Delta H_{ads} * \frac{T_2 - T_1}{R * T_1 * T_2} \tag{4.1}$$

The isosteric heats of adsorption (ΔH) were calculated using hydrogen-adsorption isotherms measured at different temperatures (77K and 87K) based on the Clausius-Clapeyron equation.

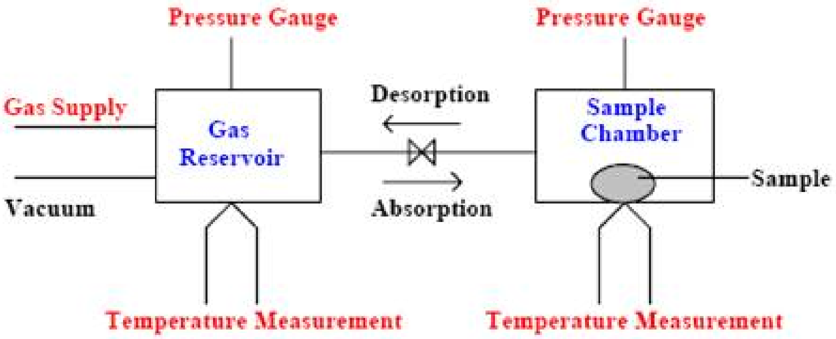

Figure 4.1: Schematic drawing of the GRC system

Where:

P_i : Pressure for isotherm i.

T_i : Temperature for the isotherm i.

R: Gas constant

Pressure as the function of the amount adsorbed was determined by using exponential fit for each isotherm, the first ten points of the isotherms were picked and fit to the exponential equation (See figures 4.6, 4.7 and 4.8 at Supplemental information section). This exponential equation gives an accurate fit over the pressure up to 10 bar and with the goodness of fit (R^1) above 0.97. The corresponding P_1 and P_2 at a certain amount H_2 adsorbed of both temperatures can be obtained by the simulated exponential equation. Then input these numbers into the equation 1, the enthalpies of the adsorption were calculated.

4.2.3 Characterization

Powder X-ray diffraction (XRD) was performed on Siemens D-500 diffractometer with Cu Kσ radiation (40KV, 40mA). The step size was 0.02^o and the counting time was 0.3s for each step. Diffraction patterns were recorded in the 2θ range 2.3 - 30^o. Samples for XRD analysis were put in a sealed capillary glass tube to protect sample from air and moisture during experiment. Nitrogen adsorption and desorption data were collected on a Micromeritics ASAP 2010 The skeletal densities of the samples were measured by a Quantachrome Micro-Ultrapycnometer 1000 using helium gas. XPS (X-ray photoelectron spectroscopy) measurements were performed at Hydro-Qubec Research Institute, Chemistry and Materials, 1800 Boul. Lionel-Boulet, Varennes, Quebec, J3X 1S1, Canada. All emissions were referenced to the carbon C 1s (CF_2) peak of a Teflon internal standard at 292.3 eV using a Physical Electronics PHI-5500 spectrometer. Charge neutralization was not necessary.

4.3 Results and discussion.

In this chapter, we report a new class of transition metal-based materials in which hydrazine is used as a low molecular weight bridging ligand to link together coordinately unsaturated cyclopentadienyl Cr centers into an amorphous network, hence minimizing void space while also preventing clustering and maximizing the concentration of high enthalpy Kubas binding sites. These materials possess hydrogen storage capacities of 1.75 wt % at 77 K at 80 bar, with a negligible contribution from physisorption, and show a surprisingly high 47.6 % retention of performance at 298 K relative to 77 K with heats of adsorption that rise from 10-47 kJ mol^{-1} with surface coverage. They also display fully reversible linear isotherms that do not saturate at 80 bar. These physical properties make them distinct from both physisorption materials and metal hydrides, and for this reason they are best considered to belong to a new class of materials that appear to use Kubas binding as a primary means of hydrogen storage.

When bis (cyclopentadienyl) chromium reacts with hydrazine at molar ratios of 2:1, 1:1 and 2:1 in toluene dark air-sensitive precipitates are formed. These precipitates are heated at 60 ^oC, 100 ^oC and 150 ^oC to obtain the materials CrNXX60, CrNXX100 and CrNXX150, respectively, where XX denotes the Cr:hydrazine ratio (Table 4.1). A possible mechanism for this reaction is shown in Figure A.1. Nitrogen adsorption/desorption isotherms (Figure A.2, A.3,and A.4) for these solids are indicative of low surface areas with a broad distribution of pore sizes[15]. The BET surface areas (Figure A.2, A.3,and A.4) fall in the range of 10 - 30 m^2/g (Table A.1). The XRD patterns (Figure A.5a, b and c) display a single broad peak in the 2θ range 3-5^o suggesting a lack of long-range order. The elemental analysis is shown in Table A.2. In general, increasing the amount of hydrazine increases the percentage of nitrogen in the sample while also decreasing the percentage of carbon. Heating the sample has the same effect, presumably by driving the protolysis and elimination of the Cp ligands further to completion. The C and N percentages in the elemental analysis are low as compared to the expected values for the hypothetical polymer "$C_5H_8N_2Cr$" (40.81%C, 19.04%N, 35.37%Cr). This is likely due to carbide and nitride formation during combustion analysis of the sample, common in the elemental analysis of early transition metal species.

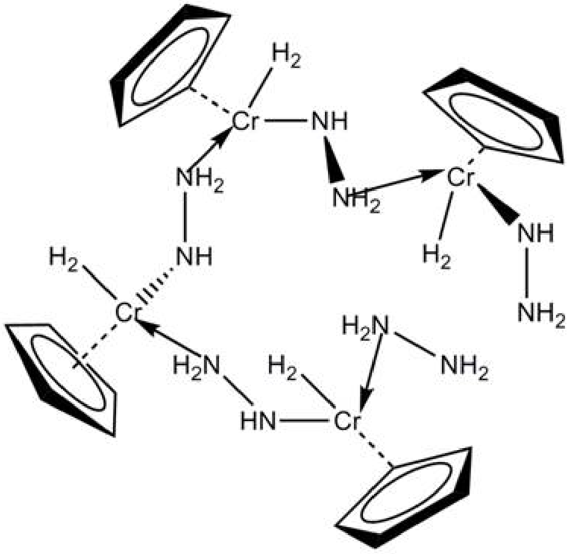

Figure 4.2: Proposed structure of CpCr hydrazide gel.

The XPS spectrum of all materials (Figure A.6) exhibit a broad emission at 400.3 eV in the N 1s region with a weak satellite 1-2 eVs lower than the principal peak position. This can be simulated as two emissions in the N 1s region, with one major peak at 400.4 eV and another smaller peak at 398.7 eV. On the basis of previous values reported in the literature for related monomeric compounds[16], the emission at higher binding energy is assigned to time averaged NH and quaternary NH_2 species bound to Cr. The minor emission at lower binding energy is assigned to terminal NH_2 groups. The Cr $3p^{1/2}$,$3p^{3/2}$ region of the spectra (Figure A.7, A.8 and A.9) can be simulated as four major species with emissions at 569.8 eV, 571.7 eV, 572.7 eV, and 573.5 eV (with spin-orbit counterparts at 578.7 eV, 580.8 eV, 581.9 eV and 582.7 eV), with several low-intensity emissions falling above 575 eV and 584 eV, respectively. This is consistent with Cr sites with oxidation states ranging from Cr (II) to Cr(III)[17]. For comparison, bis CpCr (II)[16a],[18] displays 3p 1/2, 3/2 emissions at 574.8 eV and 583.6 eV and CrN (III) shows $3p^{1/2}$,$3p^{3/2}$ emissions at 575.8 eV and 584.7 eV[18]. The fact that the major species all possess emissions that fall lower than 575.8 eV and 584.7 eV for the spin-orbit doublet pairs is consistent with Cr (II) species with only one Cp group, as this ligand is electron withdrawing. The presence of Cr(III) is not unexpected, as the oxidation of Cr (II) to Cr (III) has been observed previously in reactions between Cp_2Cr with silica[19].

The excess storage isotherms of these materials from 0-80 bar at 298 K are shown in Figure 4.3. The gravimetric and volumetric adsorption capacity of CrN11100 is 0.73 wt. % (Figure 4.2) and 11.77 kg.m^{-3} (Table A.1), the highest of all samples. The isotherms are also linear and do not saturate. The appearance of these isotherms relative to that of a standard physisorption isotherm typified by carbon AX-21 (Figure A.10) coupled with the low surface areas indicate that the principal mechanism of storage is not physisorption. Excess storage isotherms of all materials were also measured at 77 K (Table A.1) and showed gravimetric adsorption of 1.75 wt % and a volumetric adsorption 31.68 kg.m^{-3} for CrN11100. From these results the molar ratio of 1:1 and heating temperature of 100 ^{o}C were determined to be the best synthesis conditions for optimal hydrogen storage performance. On the basis of the elemental analysis results these values equate to 0.40 H_2 per Cr at 298 K and 0.97 H_2 per Cr at 77 K for CrN11100 (Table A.4). Comparing the values measured at 77 K to those recorded at room temperature, there is surprisingly high retention of storage capacity (Table A.3) of up to 47.6%. This is much greater than MOF-5 and AX21, which retain 22.2% and 13.2%, respectively. A 20 cycle-run at 298 K to 80 bar was conducted on CrN11100 without any detectable loss of storage capacity (Figure A.11).

The isosteric heats of adsorption (ΔH) were calculated from hydrogen-adsorption isotherms measured at 77 K and 87 K using the Clausius-Clapeyron equation. The data for materials heated at 100 ^{o}C and 150 ^{o}C as well as that for carbon AX-21 measured in our lab under the same conditions are shown in Figure 4.4. The isosteric heats of adsorption for

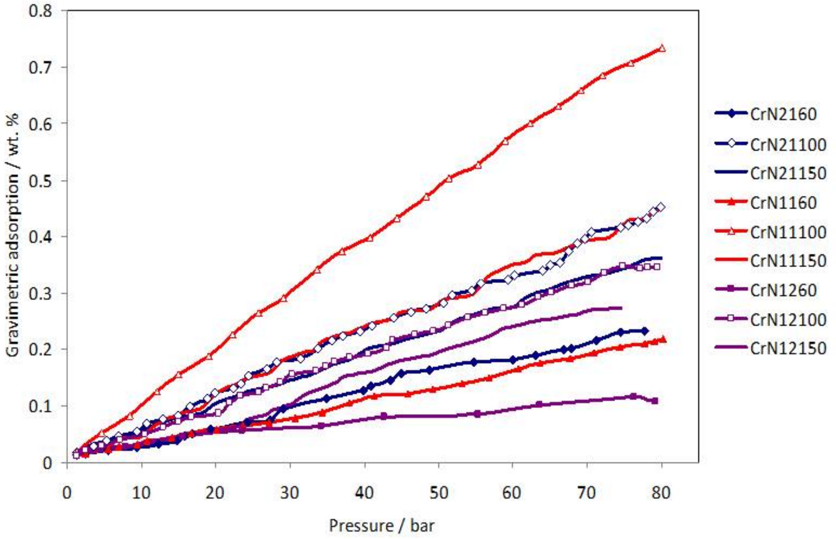

Figure 4.3: Excess storage isotherms of Chromium hydrazide materials at 298 K recorded up to 80 bar

all CrN materials rise on surface coverage from roughly 10 kJ.mol^{-1} to over 40 kJ.mol^{-1} with the average falling in the 20-30 kJ.mol^{-1} range predicted for room temperature performance. This contrasts to AX-21 which possesses enthalpies that decrease with surface coverage from 6-4 kJ.mol^{-1}. The rising enthalpy behavior has been observed previously by our group in all cases where transition metal binding sites are suspected to be contributing to hydrogen storage[19] and suggests, along with the linear isotherms, a different mechanism of adsorption distinct from physisorption (ΔH ~5-13 kJ.mol^{-1})[20] and hydrides (ΔH ~ 80 kJ.mol^{-1}). Physisorption is ruled out on the basis of high enthalpies and low surface areas relative to the hydrogen storage values (for 1.6 wt% at 77 K and 80 bar a surface area of ca. 1000 $m^2.g^{-1}$ would be required if physisorption was the operative mechanism). Metal hydride formation is ruled out because there is little or no kinetic barrier to adsorption and the oxidative addition of hydrogen to Cr(II) to form a Cr(IV) dihydride is unfavourable. The binding enthalpies are also too low for hydride formation, but fall within the expected range for the Kubas interaction[13][21]. The reason for the rising trend in these enthalpies is not fully understood, but may be related to the presence of multiple binding sites of varying enthalpies or a trend in increasing enthalpy with subsequent hydrogen ligation as predicted by Yilidrim[22] and Heben[23].

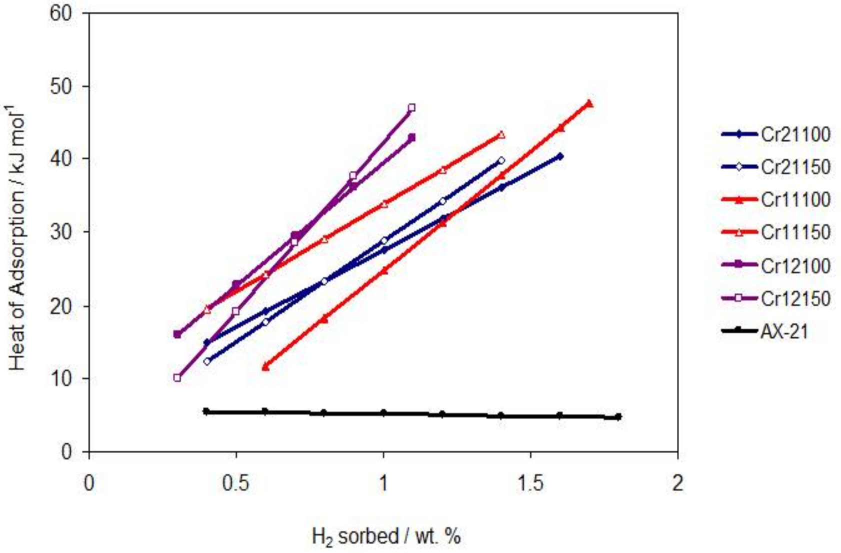

Figure 4.4: Enthalpies of H_2 adsorption for CrN11100, CrN12100, CrN11150, CrN12150, CrN21100, CrN21150 and carbon AX21r

4.4 Conclusion

In summary, novel cyclopentadienyl chromium hydrazide gels were synthesized and tested for hydrogen storage with a view towards exploiting the vacant Cr sites for Kubas binding. These materials displayed the highest retention of hydrogen storage capacity ever recorded (47.6% over the range of 298 K to 77 K) and isosteric heats of adsorption that rise from 10-40 kJ.mol^{-1}. The fact that saturation was not reached at 80 bar and a maximum of 1 functional binding site per Cr was generated suggests that even greater storage capacities can be attained at higher pressures or in systems with more than 1 active site per metal. This research thus stands as a starting point for the development of a new class of materials for practical on-board hydrogen storage operating at or near ambient temperature at moderate pressure.

References

[1] a) Schlapbach, L.; Zuettel, A. *Nature* **2001**, 414, 353; b) Cohen, R. L.; and Wernick, J. H., *Science* **1981**, 214, 1081.

[2] Zuettel, A.; Borgschulte, A.; Schlapbach, L., Hydrogen as a Future Energy Carrier, WILEY-VCH Verlag GmbH & Co. KGaA, Weinheim, **2008**.

[3] http://www1.eere.energy.gov/hydrogenandfuelcells/storage/current-technology.html, US Department of Energy Website. Retrieved on November 20th, **2009**.

[4] Seayad, A. M.; Antonelli, D. M. *Adv. Mater.* **2004**, 16, 765;

[5] a) Wiswall, Jr. R. H.; Reilily, J. J. *Science* **1974**, 186, 1158; b) Orimo, S.; Nakamori, Y.; Eliseo, J. R.; Zuettel, A.; Jensen, C. M. *Chem. Rev.* **2007**, 107, 4111.

[6] Yang, R. T.; Wang, Y. *J. Am. Chem. Soc.*, **2009**, 131, 4224.

[7] Pacula, A.; Mokaya, R. *J. Phys. Chem. C* **2008**, 112, 2764.

[8] a) Thomas, K. M. *Dalton Trans.* **2009**, 1487 - 1505; b) Kaye, S. S.; Dailly, A.; Yaghi, O. M.; Long, J. R. *J. Am. Chem. Soc.* **2007**,

129, 14176. c) Rosi, N. L.; Eddaoudi, M.; Vodak, D. T.; Kim, J.; O'Keeffe, M.; Yaghi, O. M. *Science* **2003**, 300, 1127.

[9] a) Dailly, A.; Vajo, J. J.; Ahn, C. C. *J. Phys. Chem. B* **2006**, 110, 1099; b) Rowsell, J. L. C.; Yaghi, O. M. *Angew. Chem. Int. Ed.* **2005**, 44, 4670.

[10] Lochan, R. C.; Gordon, M. H. *Phys. Chem. Chem. Phys.* **2006**, 8, 1357.

[11] a) Eberle, U.; Felderhoff, M. Schth, F., *Angew. Chem. Int. Ed.* **2009**, 48, 2; b) Li, Y.; Yang, R. T. *J. Am. Chem. Soc.* **2006**, 128, 726; c) Dinca, M., Long, J. R., *Angew. Chem. Int. Ed.* **2008**, 47, 6766.

[12] a) Han, S. S.; Mendoza-Corts, J. L.; Goddard III, W. A. *Chem. Soc. Rev.* **2009**, 38, 1460; b) Trudeau, B. Ye; M., Antonelli, D. M. *Chem. Mater.*, **2002**, 14, 2774; c) Sillar, K.; Hofmann, A.; Sauer, J. *J. Am. Chem. Soc.* **2009**, 131, 4143.

[13] Kubas, G. J. Metal dihydrogen and π-Bond complexes, Kluwer Academic Publishers, 2001; Heinekey, D. M.; Oldham, W. J. *Chem. Rev.* **1993**, 93, 913 - 926.

[14] a)Hoang, T. K. A.; Antonelli, D. M. *Adv. Mater.* **2009**, 21, 1787; b) Hamaed, A.; Trudeau, M.; Antonelli, D. M. *J. Am. Chem. Soc.* **2008**, 130, 6992.

[15] Gregg,S. J.; Sing, K. S. W. Adsorption, surface area and porosity, Academic press, Harcourt Brace & Company, Publishers, **1981**.

[16] a) Biner, H.; Sellman, D. *Z. Naturforsch.* 1978, B33, 173; b) Shulg'a, Y. M.; Troitskii, V. N.; Aivazov, M. I.; Borodk'o, Y. G. *Zh. Neorg. Khimii* **1976**, 21, 2621.

[17] a) Connor, J. A.; Derrick, L. M. R.; Hillier, I. H. *J. Chem. Soc. Faraday Trans.* II 1974, 70, 941; b) Blass, P. M.; Akhter, S.; Seymour, C. M.; Lagowski, J. J.; White,J. M., *Surf. Sci.* 1989, 217, 85.

[18] a) Barber, M.; Connor, J. A.; Derrick, L. M. R.; Hall, M. B.; Hillier, I. H. *J. Chem. Soc.* 1973, 560; b) Groenenboom, C. J.; Sawatzky, G.; Meijer, H. J. D.; Jellinek, F. *J. Organometal. Chem.* **1974**, 76, C4.

[19] Hoang, T. K. A.; Hamaed, A.; Trudeau. M.; Antonelli, D. M. *J. Phys. Chem. C* **2009**, 113, 17240.

[20] a) Nishimura, O.; Yabe, K.; Iwaki, M. *J. Electron Spectrosc. Relat. Phemon.* **1989**, 49, 335; b) Romand, M.; Roubin, M. *Analysis* **1976**, 4, 309.

[21] Saillard, J. -Y.; Hoffmann, R. *J. Am. Chem. Soc.* **1984**, 106, 2006.

[22] Yiridrim,T. ; Cirati, S. *Phys Rev Lett.* **2005**, 94, 1755501

[23] Zhao, Y.; Kim, Y. H.; Dillon, A. C.; Heben, M. J.; Zhang, S. B. *Phys Rev Lett.* **2005**, 94, 155504.

[24] Schmidt, E. W. Hydrazine and its Derivatives. Preparation, Properties, Application. John Wiley & Sons, Inc., **2001**. c) Rosi, N. L., Eddaoudi, M. D. T., 99.007, 129, 14176.

Appendix A

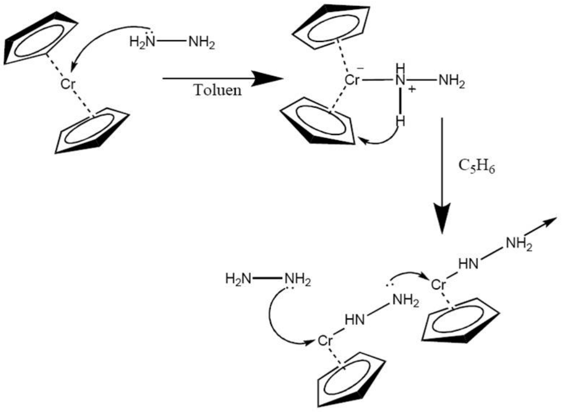

Figure A.1: Proposal mechanism of reaction between bis (cyclopentadienyl) chromium with hydrazine.

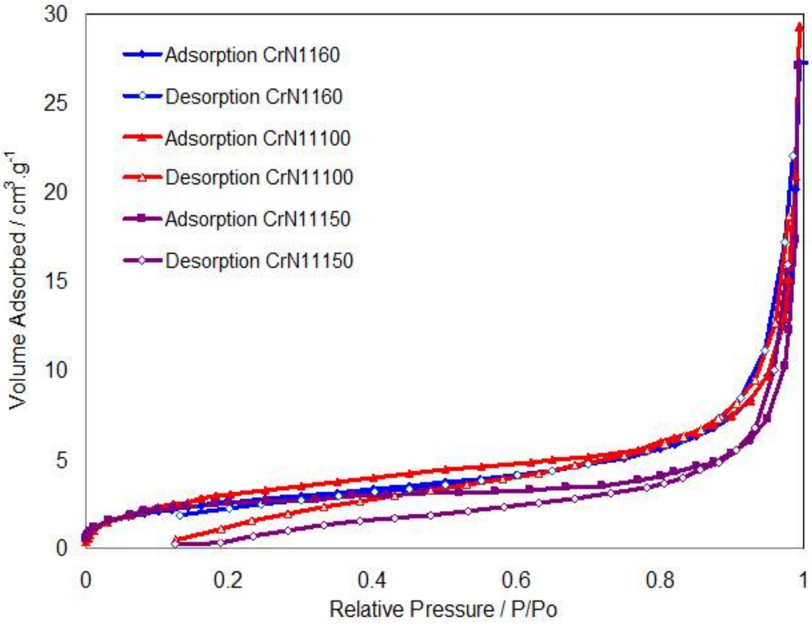

Figure A.2: Nitrogen adsorption/desorption isotherm of CrN11 materials.

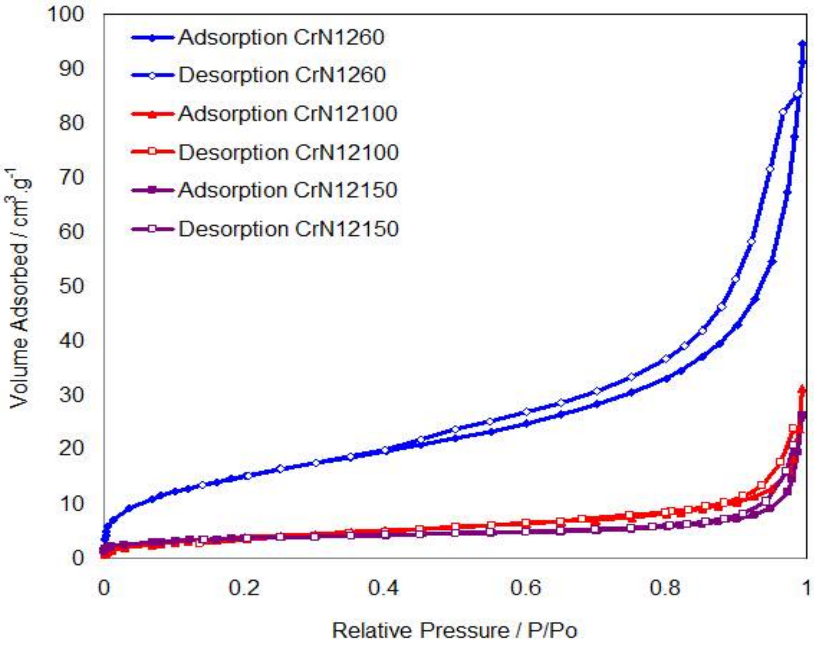

Figure A.3: Nitrogen adsoprtion/desorption isotherm of CrN12 materials

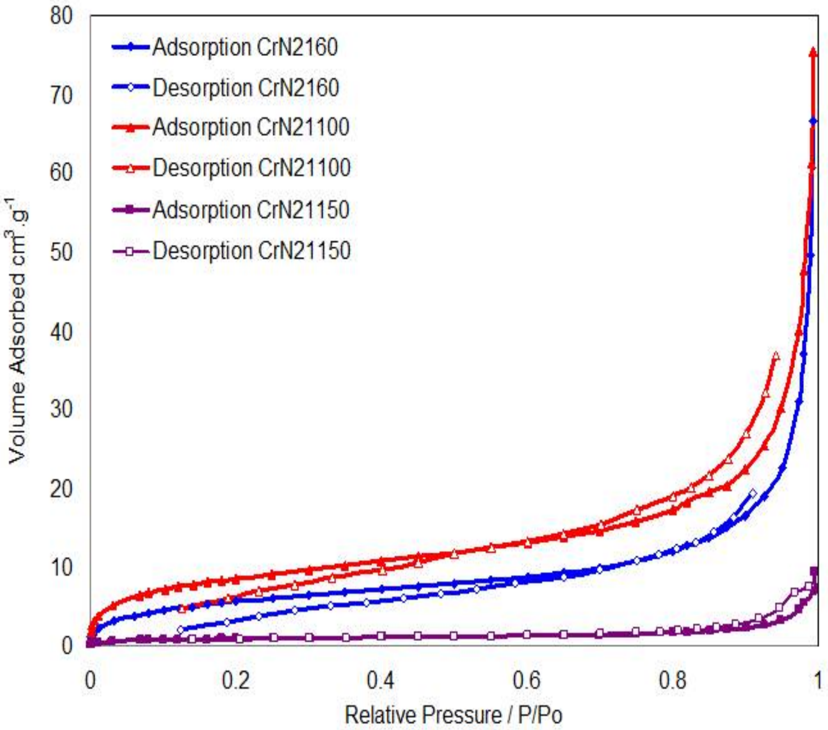

Figure A.4: Nitrogen adsorption/desorption isotherm of CrN21 materials.

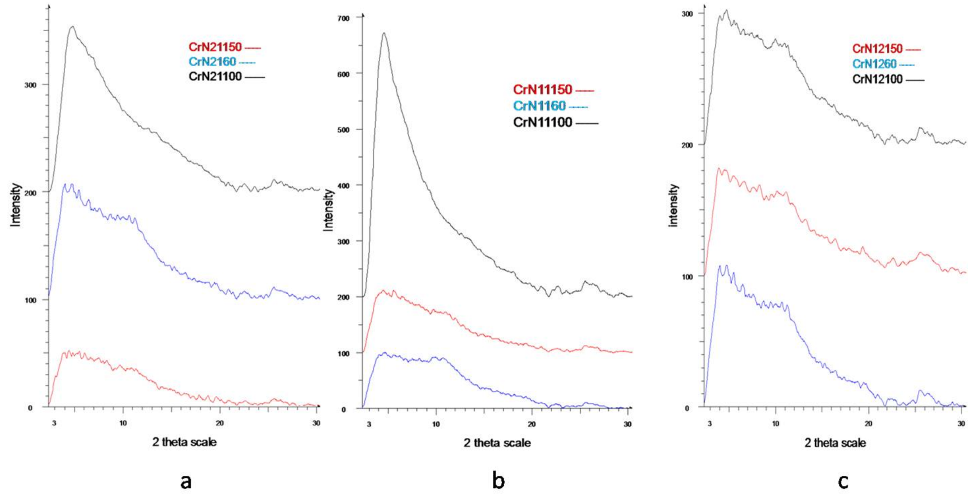

Figure A.5: XRD powder patterns of CrN21, CrN11, CrN12

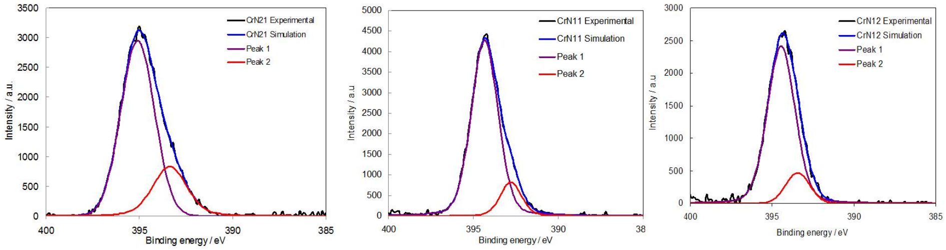

Figure A.6: N 1s region of the XPS spectrum of CrN21100,CrN11100 and CrN12100

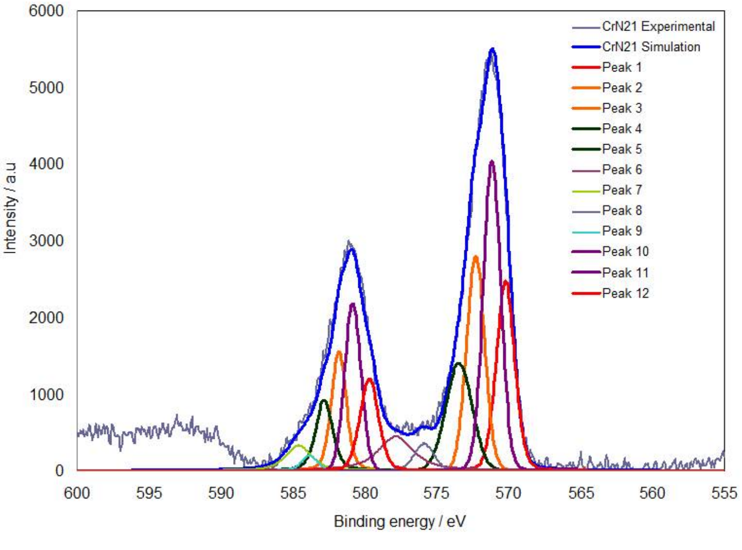

Figure A.7: Cr 2p region of the XPS spectrum of CrN21100

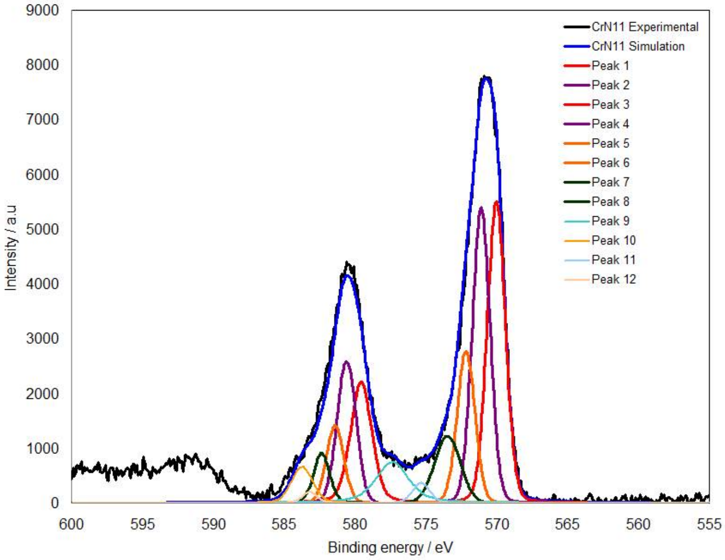

Figure A.8: Cr 2p region of the XPS spectrum of CrN11100

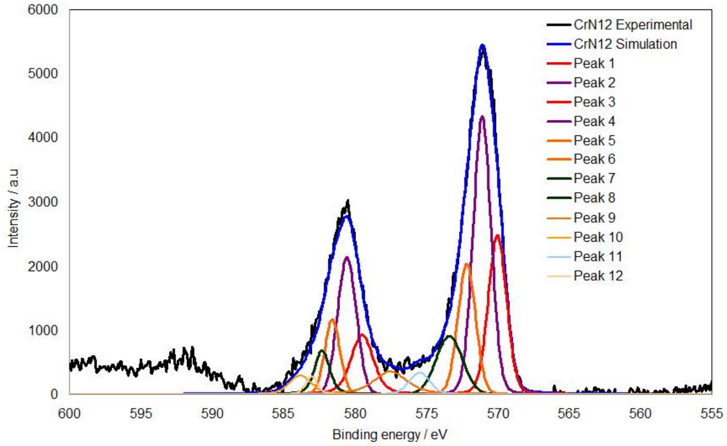

Figure A.9: Cr 2p region of the XPS spectrum of CrN12100

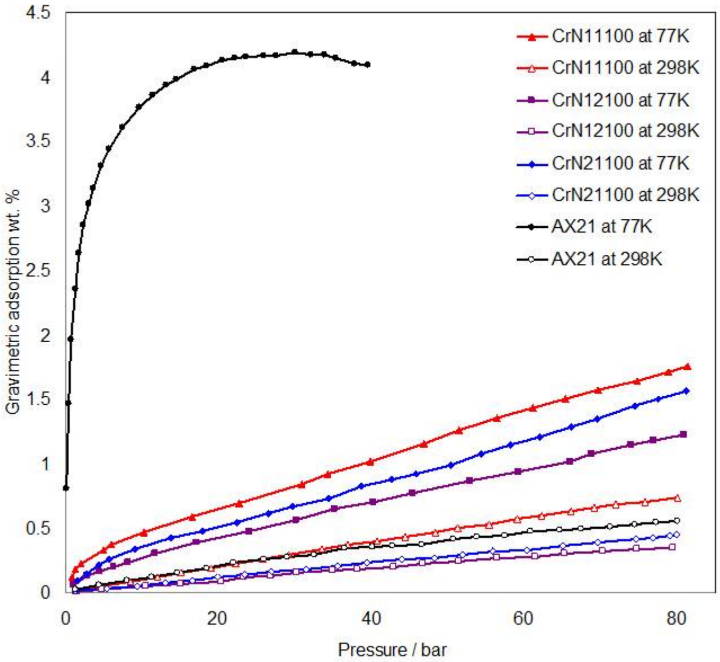

Figure A.10: Excess storage isotherms of CrN11100, CrN12100, CrN21100 and carbon AX21 at 77 K and 298 K

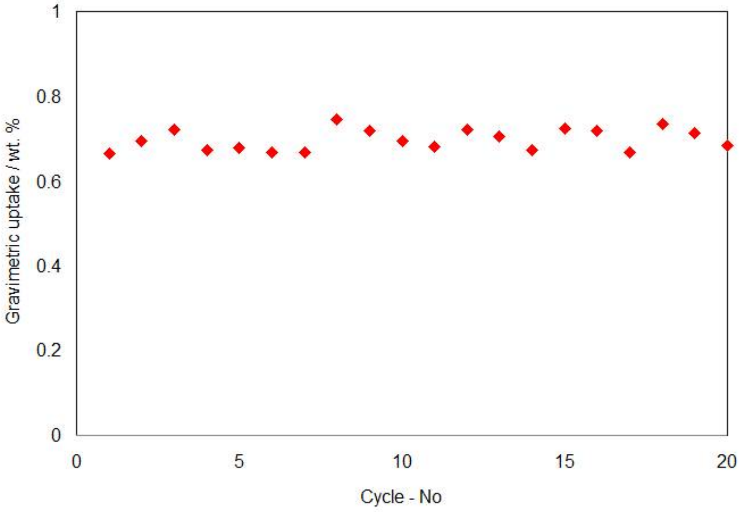

Figure A.11: 20 cycles of adsorption and desorption of CrN11100 at 298K and 80 bar

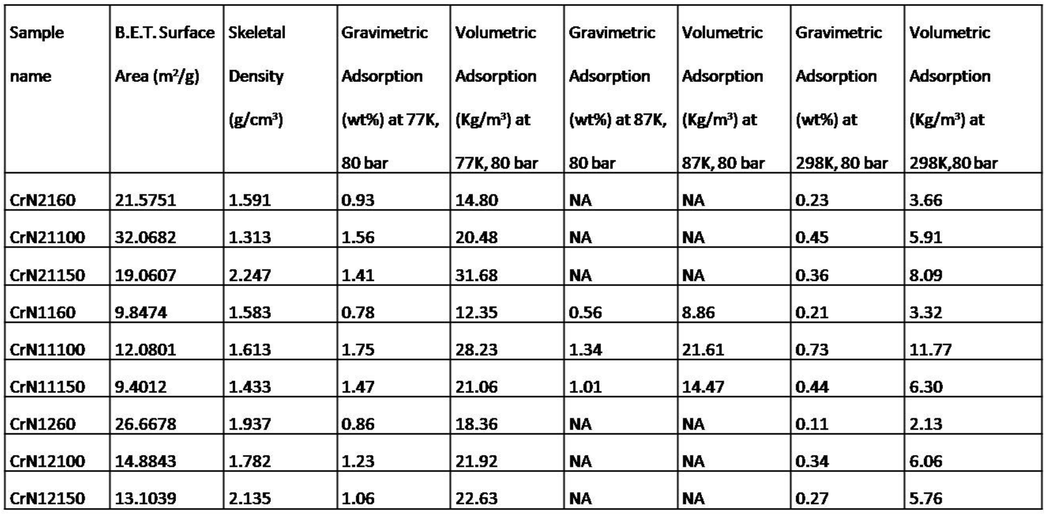

Sample name	B.E.T. Surface Area (m^2/g)	Skeletal Density (g/cm^3)	Gravimetric Adsorption (wt%) at 77K, 80 bar	Volumetric Adsorption (Kg/m^3) at 77K, 80 bar	Gravimetric Adsorption (wt%) at 87K, 80 bar	Volumetric Adsorption (Kg/m^3) at 87K, 80 bar	Gravimetric Adsorption (wt%) at 298K, 80 bar	Volumetric Adsorption (Kg/m^3) at 298K,80 bar
CrN2160	21.5751	1.591	0.93	14.80	NA	NA	0.23	3.66
CrN21100	32.0682	1.313	1.56	20.48	NA	NA	0.45	5.91
CrN21150	19.0607	2.247	1.41	31.68	NA	NA	0.36	8.09
CrN1160	9.8474	1.583	0.78	12.35	0.56	8.86	0.21	3.32
CrN11100	12.0801	1.613	1.75	28.23	1.34	21.61	0.73	11.77
CrN11150	9.4012	1.433	1.47	21.06	1.01	14.47	0.44	6.30
CrN1260	26.6678	1.937	0.86	18.36	NA	NA	0.11	2.13
CrN12100	14.8843	1.782	1.23	21.92	NA	NA	0.34	6.06
CrN12150	13.1039	2.135	1.06	22.63	NA	NA	0.27	5.76

Table A.1: Hydrogen adsorption capacity and surface areas of cyclopentadienyl chromium hydrazide materials

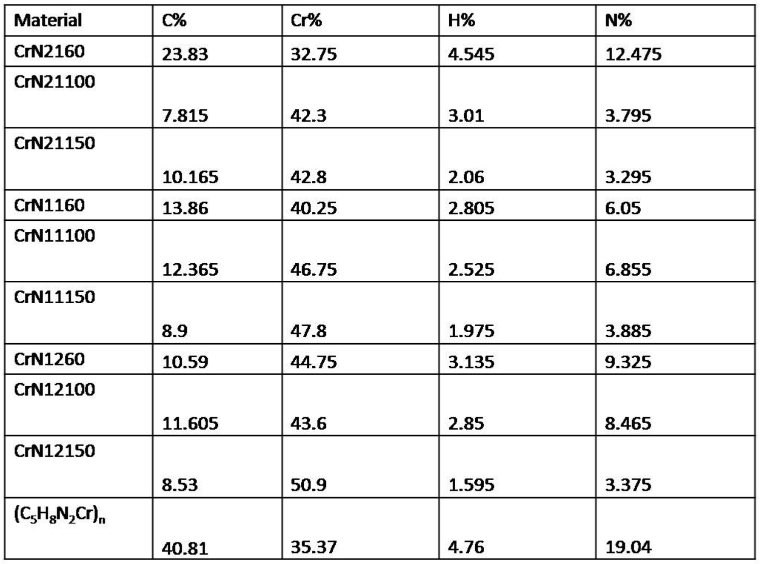

Material	C%	Cr%	H%	N%
CrN2160	23.83	32.75	4.545	12.475
CrN21100	7.815	42.3	3.01	3.795
CrN21150	10.165	42.8	2.06	3.295
CrN1160	13.86	40.25	2.805	6.05
CrN11100	12.365	46.75	2.525	6.855
CrN11150	8.9	47.8	1.975	3.885
CrN1260	10.59	44.75	3.135	9.325
CrN12100	11.605	43.6	2.85	8.465
CrN12150	8.53	50.9	1.595	3.375
$(C_5H_8N_2Cr)_n$	40.81	35.37	4.76	19.04

Table A.2: Elemental analysis of Cyclopentadienyl Chromium Hydrazide materials

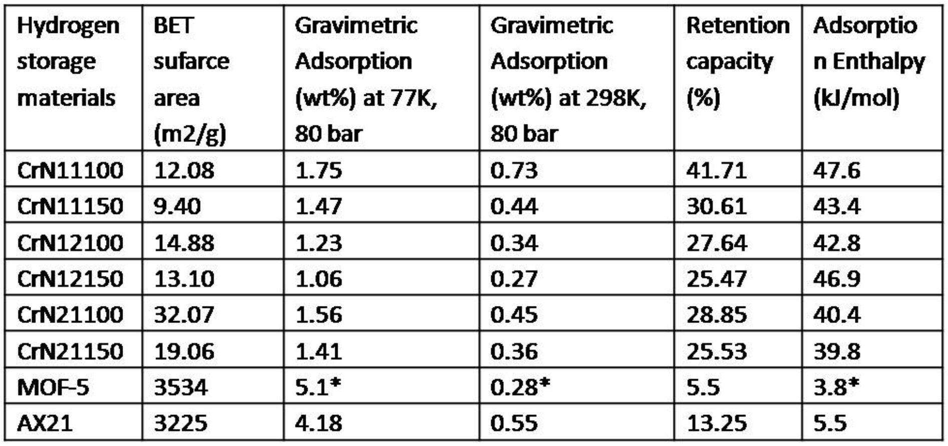

Hydrogen storage materials	BET sufarce area (m2/g)	Gravimetric Adsorption (wt%) at 77K, 80 bar	Gravimetric Adsorption (wt%) at 298K, 80 bar	Retention capacity (%)	Adsorption Enthalpy (kJ/mol)
CrN11100	12.08	1.75	0.73	41.71	47.6
CrN11150	9.40	1.47	0.44	30.61	43.4
CrN12100	14.88	1.23	0.34	27.64	42.8
CrN12150	13.10	1.06	0.27	25.47	46.9
CrN21100	32.07	1.56	0.45	28.85	40.4
CrN21150	19.06	1.41	0.36	25.53	39.8
MOF-5	3534	5.1*	0.28*	5.5	3.8*
AX21	3225	4.18	0.55	13.25	5.5

Table A.3: Retention capacity, BET surface area and adsorption enthalpy of cyclopentadienyl chromium hydrazide materials compared to MOF-5 and carbon AX-21.

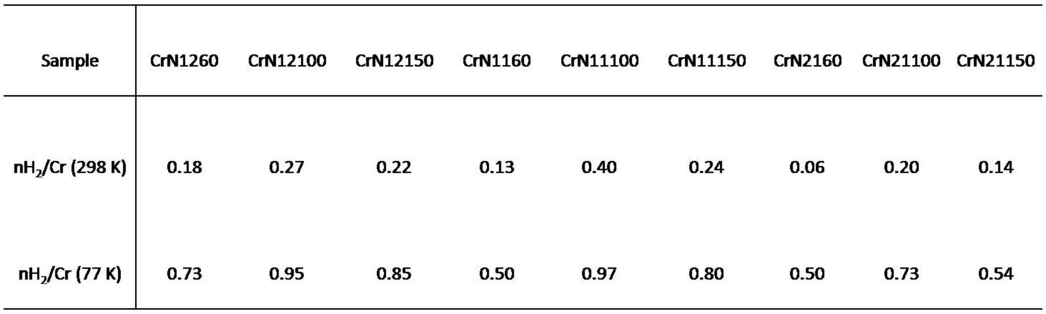

Sample	CrN1260	CrN12100	CrN12150	CrN1160	CrN11100	CrN11150	CrN2160	CrN21100	CrN21150
nH_2/Cr (298 K)	0.18	0.27	0.22	0.13	0.40	0.24	0.06	0.20	0.14
nH_2/Cr (77 K)	0.73	0.95	0.85	0.50	0.97	0.80	0.50	0.73	0.54

Table A.4: H_2 adsorbed per Cr atom for cyclopentadienyl chromium hydrazide materials.

Vita Auctoris

Van Hung Mai was born in 1982 in Vietnam. He received the B.E. degree in food and chemical engineering from the Ho Chi Minh City University of Technology, Ho Chi Minh City, Vietnam, in 2005. He received a Master degree from the Department of Chemistry and Biochemistry, University of Windsor, Windsor, ON, Canada, in September 2011.

Publications

[1] Hung V. Mai, Tuan K. A. Hoang, Ahmad Hamaed, Michel Trudeau, David M. Antonelli ”Cyclopentadienyl Chromium Hydrazide Gel for Kubas - Type Hydrogen Storage”. Chem. Comm. 2010, 46, 3206 - 3208.

[2] Tuan K. A. Hoang, Michael I. Webbs, Hung V. Mai, Ahmad Hamaed, Charles J. Walsby, Michel Trudeau, David M. Antonelli* ”Design and synthesis of vanadium hydrazide gels for Kubas - type hydrogen adsorption: a new class of hydrogen storage materials”. J. Am. Chem. Soc. 2010, 132, 11792 - 11798.

[3] Ahmad Hamaed, Hung V. Mai, Tuan K. A. Hoang, Michel Trudeau, David M. Antonelli* ”Functionalized porous silicas with unsaturated early transition metal moieties as hydrogen storage materials: Comparison of metal and oxidation state”. J. Phys. Chem. C 2010, 114 (18), 8651 - 8660.

Professional Activities

[1] 2008 - 2011: Teaching Assistant and Researching Assistant at University of Windsor

[2] April 2010: 2 posters at Canadian Society for Chemistry Conference 2010

[3] September 2007: A presentation at Korea - Vietnam Conference.

[4] 2006 - 2008: Researching Assistant at IAMS (Institute of Applied Material Science) in Vietnam.

[5] 2005 - 2006: Teaching assistant at Ho Chi Minh City University of Technology - Vietnam.

Academic Honours and Awards

[1] September 2008 - 2011: Tuition Scholarship for International Student (University of Windsor).

[2] March 03rd, 2006. Eureka First Prize in the 7th Competition Science for Students- Eureka (the people's committee - Ho Chi Minh City - Vietnam).

[3] December 25th, 2005. Encouraging Prize for Students' Sciencetific Research (Ministry of Education and Training of Vietnam).

[4] September 2000 - April 2005: Tuition Scholarship (Ho Chi Minh City University of Technology - Vietnam).